MR thermometry in fat-containing tissues for MR-guided High Intensity Focused Ultrasound therapy

Paul Baron

MR thermometry in fat-containing tissues for
MR-guided High Intensity Focused Ultrasound therapy
PhD thesis, Utrecht University, The Netherlands

This research was performed within the framework of the Center for Translational Molecular Medicine, project VOLTA

Financial support for the publication of this thesis was kindly provided by the Röntgenstichting Utrecht.

ISBN:	978-90-393-6317-1
Cover design:	Paul Baron
Lay-out:	Bolivar Creative Design & Paul Baron
Printed by:	Proefschriften.nl || Uitgeverij BOXPress

MR thermometry in fat-containing tissues for MR-guided High Intensity Focused Ultrasound therapy

MR thermometrie in vet bevattende weefsels voor MR-geleide High Intensity Focused Ultrasound therapie
(met een samenvatting in het Nederlands)

Proefschrift

ter verkrijging van de graad van doctor aan de Universiteit Utrecht
op gezag van de rector magnificus, prof.dr. G.J. van der Zwaan,
ingevolge het besluit van het college voor promoties in het openbaar
te verdedigen op dinsdag 14 april 2015 des middags te 2.30 uur

door

Paul Baron

geboren op 15 september 1977
te Ukarumpa, Papoea Nieuw Guinea

Promotoren:	Prof. dr. ir. M.A. Viergever Prof. dr. C.T.W. Moonen
Co-promotor:	Dr. ir. L.W. Bartels

Contents

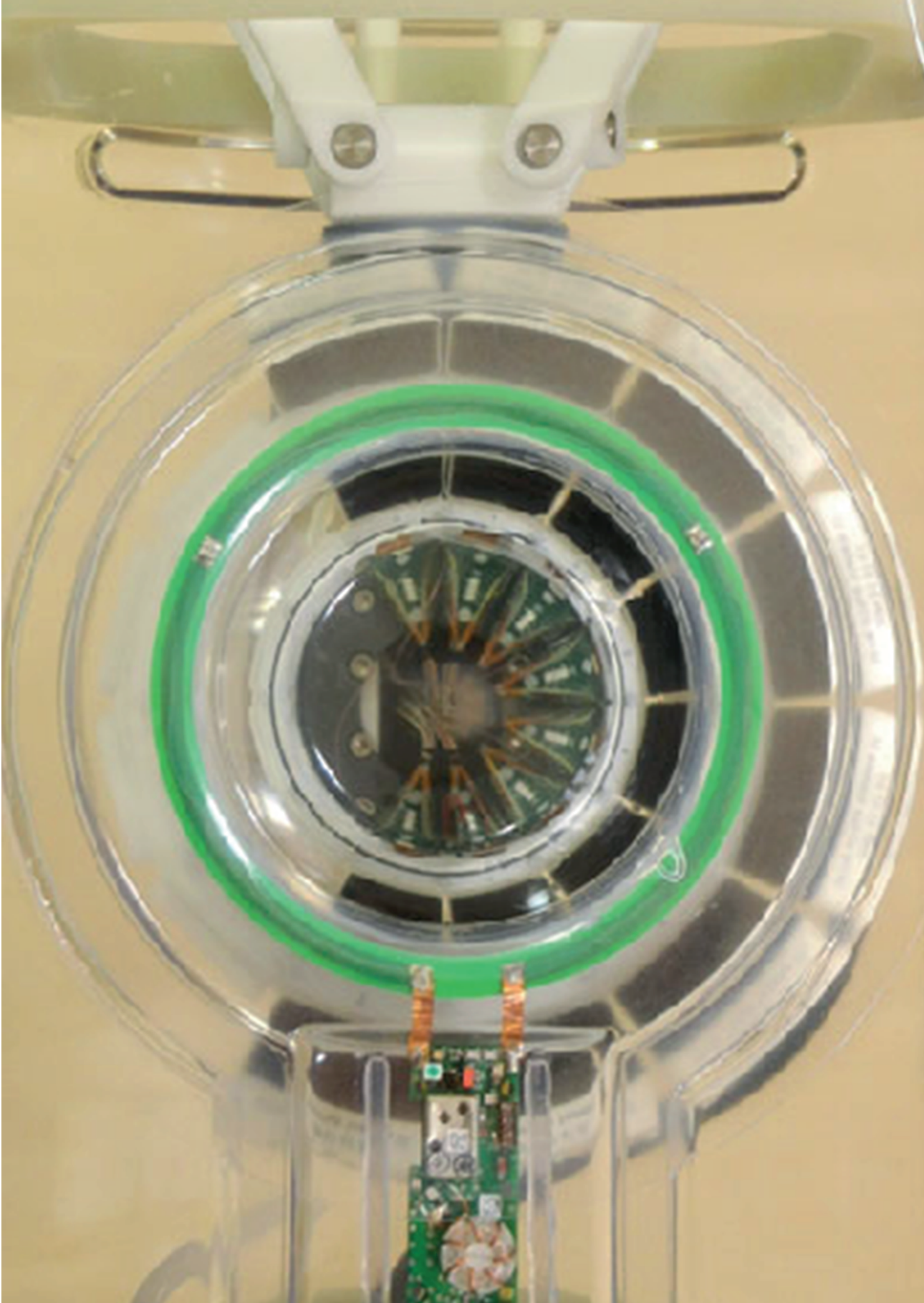

CHAPTER 1

Introduction

1.1. MR-guided High Intensity Focused Ultrasound

During the past few decades less invasive surgical and interventional procedures have been developed for many clinical indications, with the aim to reduce perioperative complications, preserve more healthy tissue, and allow for a more rapid recovery (1,2). These procedures include laparoscopic surgery (3), transluminal angioplasty (4), radiation therapy (5), and the therapeutic use of ultrasound (6). From all of these treatments, therapeutic ultrasound is the only technique that may be applied non-invasively, without the use of ionizing radiation. For the application of therapeutic ultrasound, ultrasound waves are transmitted into the body from acoustically coupled transducers. The deposition of ultrasound energy may result in thermal and/or mechanical effects in the tissue (7,8). Therapeutic ultrasound is commonly used in physiotherapy with the aim of reducing pain and for tissue healing, but there is conflicting evidence of its effectiveness (9).

High Intensity Focused Ultrasound (HIFU) is a procedure in which ultrasound waves are focused to one spot, resulting in a local region of high intensity deep within the body (Fig. 1). The ultrasound intensities reached at the focal zone are many orders of magnitude higher than those used for diagnostic ultrasound (10). A variety of therapeutic applications of HIFU are being investigated, including its potential for drug delivery (11), increasing the permeability of the blood-brain barrier (12), controlling gene expression (13), chemo- or radiotherapy sensitization (14,15), and for local tissue destruction (10). In a process called thermal ablation (10), the thermal effect is used to increase the temperature high enough for a certain duration to cause tissue necrosis (Fig. 2). The bio-effects of heating on tissues is related to the thermal dose, which is a function of the temperature-time history of the tissue (16). The lethal thermal dose depends on the tissue type (17), with an equivalent dose of 240 minutes at 43 °C commonly used as the minimum threshold (18,19). Focused ultrasound has been shown capable of producing well delineated volumes of tissue necrosis (10), and therefore may allow for precise spatial control of the target volume. A disadvantage of focused ultrasound is the typically small focal zone produced from single element transducers (20). This problem has been partly resolved by the introduction of phased array transducers, which allow for rapid electronic beam steering (20), which can be used to ablate larger volumes without having to physically move the transducer (Fig. 1: dashed lines). Philips Healthcare (Vantaa, Finland) has incorporated electronic beam path trajectories in their MR-HIFU systems known as volumetric sonications, which use point-to-point focusing on concentric rings and achieve homogenous tissue necrosis (19).

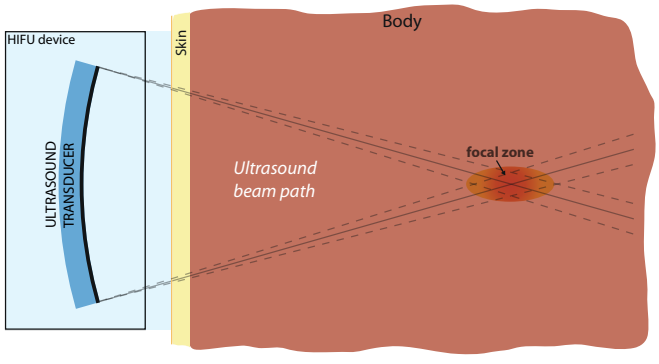

FIG. 1. Illustration of ultrasound waves being focused in the body. Electronic beam steering is indicated by the dashed lines (see text.)

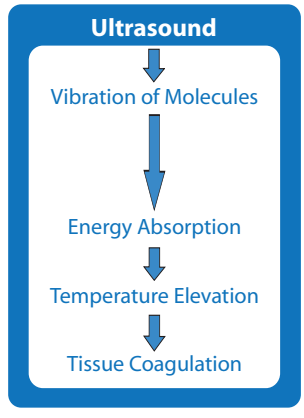

FIG. 2. Process of thermal ablation.

Combining medical imaging with HIFU has allowed for treatment planning, inter-operative guidance and monitoring, and for *in situ* treatment evaluation. HIFU is commonly monitored with ultrasound imaging (21-23) or Magnetic Resonance Imaging (MRI) (12,13,19,24-26), although these modalities are not mutually exclusive (27). The advantages of ultrasound imaging compared to MRI are its portability, lower costs, and generally higher temporal resolution. Furthermore, the ultrasound imaging and therapeutic transducers may be integrated into the same treatment unit (21,23) so that they are always aligned and share the same acoustic window (21). The advantages of MRI include its excellent soft tissue contrast (28) and the opportunity for temperature monitoring (29) during thermal therapeutic procedures. Temperature monitoring may be used for calculating the applied thermal dose, for monitoring the temperature evolution in healthy tissue structures outside the target area, or to provide feedback for controlled heating.

Focused ultrasound guided by MRI (MR-HIFU) has resulted in a state-of-the-art platform for interventional therapies (Fig 3). Figure 4a shows the dedicated breast MR-HIFU (Sonalleve) platform developed by Philips Healthcare (Vantaa, Finland). Ultrasound transducer elements surround the breast in an arc (Figure 4b) and the tumor is sonicated from the sides (Figure 4c). MR-HIFU thermal ablation is currently FDA approved for the treatment of uterine fibroids and for the palliative treatment of bone metastases (24). MR-HIFU is being further developed for other indications, such as for the treatment of breast (25) and liver (26) cancers, bringing new technological challenges to the field. For example, for breast applications, accurate MR temperature monitoring is required (preferably simultaneously) in both the glandular (water) and adipose (fat) breast tissue. For MR-HIFU thermal therapies there is also risk of undesired heating of healthy tissues, for instance in part of the HIFU beam traveling towards the focus, called the near field. Additionally, absolute temperature information is required to determine the thermal dose (16) and control the release from heat-sensitive drug carriers (11).

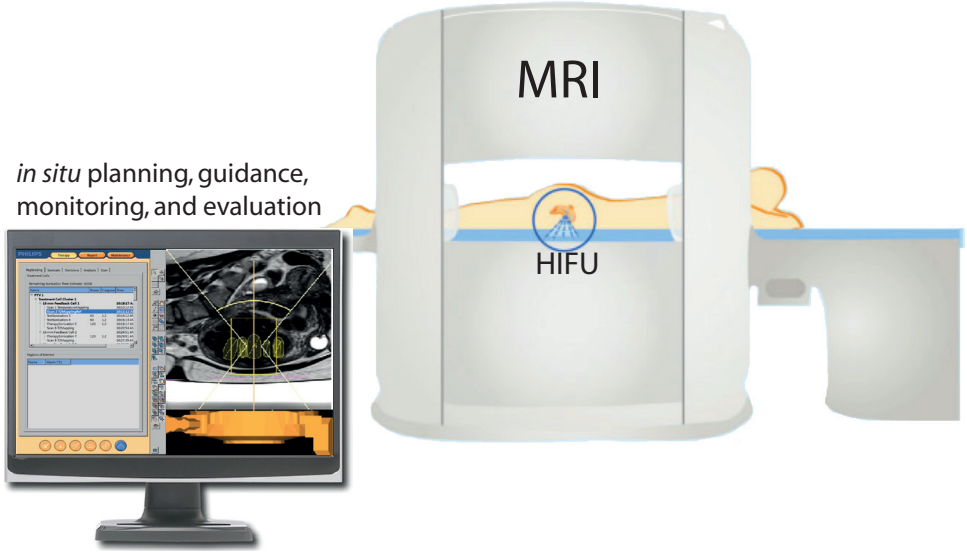

FIG. 3. The MR-HIFU operating theater allowing for a variety of non-invasive therapies. (The Figure was partly reproduced from the Philips Sonalleve MR-HIFU Instructions for Use manual for the fibroid therapy system.)

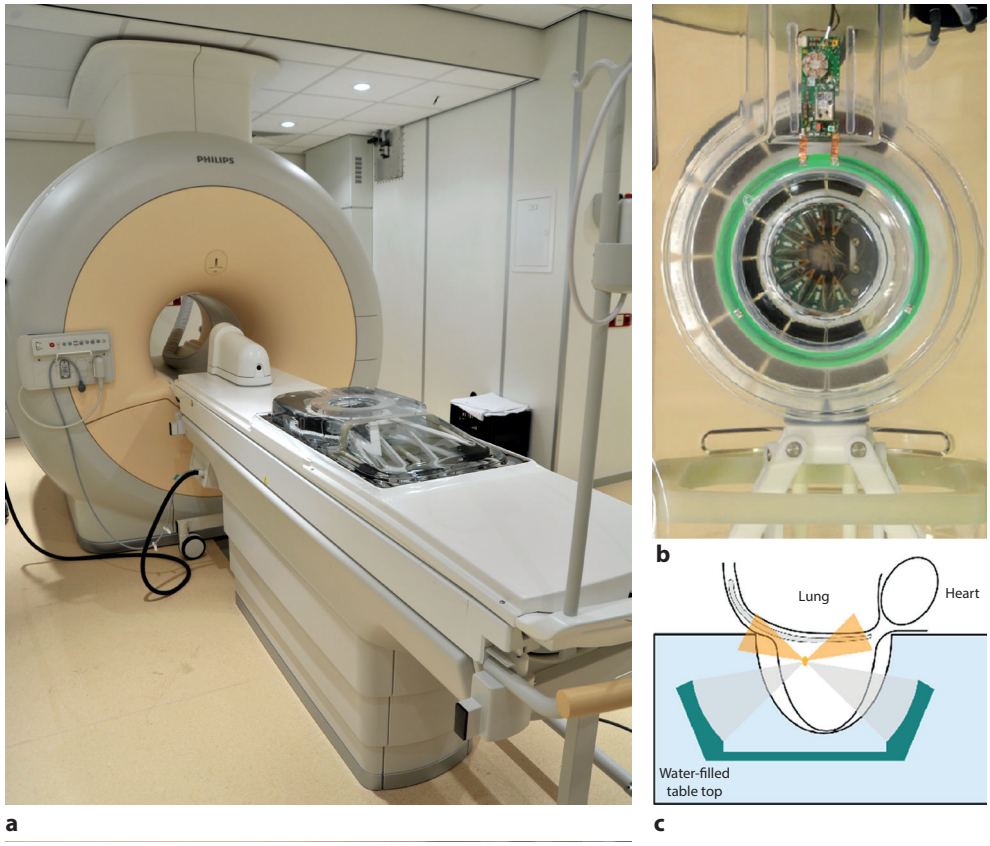

FIG. 4. (**a**) The dedicated breast MR-HIFU platform and (**b**) above view of the ultrasound transducers, and (**c**) schematic diagram of the position of the transducers with respect to the breast.

1.2. MR thermometry

MR thermometry is a technique which uses MR imaging to non-invasively probe the temperature of the body or other media. In principle any temperature dependent tissue property that influences the MR signal may be employed for MR thermometry. These properties include the apparent proton density (30), diffusivity of water molecules (31), magnetization transfer between the bound and free protons (32), intermolecular quantum coherences (33), and the magnetic susceptibility of the tissue (34). However, the most common methods for measuring temperature with MRI are based on the temperature dependence of the proton resonance frequency shift (PRFS) (35,36) and of the magnetic relaxation rates (37,38), as will be discussed in the paragraphs below.

1.3. PRFS thermometry

A common method for measuring temperature change is based on the proton resonance frequency shift (PRFS) of the water hydrogen nucleus with changing temperature (35). As the temperature of aqueous tissues or gels increases, the molecular motion of the water

molecules increases. As a consequence, hydrogen bonds stretch, bend, and break (35,36), and the water molecules spend less time on average in a hydrogen-bonded state (35). This, in turn, increases the electron shielding of the water hydrogen nuclei and decreases the nuclear magnetic field (B_{nuc}) that these nuclei experience. Changes in the hydrogen nuclear magnetic field can be measured with MRI by measuring the corresponding change in the nuclear magnetic resonance frequency (i.e. $\omega = \gamma B_{nuc}$) either via phase mapping or spectroscopic acquisitions. If only the electron shielding effects are considered, the relationship between ω and the electron shielding constant (σ) is given by:

$$\omega = \gamma\left(1-\sigma\left(T\right)\right)B_0 \qquad [1]$$

where γ is the gyromagnetic ratio for water protons and B_0 the magnetic field strength. Phase mapping techniques are commonly used to measure the PRFS shift, by applying consecutive gradient echo acquisitions at the same spatial location and with the same echo times. The change in the accumulated phase between acquisitions is then used to determine the change in resonance frequency and corresponding temperature change.

Advantages of PRFS-thermometry include the almost tissue-type independence of the temperature coefficient of the electron shielding constant and insensitivity to coagulation (35). Many research groups have investigated the temperature dependence of the electron shielding constant in various tissues and for water (see Table 1) (35,36,39,40), finding a linear relationship with a slope of about 0.01 ppm/°C. For hydrogen nuclei in fat this mechanism of temperature dependence is not present because of the absence of hydrogen bonding in fat molecules (40).

The proton resonance frequency is not only sensitive to temperature changes via electron shielding, but is influenced by any source of nuclear magnetic field variation, such as field drift (41), respiration and cardiac motion (42), or -in the specific case of MR-HIFU- ultrasound transducer movement (43). Such effects can lead to errors in PRFS Thermometry. One source of magnetic field change is from the inherent temperature dependence of the volume magnetic susceptibility (χ) of tissues (35). The magnetic susceptibility change influences the nuclear magnetic field both directly (via the sphere of Lorentz) and indirectly via the global magnetic field change it induces. Table 1 gives an overview of the range of values measured for the temperature coefficient of magnetic susceptibility for various tissues and for water (34,39,40). Generally, a higher temperature coefficient of the magnetic susceptibility was found in adipose tissue than for water-based tissues.

Table 1. Temperature coefficient for the electron screening constant (σ) and volume magnetic susceptibility (χ) for various media.

Medium	***dσ/dT*** **(×10^{-8}/°C)**		***dχ/dT*** **(×10^{-8}/°C)**	
water	0.99 – 1.02	(36,39)	0.20 – 0.26	(39,40)
water-based tissues	0.95 – 1.03	(35,40)	0.16	(40)
adipose tissue	0	(40)	0.46 – 0.94	(34,39,40)

1.4. Relaxation–based thermometry

Another approach to measure temperature change with MRI is based on the temperature dependence of the relaxation times T_1 and T_2 (38,44,45). Unlike the proton resonance

frequency, T_1 and T_2 are not disturbed by magnetic field disturbances (46), which are commonly in the order of μT. The longitudinal relaxation (characterized by time constant T_1) involves the energy transfer from the nuclear spin system to the environment. T_1 relaxation is a stimulated process which depends on the match between the molecular tumbling rate and the larmor frequency. One model proposed to describe the relationship between T_1 and temperature for aqueous tissues is given by (47,48):

$$T_1 \propto e^{-E/kT} \quad [2]$$

where E is the activation energy of the relaxation process, k the boltzmann constant, and T the absolute temperature. For small temperature ranges (i.e. $\Delta T < 25$ °C) a linear relationship was observed between T_1 and temperature for aqueous tissues (45,48). However, when the aqueous tissues were heated to temperatures above 40 °C, non-linear, and irreversible T_1 temperature changes occurred (45,48). This effect has been associated with protein denaturation which occurs at the same temperature range. For MR magnetic field strengths (B_0) ranging from 0.2 to 11 Tesla, the T_1 and T_2 of muscle and adipose tissues have been observed to increase with temperature (Table 2) (44,45,49-51).

Table 2. Temperature coefficients for T_1 and T_2. All tissues were measured ex vivo. (T range: Temperature range)

Tissue	B_0 (T)	Parameter	Coefficient (ms/°C)	T range (°C)	Reference
porcine adipose	0.2	T_1	5.3 ± 0.7	21 – 57	Peller et al. (45)
porcine muscle	0.2	T_1	4.1 ± 1.0	21 – 43	Peller et al. (45)
bovine adipose	0.5	T_1	5.0	21 – 71	Ghandi et al. (44)
bovine adipose	0.5	T_2	0.9	21 – 71	Ghandi et al. (44)
porcine adipose	1.5	T_1	5.8 ± 2.1	30 – 70	Hey et al. (49)
breast adipose	3.0	T_1	6.21 - 10.97	24 – 78	Diakite et al. (50)
bovine adipose (CH_2)	11.0	T_1	11.6 ± 0.42	20 - 60	Kuroda et al. (51)
bovine adipose (CH_3)	11.0	T_1	31.2 ± 3.92	20 - 60	Kuroda et al. (51)
bovine adipose (CH_2)	11.0	T_2	9.99 ± 0.93	20 - 60	Kuroda et al. (51)
bovine adipose (CH_3)	11.0	T_2	16.9 ± 1.39	20 - 60	Kuroda et al. (51)

1.5. Issues regarding MR thermometry for HIFU guidance

1.5.1. Corruption of PRFS thermometry in aqueous tissues

As mentioned in the PRFS-thermometry section above, PRFS-thermometry with its low temperature sensitivity of only 0.01 ppm/°C, is very sensitive to all types of sources of magnetic field change. Various methods have been proposed to correct for PRFS changes that are not directly related to the temperature induced change in electron screening constant. For example, in voxels that contain both water and fat, it has been proposed to use fat as *internal reference* (52-57). The concept is to use the resonance frequency shift of fat as a generic probe for magnetic field disturbances, in order to correct the magnetic field disturbance experienced

by water in the same voxel. Another generic correction method is the *referenceless* method (58), which interpolates the magnetic field change around the heated region to estimate the magnetic field change in the heated region. Other correction methods are more specific to the source of the field disturbance. For example, the multi baseline approach samples the periodic field disturbances occurring during breathing in order to apply the correction later during heating when in the same moment of the breathing cycle (59). Correcting or avoiding magnetic field disturbances is an important aspect in the on-going research on PRFS MR thermometry.

1.5.2. MR thermometry in adipose tissues

Because of the small quantities of water in adipose tissue (60), and absence of hydrogen bonding in fat (Table 1) (40), PRFS-based thermometry in adipose tissue is very challenging. Therefore, other MR thermometry methods are required to monitor the temperature in adipose tissues. One method that has shown to be promising is to use the temperature dependence of relaxation times of fat, for example via fast T_1-weighted turbo spin echo acquisitions (61). Techniques that would allow for simultaneous MR thermometry in aqueous and adipose tissues would be advantageous (62), especially for temperature monitoring in tissues or organs that may contain both water and fat components, like the female breast, the liver and bone marrow.

1.5.3. Monitoring of heat-sensitive tissues

Although, the heating during HIFU ablation is mainly localized to the focal area, there may be undesired tissue heating in regions outside the target area (19). This may involve heat-sensitive tissues such as nerves, skin, lungs, and heart tissue. MR thermometry may play an important role in preventing thermal damage outside of the target region. Ideally, MR thermometry techniques would be used to monitor the therapeutic effect at the target region as well as for ensuring the absence of unwanted heating outside of this region.

1.5.4. Need for absolute temperature information

Although most MR thermometry techniques measure *changes* in temperature, in some cases there is also a desire to know the absolute tissue temperature. For example, the thermal dose, an important indicator of tissue damage, is a function of the absolute temperature-time history of the tissue (63). Additionally, drug release from heat-sensitive carries occurs when the temperature is raised above a critical absolute temperature (11). Furthermore, being able to determine the absolute temperature would obviate the use of reference scans for subtraction, thereby making the technique more robust against motion (64). Additionally, tissues may be actively cooled during HIFU to prevent thermal injuries (65), but this may be a problem for MR thermometry protocols that assume a baseline temperature of 37 °C. Also for mild (non-destructive) hyperthermia, the temperature should be maintained within the absolute temperature range of 40-45 °C for long periods of time.

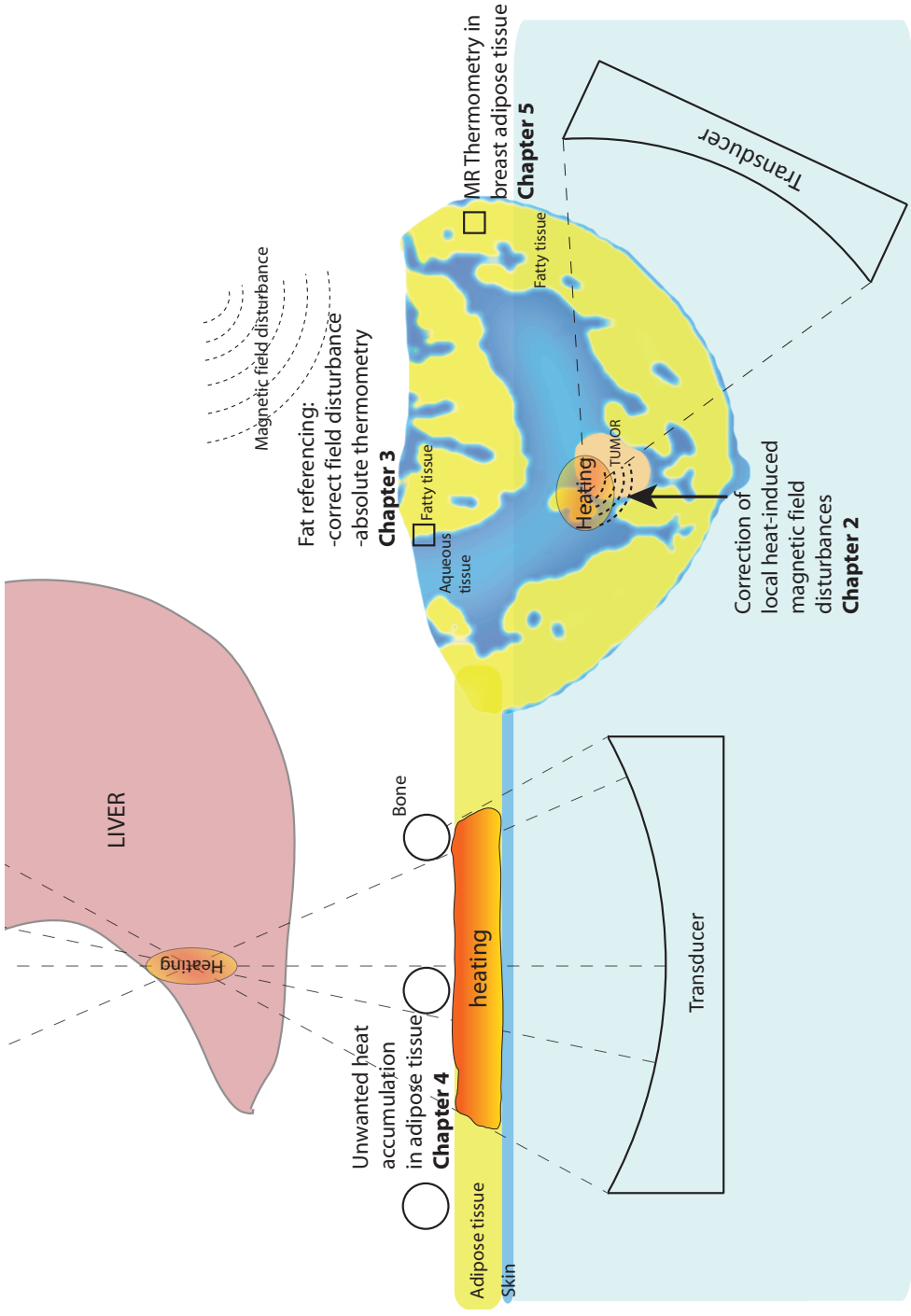

FIG. 5. Overview of the scenarios investigated in this thesis for the development of MR-HIFU for the treatment of breast and liver cancer.

1.6. Outline of this thesis

The aim of the research underlying this thesis was to develop and apply MR thermometry techniques for applications during volumetric MR-HIFU ablation in the breast and liver. The focus is on MR thermometry methods in tissues containing fat. The outline of this thesis is schematically summarized in Figure 5.

In the breast, the heating of adipose tissue may be unavoidable. For example, the tumor itself may be partly embedded in adipose tissue and be part of the treatment target region. Given that the temperature coefficient of magnetic susceptibility for adipose tissue is on the same order of magnitude as that of the electron screening constant for aqueous tissues (Table 1), the heating of fat may result in appreciable magnetic field disturbances in adjacent aqueous tissue structures. If this adjacent tissue structure is the tumor being treated, the magnetic field disturbance may corrupt the PRFS temperature measurements there (66). Essentially, all heat-induced changes of tissue magnetic susceptibility, when not accounted for, may result in PRFS thermometry errors. The magnitude of these errors will depend on the exact heating profile, orientation of the heating profile with respect to the main magnetic field, and distance of the disturbance to the PRFS measurement (66). In **chapter 2** (see Fig. 5), the magnetic field disturbance originating from the heat-induced HIFU heating of breast adipose tissue was visualized directly with phase mapping. A correction method was then proposed for these sources of thermometry errors in surrounding aqueous tissues.

In **chapter 3** the role of the water/fat spatial distribution was investigated in evaluating the feasibility of fat referenced absolute MR thermometry. This was evaluated in samples with different scales of water/fat heterogeneities such as pork tissue and margarine. Additionally, the implication of heat-induced magnetic susceptibility changes on the accuracy of relative fat referenced MR thermometry was investigated.

For MR-HIFU thermal applications there is risk of undesired heating of tissues outside of the target area. Especially the liver tissue, which is highly perfused, may require high levels of ultrasound powers to achieve tissue necrosis due to the cooling effect of the blood flow. Additionally, the ultrasound beam path access to the liver tumor may be blocked by the rib cage or lungs. Therefore, the US intensity in this smaller acoustic window would have to be higher to achieve the same rate of energy deposition at the focal zone. Furthermore, because multiple sonications are generally required to treat the whole tumor volume, there may be an accumulation of heat in regions where the beam paths overlap when inadequate cooling times are used between the sonications. All these aspects put tissues outside of the target area at risk. Especially adipose tissue is a concern because of its low heat capacity (67), low conductivity (67,68), and low perfusion (69). Adipose tissue may therefore accumulate heat, and put adjacent structures, such as the skin or muscle at risk. In **chapter 4**, apparent T_2 mapping was investigated for temperature monitoring in the subcutaneous adipose tissue layers to prevent skin burns during MR-HIFU of the liver.

For MR-HIFU in the breast, temperature monitoring in adipose tissues is desirable. To employ relaxation based methods, the temperature dependence of the relaxation times of breast adipose tissue would need to be measured at the MR field strength (1.5 T) currently used by our institute for MR-HIFU. Other studies have reported large inter-subject variations of the temperature coefficient of T_1 in breast adipose tissue measured at 3 T (50,51). In **chapter 5**, the T_1 and T_2 temperature dependence of human breast adipose tissue was investigated at 1.5 T to determine if these relaxation times could be used for thermometry during thermal therapies of the breast.

In **chapter 6** the main contributions and limitations of the research presented in this thesis is discussed. Additionally, some current and future work in the field of MR thermometry is described. **Chapter 7** contains a summary of this thesis.

1.7. References

1. Wickham JEA. The New Surgery. Brit Med J 1987;295(6613):1581-1582.
2. Wyld L, Audisio RA, Poston GJ. The evolution of cancer surgery and future perspectives. Nat Rev Clin Oncol 2014.
3. Velanovich V. Laparoscopic vs open surgery - A preliminary comparison of quality-of-life outcomes. Surg Endosc-Ultras 2000;14(1):16-21.
4. Shawl FA. Minimally Invasive Angioplasty - Acute and Long-Term Results of Low-Pressure Dilatation with a Noncompliant Balloon during Percutaneous Transluminal Coronary Angioplasty. J Invasive Cardiol 1993;5(3):122-127.
5. Bernier J, Hall EJ, Giaccia A. Timeline - Radiation oncology: a century of achievements. Nat Rev Cancer 2004;4(9):737-U715.
6. ter Haar G. Ultrasound focal beam surgery. Ultrasound in medicine & biology 1995;21(9):1089-1100.
7. Bailey MR, Khokhlova VA, Sapozhnikov OA, Kargl SG, Crum LA. Physical mechanisms of the therapeutic effect of ultrasound - (A review). Acoust Phys+ 2003;49(4):369-388.
8. Johns LD. Nonthermal effects of therapeutic ultrasound: The frequency resonance hypothesis. J Athl Training 2002;37(3):293-299.
9. Robertson VJ, Baker KG. A review of therapeutic ultrasound: effectiveness studies. Phys Ther 2001;81(7):1339-1350.
10. Ter haar G. Ultrasound Focal Beam Surgery. Ultrasound in Medicine and Biology 1995;21(9):1089-1100.
11. Grull H, Langereis S. Hyperthermia-triggered drug delivery from temperature-sensitive liposomes using MRI-guided high intensity focused ultrasound. Journal of controlled release : official journal of the Controlled Release Society 2012;161(2):317-327.
12. Hynynen K, McDannold N, Vykhodtseva N, Jolesz FA. Noninvasive MR imaging-guided focal opening of the blood-brain barrier in rabbits. Radiology 2001;220(3):640-646.
13. Deckers R, Quesson B, Arsaut J, Eimer S, Couillaud F, Moonen CTW. Image-guided, noninvasive, spatiotemporal control of gene expression. P Natl Acad Sci USA 2009;106(4):1175-1180.
14. Issels RD, Lindner LH, Verweij J, Wust P, Reichardt P, Schem BC, Abdel-Rahman S, Daugaard S, Salat C, Wendtner CM, Vujaskovic Z, Wessalowski R, Jauch KW, Durr HR, Ploner F, Baur-Melnyk A, Mansmann U, Hiddemann W, Blay JY, Hohenberger P. Neo-adjuvant chemotherapy alone or with regional hyperthermia for localised high-risk soft-tissue sarcoma: a randomised phase 3 multicentre study. Lancet Oncol 2010;11(6):561-570.
15. Raaphorst GP, Szekely JG. Thermal Enhancement of Cellular Radiation-Damage - a Review of Complementary and Synergistic Effects. Scanning Microscopy 1988;2(1):513-535.
16. Sapareto SA, Dewey WC. Thermal Dose Determination in Cancer-Therapy. Int J Radiat Oncol 1984;10(6):787-800.
17. Dewey WC. Arrhenius relationships from the molecule and cell to the clinic. Int J Hyperther 2009;25(1):3-20.
18. McDannold NJ, King RL, Jolesz FA, Hynynen KH. Usefulness of MR imaging-derived thermometry and dosimetry in determining the threshold for tissue damage induced by thermal surgery in rabbits. Radiology 2000;216(2):517-523.

19. Kohler MO, Mougenot C, Quesson B, Enholm J, Le Bail B, Laurent C, Moonen CT, Ehnholm GJ. Volumetric HIFU ablation under 3D guidance of rapid MRI thermometry. Med Phys 2009;36(8):3521-3535.
20. ter Haar G. Acoustic surgery. Phys Today 2001;54(12):29-34.
21. Wu F, Chen WZ, Bai J, Zou JZ, Wang ZL, Zhu H, Wang ZB. Pathological changes in human malignant carcinoma treated with high-intensity focused ultrasound. Ultrasound Med Biol 2001;27(8):1099-1106.
22. Ritchie RW, Leslie T, Phillips R, Wu F, Illing R, ter Haar G, Protheroe A, Cranston D. Extracorporeal high intensity focused ultrasound for renal tumours: a 3-year follow-up. Bju Int 2010;106(7):1004-1009.
23. Leung JHY, Yu SCH, Cheung ECW, Wong ASW, Tong MMB, Ho SSY, Leung VYF, Ahuja AT. Safety and Efficacy of Sonographically Guided High-Intensity Focused Ultrasound for Symptomatic Uterine Fibroids Preliminary Study of a Modified Protocol. J Ultras Med 2014;33(10):1811-1818.
24. Schlesinger D, Benedict S, Diederich C, Gedroyc W, Klibanov A, Larner J. MR-guided focused ultrasound surgery, present and future. Med Phys 2013;40(8).
25. Merckel LG, Bartels LW, Kohler MO, van den Bongard HJGD, Deckers R, Mali WPTM, Binkert CA, Moonen CT, Gilhuijs KGA, van den Bosch MAAJ. MR-Guided High-Intensity Focused Ultrasound Ablation of Breast Cancer with a Dedicated Breast Platform. Cardiovasc Inter Rad 2013;36(2):292-301.
26. Wijlemans JW, Bartels LW, Deckers R, Ries M, Mali WPTM, Moonen CTW, van den Bosch MAAJ. Magnetic resonance-guided high-intensity focused ultrasound (MR-HIFU) ablation of liver tumours. Cancer Imaging 2012;12(2):387-394.
27. Arvanitis CD, Livingstone MS, McDannold N. Combined ultrasound and MR imaging to guide focused ultrasound therapies in the brain. Phys Med Biol 2013;58(14):4749-4761.
28. Taylor DG, Bore CF. A Review of the Magnetic-Resonance Response of Biological Tissue and Its Applicability to the Diagnosis of Cancer by NMR Radiology. Ct-J Comput Tomogr 1981;5(2):122-134.
29. Rieke V, Pauly KB. MR thermometry. J Magn Reson Imaging 2008;27(2):376-390.
30. Chen J, Daniel BL, Pauly KB. Investigation of proton density for measuring tissue temperature. J Magn Reson Imaging 2006;23(3):430-437.
31. Kozak LR, Bango M, Szabo M, Rudas G, Vidnyanszky Z, Nagy Z. Using diffusion MRI for measuring the temperature of cerebrospinal fluid within the lateral ventricles. Acta Paediatr 2010;99(2):237-243.
32. Young IR, Hand JW, Oatridge A, Prior MV. Modeling and Observation of Temperature-Changes in-Vivo Using Mri. Magn Reson Med 1994;32(3):358-369.
33. Jenista ER, Branca RT, Warren WS. Absolute temperature imaging using intermolecular multiple quantum MRI. Int J Hyperther 2010;26(7):725-U155.
34. Sprinkhuizen SM, Bakker CJG, Ippel JH, Boelens R, Viergever MA, Bartels LW. Temperature dependence of the magnetic volume susceptibility of human breast fat tissue: an NMR study. Magn Reson Mater Phy 2012;25(1):33-39.
35. Peters RD, Hinks RS, Henkelman RM. Ex vivo tissue-type independence in proton-resonance frequency shift MR thermometry. Magnet Reson Med 1998;40(3):454-459.
36. Hindman JC. Proton Resonance Shift of Water in Gas and Liquid States. J Chem Phys 1966;44(12):4582.
37. Bloembergen N, Purcell EM, Pound RV. Relaxation Effects in Nuclear Magnetic Resonance Absorption. Phys Rev 1948;73(7):679-712.

38. Parker DL. Applications of NMR Imaging in Hyperthermia - an Evaluation of the Potential for Localized Tissue Heating and Noninvasive Temperature Monitoring. Ieee T Bio-Med Eng 1984;31(1):161-167.
39. Stollberger R, Ascher PW, Huber D, Renhart W, Radner H, Ebner F. Temperature monitoring of interstitial thermal tissue coagulation using MR phase images. Journal of magnetic resonance imaging : JMRI 1998;8(1):188-196.
40. De Poorter J. Noninvasive MRI thermometry with the proton resonance frequency method: study of susceptibility effects. Magn Reson Med 1995;34(3):359-367.
41. De poorter J, Dewagter C, Dedeene Y, Thomsen C, Stahlberg F, Achten E. The Proton-Resonance-Frequency-Shift Method Compared with Molecular-Diffusion for Quantitative Measurement of 2-Dimensional Time-Dependent Temperature Distribution in a Phantom. J Magn Reson Ser B 1994;103(3):234-241.
42. Peters NHGM, Bartels LW, Sprinkhuizen SM, Vincken KL, Bakker CJG. Do Respiration and Cardiac Motion Induce Magnetic Field Fluctuations in the Breast and Are There Implications for MR Thermometry? Journal of Magnetic Resonance Imaging 2009;29(3):731-735.
43. Zhou XD, He QA, Zhang A, Beckmann M, Ni C. Temperature measurement error reduction for MRI-guided HIFU treatment. Int J Hyperther 2010;26(4):347-358.
44. Gandhi S, Daniel BL, Butts K. Temperature Dependence of Relaxation Times in Bovine Adipose Tissue. Proceedings 6th ISMRM; Sydney, Australia. 1998. p. 701.; 1998; Australia.
45. Peller M, Reinl HM, Weigel A, Meininger M, Issels RD, Reiser M. T1 relaxation time at 0.2 Tesla for monitoring regional hyperthermia: feasibility study in muscle and adipose tissue. Magn Reson Med 2002;47(6):1194-1201.
46. Bottomley PA, Foster TH, Argersinger RE, Pfeifer LM. A Review of Normal Tissue Hydrogen NMR Relaxation-Times and Relaxation Mechanisms from 1-100 Mhz - Dependence on Tissue-Type, NMR Frequency, Temperature, Species, Excision, and Age. Med Phys 1984;11(4):425-448.
47. Parker DL, Smith V, Sheldon P, Crooks LE, Fussell L. Temperature distribution measurements in two-dimensional NMR imaging. Med Phys 1983;10(3):321-325.
48. Lewa J, Majewska Z. Temperature Relationships of Proton Spice-Lattice Relaxation Time T1 in Biological Tissues. Bulletin du Cancer 1980;67(5):525-530.
49. Hey S, de Smet M, Stehning C, Grull H, Keupp J, Moonen CT, Ries M. Simultaneous T1 measurements and proton resonance frequency shift based thermometry using variable flip angles. Magn Reson Med 2012;67(2):457-463.
50. Diakite M, Odeen H, Todd N, Payne A, Parker DL. Toward real-time temperature monitoring in fat and aqueous tissue during magnetic resonance-guided high-intensity focused ultrasound using a three-dimensional proton resonance frequency T1 method. Magn Reson Med 2014;72(1):178-187.
51. Kuroda K, Iwabuchi T, Obara M, Honda M, Saito K, Imai Y. Temperature Dependence of Relaxation Times in Proton Components of Fatty Acids. Magnetic Resonance in Medical Sciences 2011;10(3):177-183.
52. Kuroda K, Mulkern RV, Oshio K, Panych LP, Nakai T, Moriya T, Okuda S, Hynynen K, Jolesz FA. Temperature mapping using the water proton chemical shift: self-referenced method with echo-planar spectroscopic imaging. Magn Reson Med 2000;44(1):167.
53. Pan X, Li C, Ying K, Weng D, Qin W, Li K. Model-based PRFS thermometry using fat as the internal reference and the extended Prony algorithm for model fitting. Magn Reson Imaging 2010;28(3):418-426.

54. Shmatukha AV, Harvey PR, Bakker CJ. Correction of proton resonance frequency shift temperature maps for magnetic field disturbances using fat signal. J Magn Reson Imaging 2007;25(3):579-587.
55. Li C, Pan X, Ying K, Zhang Q, An J, Weng D, Qin W, Li K. An internal reference model-based PRF temperature mapping method with Cramer-Rao lower bound noise performance analysis. Magn Reson Med 2009;62(5):1251-1260.
56. Soher BJ, Wyatt C, Reeder SB, MacFall JR. Noninvasive temperature mapping with MRI using chemical shift water-fat separation. Magn Reson Med 2010;63(5):1238-1246.
57. Taylor BA, Elliott AM, Hwang KP, Shetty A, Hazle JD, Stafford RJ. Measurement of temperature dependent changes in bone marrow using a rapid chemical shift imaging technique. Journal of magnetic resonance imaging : JMRI 2011;33(5):1128-1135.
58. Rieke V, Vigen KK, Sommer G, Daniel BL, Pauly JM, Butts K. Referenceless PRF shift thermometry. Magn Reson Med 2004;51(6):1223-1231.
59. Vigen KK, Daniel BL, Pauly JM, Butts K. Triggered, navigated, multi-baseline method for proton resonance frequency temperature mapping with respiratory motion. Magnet Reson Med 2003;50(5):1003-1010.
60. Ren JM, Dimitrov I, Sherry AD, Malloy CR. Composition of adipose tissue and marrow fat in humans by (1)H NMR at 7 Tesla. J Lipid Res 2008;49(9):2055-2062.
61. Hynynen K, McDannold N, Mulkern RV, Jolesz FA. Temperature monitoring in fat with MRI. Magn Reson Med 2000;43(6):901-904.
62. Todd N, Diakite M, Payne A, Parker DL. Hybrid proton resonance frequency/T1 technique for simultaneous temperature monitoring in adipose and aqueous tissues. Magn Reson Med 2013;69(1):62-70.
63. Sapareto SA, Dewey WC. Thermal dose determination in cancer therapy. Int J Radiat Oncol Biol Phys 1984;10(6):787-800.
64. Rieke V, Butts Pauly K. MR thermometry. Journal of magnetic resonance imaging : JMRI 2008;27(2):376-390.
65. Wijlemans J, de Greef M, Schubert G, van den Bosch M, Moonen C, Ries M. Near-field management during MR-HIFU ablation in highly perfused organs.In Proceedings of the 23th Annual Meeting of the ISMRM, Milan, Italy, 2014. p. 2340.
66. Sprinkhuizen SM, Konings MK, van der Bom MJ, Viergever MA, Bakker CJ, Bartels LW. Temperature-induced tissue susceptibility changes lead to significant temperature errors in PRFS-based MR thermometry during thermal interventions. Magn Reson Med 2010;64(5):1360-1372.
67. Henriques FC, Moritz AR. Studies of Thermal Injury .1. The Conduction of Heat to and through Skin and the Temperatures Attained Therein - a Theoretical and an Experimental Investigation. Am J Pathol 1947;23(4):531-&.
68. Cohen ML. Measurement of the thermal properties of human skin. A review. The Journal of investigative dermatology 1977;69(3):333-338.
69. ESHO Task Group Committee. Treatment planning and modeling in hyperthermia: a task group report of the European Society for Hyperthermic Oncology. Rome: Tor Vergata 1992.

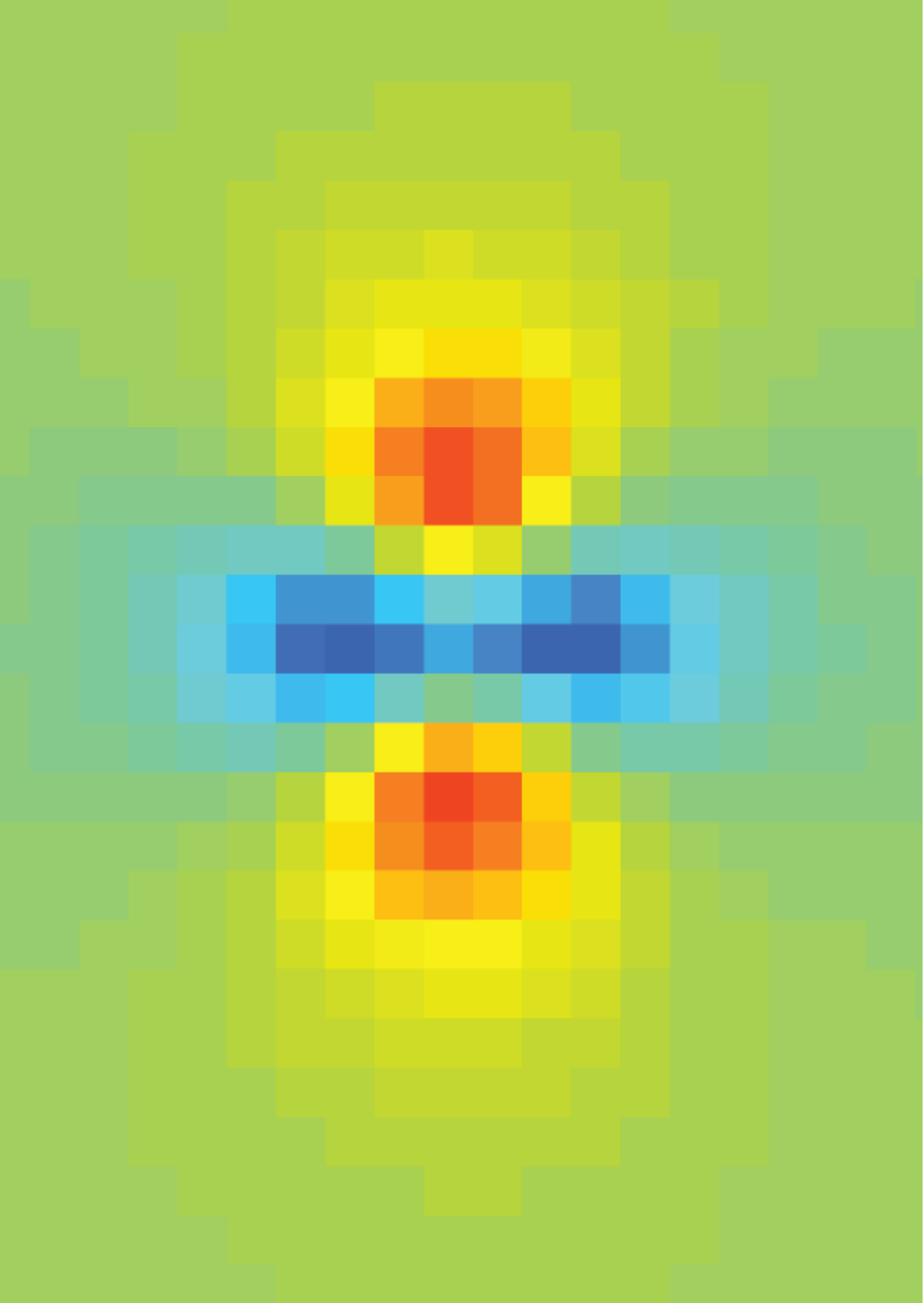

CHAPTER 2

Correction of proton resonance frequency shift MR thermometry errors caused by heat-induced magnetic susceptibility changes during High Intensity Focused Ultrasound ablations in tissues containing fat

Published as:

Baron P, Deckers R, de Greef M, Merckel LG, Bakker CJG, Bouwman JG, Bleys RLAW, van den Bosch MAAJ, Bartels LW. Correction of Proton Resonance Frequency Shift MR-Thermometry Errors Caused by Heat-Induced Magnetic Susceptibility Changes during High Intensity Focused Ultrasound Ablations in Tissues Containing Fat. Magn Reson Med 2014;72(6):1580-1589.

ABSTRACT

Purpose: In this study, we aim to demonstrate the sensitivity of proton resonance frequency shift (PRFS) -based thermometry to heat-induced magnetic susceptibility changes and to present and evaluate a model-based correction procedure.

Theory and Methods: To demonstrate the expected temperature effect, field disturbances during high intensity focused ultrasound sonications were monitored in breast fat samples with a three-dimensional (3D) gradient echo sequence. To evaluate the correction procedure, the interface of tissue-mimicking ethylene glycol gel and fat was sonicated. During sonication, the temperature was monitored with a 2D dual flip angle multi-echo gradient echo sequence, allowing for PRFS-based relative and referenced temperature measurements in the gel and T_1-based temperature measurements in fat. The PRFS-based measurement in the gel was corrected by minimizing the discrepancy between the observed 2D temperature profile and the profile predicted by a 3D thermal model.

Results: The HIFU sonications of breast fat resulted in a magnetic field disturbance which completely disappeared after cooling. For the correction method, the 5th to 95th percentile interval of the PRFS-thermometry error in the gel decreased from 3.8 °C before correction to 2.0 - 2.3 °C after correction.

Conclusion: This study has shown the effects of magnetic susceptibility changes induced by heating of breast fatty tissue samples. The resultant errors can be reduced by the use of a model-based correction procedure.

2.1. Introduction

Breast cancer is the most frequently diagnosed cancer and leading cause of cancer death in women (1). Treatment involves surgery, often in combination with radiotherapy and/or chemotherapy (2). As in other fields of medicine, also in the field of oncology, there is a growing interest in minimally invasive image-guided therapy. MR-guided high intensity focused ultrasound (MR-HIFU) is currently used for thermal ablation of benign uterine fibroids (3) and shows great potential for the ablation of malignant tumors in prostate (4), bone (5), and breast (6). MR imaging is used for treatment planning and follow-up after treatment because of its excellent soft tissue contrast and the large variety of imaging biomarkers that can be measured. Furthermore, MR imaging is used for temperature mapping during the thermal ablation procedure for guidance and safety.

Accurate MR thermometry is important to ensure that the target tissue is maintained long enough at elevated temperatures (e.g., for a few seconds above 55 °C) such that the applied thermal dose causes complete tissue necrosis. Furthermore, MR thermometry is used for monitoring the temperature of healthy tissue in the near and far field of the HIFU beam to prevent unwanted damage. Conventionally, proton resonance frequency shift (PRFS) thermometry is used for temperature monitoring during HIFU treatment in water-containing tissues such as tumors. PRFS thermometry is based on the fact that the magnetic field experienced by the nuclei of the hydrogen atoms in water molecules decreases by 0.01 ppm per degree Celsius temperature increase (7). This nuclear field change as a function of temperature, which is caused by the temperature dependence of the strength of the hydrogen bonds between water molecules, can be measured using phase mapping techniques based upon gradient echo pulse sequences. However, such phase measurements can be corrupted by other sources of magnetic field change such as field drift, respiration and cardiac motion (8), ultrasound transducer movement (9), cavitation (10), and changes in air temperature and oxygen concentration (11).

It has been shown theoretically with simulations in a breast tumor numerical model that heat-induced susceptibility changes of fat (12) may give rise to disturbances in the magnetic field. This phenomenon can lead to errors in temperature maps of the water-containing tumor tissue (and margin) measured by PRFS thermometry (13). This effect has also been shown experimentally in water/oil phantoms (13), but to our knowledge has never been reported for an actual HIFU sonication of fat containing tissue, including the breast. This may in part be due to the frequent use of fat-suppression techniques during these procedures, which would mask out any induced phase changes occurring in fat. Furthermore, the phase changes induced by external magnetic field changes in the aqueous tumor may not present itself as an obvious artifact when compared with the larger electron shielding related PRFS change.

The aim of the current study was to demonstrate experimentally the predicted effect in fatty human breast tissue samples under HIFU heating. In addition, we propose and evaluate a method to measure and correct for the field disturbance resulting from a HIFU sonication of a fat/aqueous tissue boundary. The correction method uses two-dimensional (2D) MR thermometry as input to a 3D thermal model. The 3D thermal model is combined with a high resolution 3D magnetic susceptibility temperature coefficient map to calculate the 3D magnetic susceptibility change. From the change in magnetic susceptibility the change in magnetic field is calculated in the imaging slice to correct the PRFS measurement.

2.2. Theory

In this section, the sensitivity of PRFS thermometry to changes in tissue magnetic susceptibility is described. Additionally, the principles of the proposed correction method are explained.

2.2.1. Sensitivity of PRFS to B_{nuc}

The nuclear magnetic field B_{nuc} experienced by water protons is given by (13):

$$B_{nuc} = \left(1 - \sigma - \frac{2}{3}\chi\right) B_{mac}(\chi) \quad [1]$$

where χ is the magnetic volume susceptibility spatial distribution, σ the electron screening constant, and B_{mac} the macroscopic magnetic field. For human tissue, for which χ is in the order of 10^{-6}, B_{mac} may be approximated by $B_{mac} = B_{mac} + O(\chi B_0)$ and Eq. [1] becomes (13):

$$\Delta B_{nuc} \cong \left[\Delta B_{mac}(\Delta\chi) - \frac{2}{3}\Delta\chi B_0\right] - \Delta\sigma B_0 = \Delta B_{nuc,suc}(\Delta\chi) - \Delta B_{nuc,elect}(\Delta\sigma) \quad [2]$$

where $\Delta B_{nuc,suc}(\Delta\chi) = \left[\Delta B_{mac}(\Delta\chi) - 2/3\Delta\chi B_0\right]$ is the nuclear magnetic field change caused by the change in magnetic susceptibility over the whole object including the change in the Lorentz correction term, and $\Delta B_{nuc,elect}(\Delta\sigma) = \Delta\sigma B_0$ is the nuclear magnetic field change caused by the local change in hydrogen electron shielding.

Usually the influence of $\Delta B_{nuc,suc}$ is neglected in Eq. [2], and the measured temperature change (ΔT_{meas}) is calculated as:

$$\Delta T_{meas} = \frac{\Delta\phi}{\gamma\alpha B_0 TE} \quad [3]$$

where $\Delta\phi$ is the phase difference between measurements at two temperatures with difference ΔT, TE the echo time, γ the gyromagnetic ratio, α the thermal coefficient ($\alpha = d\sigma / dT = 0.01\, ppm / °C$), and B_0 the magnetic field strength.

2.2.2. Model-based correction of PRFS for $\chi(T)$ effects

To correct for $\chi(T)$ effects, two important implications of Eq. [2] should be recognized. First, the change in nuclear magnetic field may be calculated from the change in susceptibility without knowing the absolute susceptibility values. Second, the contribution to ΔB_{nuc} from the change in susceptibility can be separated from the contribution from the change in electron screening constant by a simple subtraction operation. From Eq. [2], it further follows that once $\Delta B_{nuc,suc}$ is known, the corrected temperature change (ΔT_{cor}) is given by:

$$\Delta T_{cor} = \Delta T_{meas} - \frac{\Delta B_{nuc,suc}}{\alpha B_0} \quad [4]$$

In principle, because of the dependence of $\Delta B_{nuc,suc}$ on ΔB_{mac} seen in Eq. [2], the calculation of $\Delta B_{nuc,suc}$ requires information about the susceptibility distribution in the whole heated volume, which means that 3D data of the heat-induced susceptibility changes is needed. In practice, 3D measurement of such data would lead to acquisition times that are too long for monitoring the rapid temperature changes that occur for instance during thermal ablation.

For this reason, we propose a model-based approach to estimate $\Delta B_{nuc,suc}$ using 2D data as an input, which is illustrated in Figure 1. The first step (Fig. 1, box 1) is to define water and fat masks where the 2D MR thermometry data is well defined (i.e., voxels with minimal partial volume.) The temperature change in aqueous tissue ($\Delta T_{w,meas}$) is measured with PRFS thermometry and in fat ($\Delta T_{f,meas}$) with T_1 mapping. These T_1 measurements are not disturbed by magnetic field disturbances (14), which are on the order of μT. The next step (Fig. 1, box 2) is to fit a 3D thermal model (15) to the 2D MR thermometry measurements. The 3D thermal model is then combined with a high resolution 3D magnetic susceptibility temperature coefficient map ($d\chi/dT$ map) to calculate the 3D susceptibility change. The susceptibility temperature coefficient map uses prior knowledge of the susceptibility temperature coefficients of water-containing tissue ($d\chi/dT$ = 0.0015 ppm/°C) (16) and fatty tissue ($d\chi/dT$ = 0.0085 ppm/°C) (16,17). The change in magnetic susceptibility is then used to calculate the change in nuclear magnetic field (ΔB_{nuc}) using a memory efficient and fast Fourier-based algorithm (18). The last step (Fig. 1, box 3) is to correct the measured PRFS temperature change in water ($\Delta T_{w,meas}$) by subtracting the contribution from the nuclear magnetic field disturbance ($\Delta T_{w,suc}$). The corrected temperature change in water is then used as input to the 3D thermal model, and the steps (box 1-3 of Fig. 1) are iterated until the corrected temperature change ($\Delta T_{w,cor}$) remains stable.

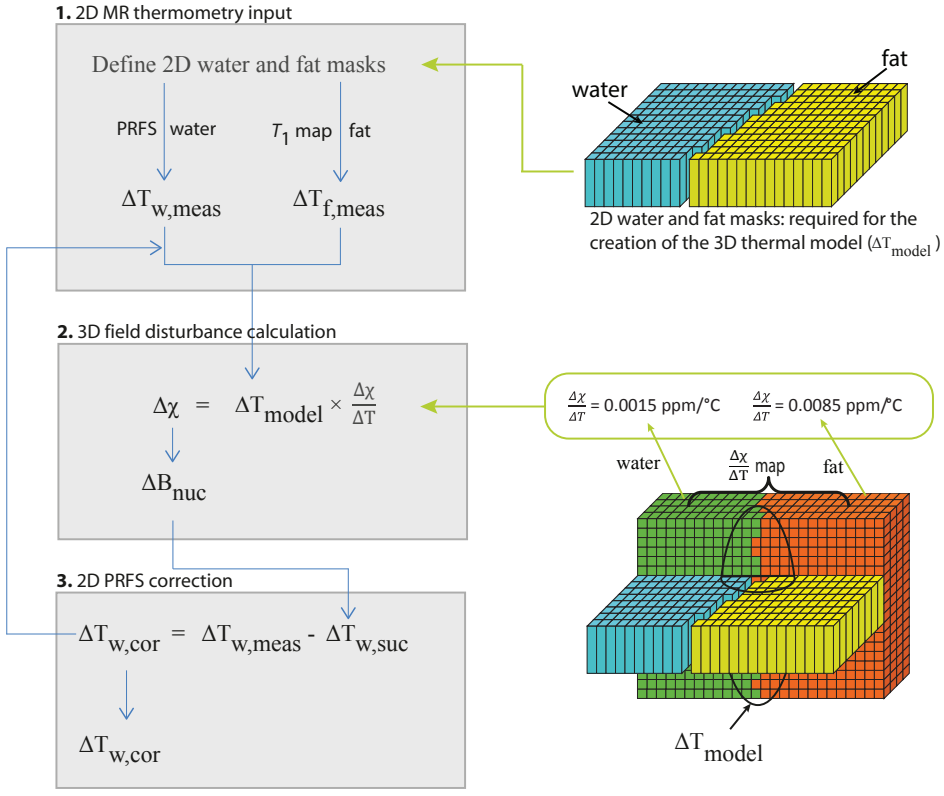

FIG. 1. Flow diagram showing the correction procedure. The three main parts are shown: **1:** 2D MR thermometry input, **2:** 3D field disturbance calculation, and **3:** 2D PRFS correction. (meas = measured, nuc = nuclear, cor = corrected, suc = susceptibility, w = water, f = fat).

2.3. Methods

In total, three experiments were conducted. The first experiment was to demonstrate the occurrence of temperature-induced field disturbances in human fat tissue. The influence of breast fat tissue HIFU heating on the local magnetic field was demonstrated for various acoustic powers and sonication volumes. Because fat does not have a temperature-dependent PRF, all measured phase changes are caused by changes in magnetic susceptibility (Eq. [1]). The second experiment was to determine the magnetic susceptibility temperature coefficient of the ethylene glycol (EG) gel, which is needed for the correct interpretation of the phantom experiments. The third experiment was performed to evaluate the proposed correction method for the errors shown in the breast experiment. For this purpose HIFU sonications in a dedicated EG gel/fat phantom were performed. All experiments were performed using a 1.5 Tesla (T) MR Scanner (Philips Healthcare, Best, The Netherlands) and a clinical MR-HIFU system (Sonalleve, Philips Healthcare, Vantaa, Finland).

2.3.1. HIFU sonications of breast fatty tissue

Five breasts were obtained from five unembalmed female human cadavers and degassed for 24 h in a vacuum tank to remove air bubbles that could lead to cavitation. The breast tissue was clamped between two ultrasound transparent membranes to prevent motion during sonication due to radiation forces and placed on top of the HIFU transducer. Below and above the breast tissue sample a block of agar gel was placed for acoustic coupling in the near field and to prevent reflection in the far field. Different fatty tissue regions, as observed on volumetric T_2-weighted scans, were ablated with various acoustic powers (40, 60, 80, 100 W) and volumetric treatment cell (19) diameters (2 mm, 4 mm) for 60 s. For magnetic field mapping, 3D T_1-weighted RF-spoiled gradient echo (SPGR) images were acquired dynamically during ablation. The parameters were: TE = 5 ms, repetition time (TR) = 10 ms, flip angle = 15°, matrix = 64 × 64 × 10, field of view (FOV) = 128 × 128 × 20 mm, and 5.7 s per dynamic. The relative change in nuclear magnetic field $\Delta B_{nuc} / B_0$ between dynamics was measured using the change in phase maps ($\Delta\phi$): $\Delta B_{nuc} / B_0 = \Delta\phi / (TE\,\gamma\,B_0)$ where TE = 5 ms, γ = 2.675 × 10^8 rad/s/T, and B_0 = 1.5 T. The center of the imaging volume was placed at the ultrasound focal target.

2.3.2. Ethylene glycol gel as temperature probe

Numerical simulations have shown (13) that HIFU sonications of fat-aqueous tissue boundaries result in a field disturbance in the aqueous tissue, mainly due to the magnetic susceptibility changes of fat (13). To experimentally show this effect, and verify the correction method, the boundary of EG gel with fat was sonicated. For practical considerations of obtaining reference temperature change measurements, the EG gel was used as a substitute for aqueous tissue. It consisted of 2/3 ethylene glycol, 1/3 deuterium, 3% agar, and 3% silica. EG has two proton resonance peaks (from the -OH and -CH_2 groups); the -OH peak shifts due to (electron shielding-induced) temperature change and external magnetic field change, whereas the -CH_2 peak only shifts due to the external magnetic field change because of the absence of hydrogen bonding. Therefore, the -OH shift represents the uncorrected PRFS thermometry measurement (i.e., $\Delta T_{w,meas}$ in Fig. 1) that would be obtained in aqueous tissue, and the true (referenced) temperature change is calculated as the shift in the OH peak position relative to the -CH_2 peak position. This allows for the verification of the correction method when the surrounding fat is heated. The referenced temperature change calculations were preferred to using fiber optic probes to verify the true temperature change for several reasons. First, because rapid spatial changes in the magnetic field disturbance (> 0.01 ppm/mm) make

correlating the fiber optic probe tip position with the corresponding imaging voxel difficult. Furthermore, the EG gel provided a temperature change map, whereas temperature probes would only give the temperature at certain locations. Finally, using fiber optic probes would cause temperature artifacts due to interaction of the ultrasound pressure waves with the probe tip.

2.3.3. Calibration of $d\chi/dT$ for ethylene glycol gel

Although $d\chi/dT$ is known for aqueous tissue (16), for the application of the correction method using EG gel, $d\chi/dT$ had to be determined. This was done by sonicating EG gel and fitting the simulated field disturbance to the measured one. A cylinder with an inner diameter of 4 cm was completely filled with EG gel (Fig. 2a). The EG gel was sonicated with a single point focus ($2 \times 2 \times 5$ mm^3 at -3 dB) for 60 s using an acoustic power of 60 W. During sonication, 2D multi-echo SPGR scans were acquired dynamically. The experimental protocol and other imaging parameters were the same as those used for the EG gel/fat interface HIFU experiment, with the exception of only using one flip angle (15°). The referenced temperature change, and corresponding thermal model was obtained similarly as was done for the model based correction. Specifically, the z = 0 intersection of the 3D Gaussian thermal model was fit to the measured referenced temperature change. The 3D temperature distribution was then sampled on a $1 \times 1 \times 1$ mm^3 grid. The change in magnetic susceptibility ($\Delta\chi$) was assumed to depend linearly on the referenced temperature change (ΔT_{ref}). The optimum of $\Delta\chi / \Delta T_{ref}$, denoted p was found such that the calculated nuclear magnetic field change $\Delta B_{nuc}\left(p \times \Delta T_{ref}\right)$ after averaging over the 5-mm imaging slice thickness fitted the measured field disturbance in the least square sense (Levenberg-Marquardt). For the calculation, the dynamic with a maximum temperature change of approximately 37 °C was used.

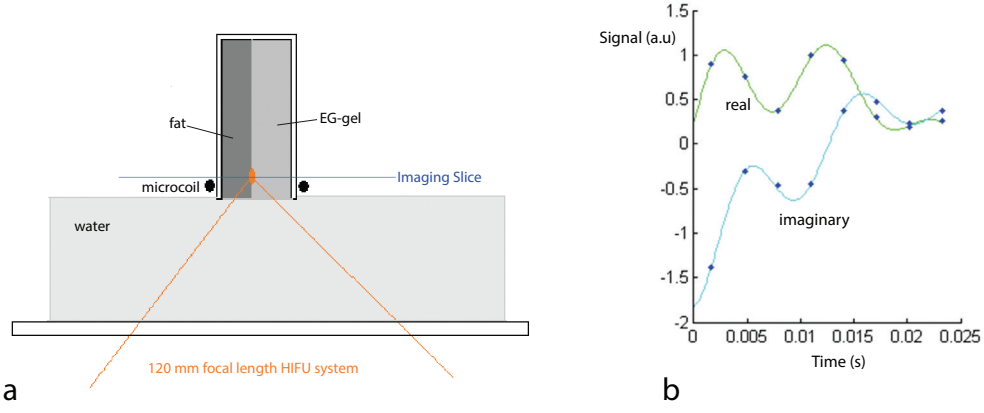

FIG. 2. (**a**) Experimental setup of the HIFU sonication with the cylinder filled either completely with EG gel or partly filled with fat and EG gel (as shown). (**b**) Example of the simultaneous fitting of the real and imaginary signal from EG.

2.3.4. HIFU sonication of an ethylene glycol gel/fat Interface

To demonstrate the efficacy of the correction method a cylinder with an inner diameter of 4 cm was partly filled with porcine fatty tissue and partly with EG gel (Fig. 2a). The boundary of the EG gel with fat was sonicated with a 4-mm diameter volumetric cell and 20 W acoustic power for 60 s. During sonication, 2D multi echo SPGR scans were acquired dynamically

with interleaved 15°/ 30° flip angles for combined -OH shift based thermometry in EG gel and T_1-based thermometry in fat (20). The following imaging parameters were used: FOV = 128 × 128 mm, matrix = 128 × 128, slice thickness = 5 mm, NSA = 1, flyback mode (equal polarity of the readout gradients) with 8 echoes, TR = 45 ms, TE_0 = 1.65 ms (first echo time), ΔTE = 3.09 ms (echo spacing), 40 dynamics and 5.8 s per dynamic. The imaging slice was positioned perpendicular to the HIFU beam and intersected the focal point. An RF receive coil with a diameter of 4.7 cm was positioned close to the sonication focus and the imaging slice. This allowed for a high SNR and thus high spatial resolution.

To correct for B_1-inhomogeneities in the T_1 calculation, a B_1 map was obtained before the sonication with the dual TR method (21) (2D SPGR, TR_1/TR_2 = 20/120 ms, TE = 1.76 ms, flip angle = 70°). Additionally, a map identifying tissue types is required for the creation of the 3D magnetic susceptibility temperature coefficient map. This was accomplished by T_1 mapping and subsequent processing. A 3D high resolution T_1 map was acquired before the sonication using the vendor specific mixed sequence (22) with the volume center positioned at the same location as for the 2D thermometry slice. The parameters used were: TR-IR = 2290 ms, TR-SE = 760 ms, TE = 2 × 35 ms, IR-delay = 370 ms, N = 64 × 64 × 15, FOV = 64 × 64 × 15 mm^3. No water or fat suppression was used for either the B_1 or T_1 map.

2.3.5. Model-based correction

EG gel and fat masks

The first step in the correction method (Fig. 1, box 1) was to define EG gel and fat masks containing voxels with minimal partial volume. These masks, identifying tissue types, were required for the correct interpretation of the thermometry measurements and for the subsequent creation of the 3D thermal model. For water and fat this may be achieved with a DIXON method, however, the EG gel used in the experiment as a substitute for aqueous tissue also has an additional -CH_2 peak which complicates this approach. Therefore, another method was used to define the masks based on the goodness of fit (in the least squares sense) of a predefined signal form for the EG gel and fat regions. For the EG gel, a two peak spectral model is expected to give a good-fit (defined as $R^2 > 0.9$). See the following section for the fitting parameters used for the fit. For the fat region, a signal form of $s(TE) = f(TE)\Delta A \exp\left(i\left(2\pi TE\Delta f + \Delta\phi\right) - TE\,\Delta R2^*\right)$ was used, where $f(TE)$ is a signal measurement of a voxel in the center of the fat tissue (with no partial volume) and ΔA , Δf, $\Delta\phi$, $\Delta R2^*$ are free variables. This procedure resulted in EG gel and fat masks that included voxels with minimal signal contamination from other sources (i.e., with minimal partial volume). The images were processed using MATLAB (MathWorks, Natick, MA).

MR thermometry input

For determining the temperature change in the EG gel, the 8 echoes of the SPGR signal were fitted in the time domain (23) with a two peak model (Fig. 2b). The signal was first normalized, and the least square difference between the model signal and data was minimized using the Levenberg-Marquardt algorithm, fitting simultaneously the real and imaginary signal. Nine variables were used: the amplitude (A), transversal relaxation time ( ), frequency (f), and initial phase (ϕ_0) for both the CH_2 and -OH peaks. Additionally, the variable g represented the degree of Lorentzian (g = 0) or Gaussian (g = 1) line form. The starting values used for the fitting algorithm were $\left[A_{CH2}\ R2^*_{CH2}\ f_{CH2}\ \phi_{0CH2}\ A_{OH}\ R2^*_{OH}\ f_{OH}\ \phi_{OH}\ g\right]$ = [1, 40 1/s, 15 Hz, 0, 1, 40 1/s, 100 Hz, 0, 1]. The OH shift represents the uncorrected PRFS thermometry measurement (

$\Delta T_{w,meas}$ in Fig. 1) and was used as input to the 3D thermal model. The true temperature change was calculated as the shift in the -OH peak position relative to the -CH_2 peak position. The temperature coefficient of 0.01 ppm/°C was used to convert peak shift to temperature change.

For the fat region, a (B_1 corrected) T_1 map was calculated for every 15°/30° flip angle pair with the DESPOT 1 method (24) using the first echo. The change in T_1 maps were then converted to temperature change using the T_1 - temperature coefficient (dT_1 / dT) of 5.8 ms/°C obtained from literature (20).

Thermal model and dχ/dT map

The thermal model of the HIFU focus used for this experiment had a 3D Gaussian (15) temperature distribution (Fig. 3) defined by the parameters (x_c, y_c, σ_r, T_0), where x_c, y_c are the x and y center coordinates of the 3D Gaussian which was fixed to the center of the 2D thermometry slice (defined as z = 0) and had radial width σ_r (= σ_x = σ_y) and temperature amplitude T_0. The axial width σ_z was defined as 2.5 × σ_r such that the ratio of the axial to radial width of the thermal model is similar to the ratio of the applied 3D Gaussian power profile.

The 3D magnetic susceptibility temperature coefficient map was obtained from the 3D high resolution T_1 map. This was achieved by thresholding the T_1 values half way between the mean T_1 of the EG gel (1021 ± 40 ms) and fat (228 ± 7 ms) components and associating 0.0085 ppm/°C (16,17) for the porcine fat region and the found magnetic susceptibility temperature coefficient from the calibration experiment for the EG gel region.

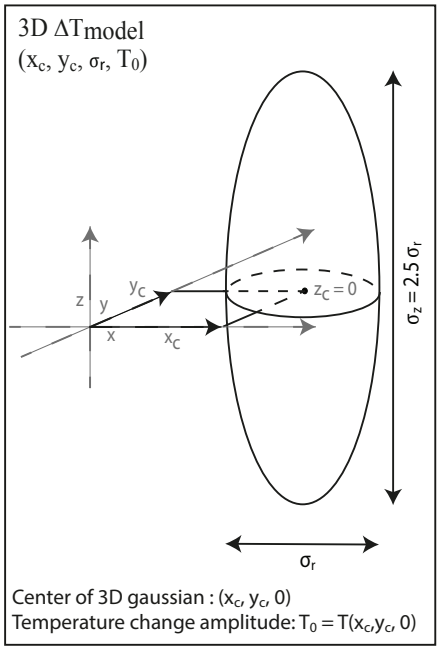

FIG. 3. Parameters of the 3D Gaussian thermal model. z = 0 is defined by the center of the 2D thermometry slice.

PRFS correction

The correction method was applied with either the uncorrected PRFS maps in EG gel (i.e., -OH shift), the T_1-based temperature change measurements in fat, or the combination of uncorrected PRFS in the EG gel and T_1 temperature change measurements in fat as input to the 3D thermal model. The optimal parameters (x_c, y_c, σ_r, T_0) of the 3D Gaussian model (Fig. 3) were determined such that the thermal model temperature change at z = 0 corresponded to the measured temperature change in the imaging slice in the least square sense (Levenberg-Marquardt). Prior calculations using analytical integration of the 3D Gaussian temperature profile over the slice thickness (results not shown) showed that the 5-mm imaging slice thickness was sufficiently small to represent the temperature change at the center of the focus (i.e., z = 0 in Fig. 3). For the focus dimensions measured, this resulted in an underestimation of the maximum temperature change by less than 5%. The 3D thermal model was then sampled on the same imaging grid as the $d\chi / dT$ map and multiplied voxel-wise with the $d\chi / dT$ map to create the 3D magnetic susceptibility change map. The field disturbance was calculated from the susceptibility change (18) and averaged over the 5-mm thermometry slice. This average field disturbance was used to correct for the PRFS measurements of EG gel. When the correction was based on the PRFS measurements, or the combined PRFS

and T_1 measurements, the steps of the correction procedure were iterated until the corrected temperature change remained stable (defined here as temperature changes under 0.1 °C).

When only using PRFS measurements as input to the 3D thermal model, the correction procedure was applied for both flip angles. Because this resulted in a two times higher temporal resolution than when using T_1 or PRFS + T_1 as input, the PRFS measurements of the same 15°/30° flip angle pairs were averaged to obtain a better temporal comparison between the three variations of the correction method.

To quantify the temperature error, the 5th to 95th percentile interval of the temperature error distribution was calculated for the maximum temperature change before and after applying the correction.

2.4. Results

2.4.1. HIFU sonications of breast fatty tissue

Phase maps made during HIFU heating of fatty breast tissue with different acoustic powers showed magnetic field disturbances with both positive and negative polarity. Figure 4a-c shows examples of the maximum magnetic field change in the coronal central slice. Large nuclear magnetic field changes were observed, ranging from -0.6 ppm for the 40 W 2-mm sonication to -1.4 ppm for the 100 W 4-mm sonication. Figure 4d shows the nuclear magnetic field change of three voxels in the central heated region as function of time during a 100 W sonication. It was observed that the magnetic field change completely disappeared after cool-down.

2.4.2. Calibration of $d\chi/dT$ for ethylene glycol gel

For the EG gel, a magnetic susceptibility temperature coefficient of 0.0061 ppm/°C was found (Fig. 5). Figure 5c shows the residual magnetic field disturbance after subtracting the simulated magnetic field disturbance (Fig. 5b, with $d\chi/dT$ = 0.0061 ppm/°C) from the measured magnetic field disturbance (Fig. 5a).

2.4.3. HIFU sonication of an ethylene glycol gel/fat interface

Figure 6a shows the temperature change measured in the EG gel and fat regions at the end of the sonication. The maximum temperature change measured of 37 °C occurred in fat. Figure 6b shows an example of the 3D temperature distribution obtained when using PRFS and T_1 as thermometry input, which corresponds with the MR measurements of Figure 6a. For all 2D thermometry inputs used, the maximum temperature change of the thermal model was lower than the measured maximum temperature change. The maximum temperature change of the thermal model was 18 °C, 30 °C, and 27 °C when using PRFS, T_1, and PRFS + T_1 as thermometry input, respectively. Figure 7 shows the temperature error map in EG gel before (Fig. 7a) and after using the model based correction with PRFS (Fig. 7b), T_1 (Fig. 7c), and PRFS + T_1 (Fig. 7d) as thermometry input. A reduction in the PRFS thermometry error with respect to the referenced temperature was observed with the exception of some voxels close to the EG gel/fat boundary. The 5th to 95th percentile interval (Fig. 8) of the temperature error distribution decreased from 3.8 °C before correction (T_{meas} [5/ 95]) to 2.3 °C, 2.2 °C, and 2.0 °C after correction (T_{cor} [5/ 95]) when using PRFS (Fig. 8a), T_1 (Fig. 8b), and PRFS + T_1 (Fig. 8c) as thermometry input, respectively. Six iterations were found sufficient for the correction procedure to stabilize.

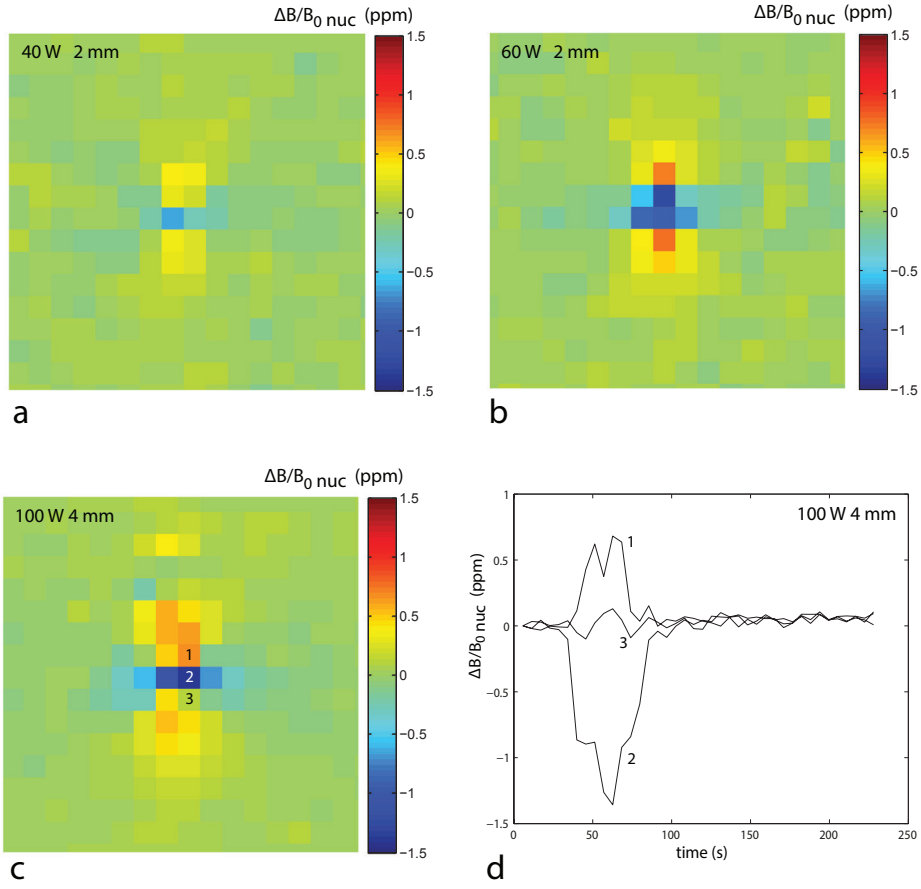

FIG. 4. (**a-c**) Field disturbances caused by HIFU heating of human breast tissue. The maximum nuclear magnetic field change of the central slice perpendicular to the long axis of the ablation cell for various sonication powers and volumes. (**d**) The nuclear magnetic field change of three voxels (indicated in c) versus time for the 100 W, 4 mm sonication.

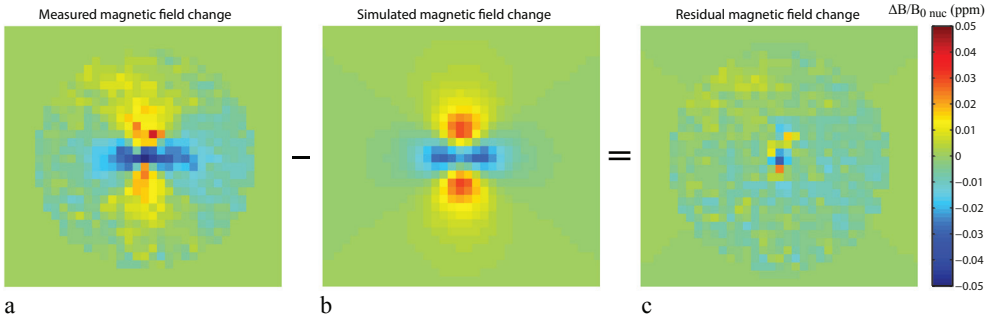

FIG. 5. Results from the estimation procedure of the magnetic susceptibility temperature coefficient of EG gel. The measured magnetic field change (**a**) and simulated magnetic field change (**b**) using the optimal $\Delta\chi/\Delta T_{ref}$ value to minimize the residual (**c**).

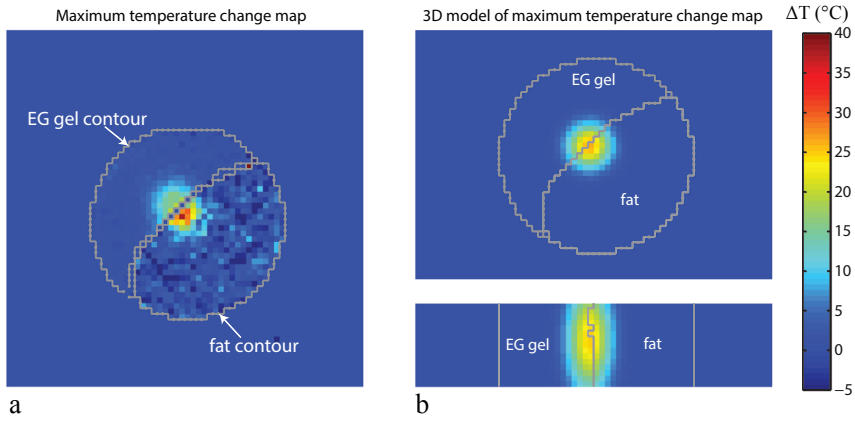

FIG. 6. (**a**) The maximum temperature change in the EG gel and fat region. (**b**) The 3D Gaussian fit of the maximum temperature change of both EG gel and fat. The volumetric EG gel and fat separation is also shown.

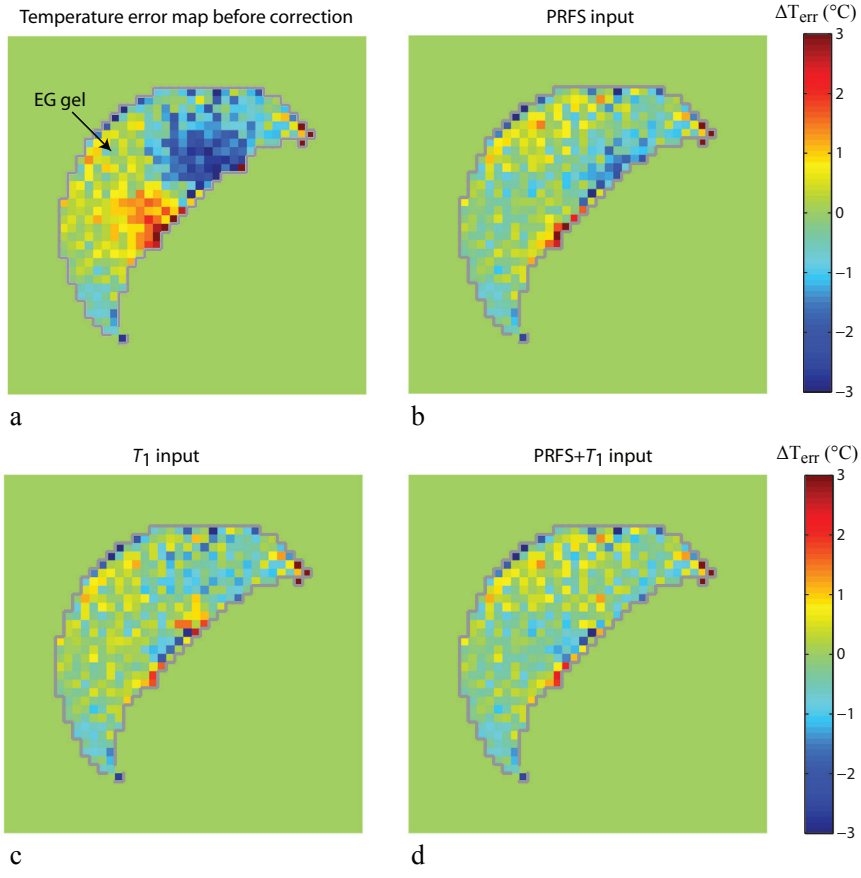

FIG. 7. Temperature error map in EG gel before (**a**) and after (**b-d**) using the model based correction method with (**b**) PRFS, (**c**) T_1, and (**d**) PRFS+T_1 as thermometry input to the thermal model.

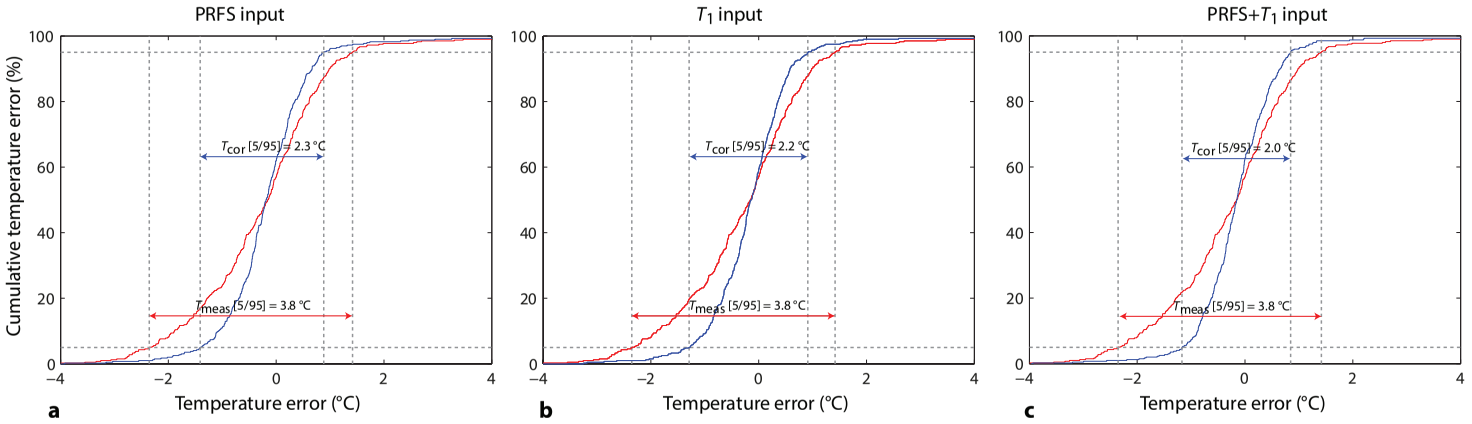

FIG. 8. Cumulative distribution functions of the temperature error before (red line) and after (blue line) application of the model based correction method with (**a**) PRFS, (**b**) T_1, and (**c**) PRFS+T_1 used as thermometry input to the thermal model.

2.5. Discussion

PRFS thermometry is commonly used in MR-HIFU treatments for monitoring temperature. This thermometry method requires a constant magnetic field strength during the measurement. For globally varying or periodic magnetic field changes, the referenceless (25) or multi-baseline (26) correction methods may be applied. Variation of the susceptibility distribution, as demonstrated here by heat-induced magnetic susceptibility changes of tissue (especially of fat), give rise to local field disturbances, extending further than the actual location of the susceptibility change. The magnetic field changes caused by the heating of fat can lead to PRFS temperature errors in water-containing tissues, even with adequate fat signal suppression. We used dynamic field mapping in fatty tissue to visualize the susceptibility-induced nuclear magnetic field changes, as was shown in breast tissue. Here, it was shown for the first time experimentally that HIFU heating of adipose tissue gives rise to magnetic field changes in the surrounding tissue.

Although large magnetic field changes (i.e., up to 1.4 ppm) were measured in the breast adipose tissues, the magnetic field drops off rapidly beyond the heated regions. For example, for a sphere-shaped uniformly heated region, the external magnetic field decreases with $a/(a+r)^3$, where a is the radius of the sphere and r the distance from the edge (27). This is consistent with the presented EG gel/fat HIFU experiment, which showed the largest temperature errors at the boundary of the fat tissue. When using MR-HIFU for the ablation of water-containing tumors in fatty tissue, e.g., with the ablation of breast cancer, these errors may lead to considerable temperature uncertainty at the tumor boundaries.

Three variations of the model-based correction method were proposed, all requiring knowledge of the susceptibility change of the whole heated volume. Despite the simplicity of the thermal model used here (apparent from the discrepancy between the maximum temperature change of the thermal model and the maximum T_1-based temperature change measurement in fat), the correction method resulted in a substantial reduction in the temperature error. The thermal model may further be improved by including physical and thermal properties of the tissues (28). The correction method performed the best when both PRFS thermometry in EG gel and T_1-based thermometry in fat were used as input, possibly because of the better estimate of the actual 3D temperature distribution.

To evaluate the efficacy of the correction method, multiple gradient echoes were required to separate the -OH and -CH_2 peaks of the EG gel. However, for the application of the model-based correction method in aqueous/ fat tissue only one echo is required. Furthermore, when only PRFS thermometry is used as an input to the thermal model, fat suppression may be used. However, the correction method would still require a pre-scan to obtain a 3D tissue distribution map. The acquisition time of the T_1-based measurements may also be decreased by measuring the temperature change in fat based on the relative signal change of a T_1-weighted gradient echo sequence (29). This technique has been used to monitor the temperature change during focused ultrasound heating of muscle tissue (29) but would have to be validated for adipose tissue.

For the correction method, five or six iterations suffice to reduce the susceptibility-induced temperature error. The fast convergence of the proposed iterative scheme can be explained by the relatively small effect of temperature-induced susceptibility changes on the proton resonance ($<< 2/3 \times 0.0085$ ppm/°C), compared with the direct effect of temperature on PRFS (0.01 ppm/°C). The only crucial requirement is a reasonably accurate estimate of the initial Gaussian temperature distribution.

For the EG gel/fat HIFU experiment, the assignment of susceptibility temperature dependent coefficients was based on a 3D spatial binary separation of EG gel and fat regions.

Including voxels containing mixed tissue types, and applying Wiedemann's additivity law of susceptibility (30), may further improve the correction results. Additionally, although we show the correction method in the presence of fat because of the larger $d\chi / dT$ of fat compared with aqueous tissues (16), the principle of the proposed correction method is also applicable for aqueous tissues alone.

Other correction methods for general magnetic field disturbances are referenceless (25) and fat referenced (31) techniques. The referenceless method interpolates the measured magnetic field change around the heated region to estimate the magnetic field change in the heated regions. However, because the heat-induced magnetic field disturbances occur locally in the heated region itself, and are rapidly changing over a small region (i.e. have high spatial frequencies), such a correction approach would be challenging. The other method, fat referencing, uses the resonance frequency of fat as a magnetic field probe, which is measured in a separate water suppressed acquisition (31,32) or with spectroscopic imaging (33,34). The magnetic field shift of fat is used to correct for the shift in the water resonance frequency in the same voxel, which is assumed to experience the same magnetic field. This technique is limited to voxels containing both fat and water, and can, therefore, not be used to correct for field effects in pure water voxels close to heated fat tissue.

We have shown the applicability of the model-based correction method experimentally. This was shown with relatively simple setups, and a few issues remain. First, steep spatial temperature gradients (observed in the center of the HIFU focus) were shown with simulations to result in an underestimation of the simulated magnetic field disturbance (results not shown). Second, the correction method assumes that iterated corrections lead to a convergence of the temperature change, and to a value with less error than the initial measurement. This was shown to be valid for the HIFU experiment presented but general applicability to different water fat distributions would need to be validated. Lastly, the correction method assumes small intra- and intersubject variation of $d\chi / dT$ values. This would have to be confirmed for the specific tissue types being sonicated.

To conclude, a magnetic field disturbance was observed during HIFU sonications of breast fatty tissue, and the proposed correction method was shown to greatly reduce such temperature errors in phantom experiments. However, residual errors remained which may be explained by the simplified thermal model used, the binary spatial allocation of susceptibility temperature coefficients, and the steep spatial temperature gradients. The emergence of fast algorithms to calculate magnetic field disturbances resulting from tissue magnetic susceptibility changes opens the opportunity for real time correction of this error source during HIFU sonications.

2.6. Acknowledgements

This research was performed within the framework of CTMM, the Center for Translational Molecular Medicine, project VOLTA.

2.7. References

1. Jemal A, Bray F, Center MM, Ferlay J, Ward E, Forman D. Global cancer statistics. CA Cancer J Clin 2011;61:69–90.
2. Buchholz TA, Lehman CD, Harris JR, et al. Statement of the science concerning locoregional treatments after preoperative chemotherapy for breast cancer: a National Cancer Institute conference. J Clin Oncol 2008;26:791–797.
3. Chapman A, ter Haar G. Thermal ablation of uterine fibroids using MR-guided focused ultrasound-a truly non-invasive treatment modality. Eur Radiol 2007;17:2505–2511.
4. Zini C, Hipp E, Thomas S, Napoli A, Catalano C, Oto A. Ultrasoundand MR-guided focused ultrasound surgery for prostate cancer. World J Radiol 2012;4:247–252.
5. Huisman M, van den Bosch MA. MR-guided high-intensity focused ultrasound for noninvasive cancer treatment. Cancer Imaging 2011; 11:S161–S166.
6. Merckel LG, Bartels LW, Kohler MO, van den Bongard HJ, Deckers R, Mali WP, Binkert CA, Moonen CT, Gilhuijs KG, van den Bosch MA. MR-guided high-intensity focused ultrasound ablation of breast cancer with a dedicated breast platform. Cardiovasc Intervent Radiol 2013;36:292–301.
7. Peters RD, Hinks RS, Henkelman RM. Ex vivo tissue-type independence in proton-resonance frequency shift MR thermometry. Magn Reson Med 1998;40:454–459.
8. Peters NHGM, Bartels LW, Sprinkhuizen SM, Vincken KL, Bakker CJG. Do respiration and cardiac motion induce magnetic field fluctuations in the breast and are there implications for MR thermometry? J Magn Reson Imaging 2009;29:731–735.
9. Zhou XD, He QA, Zhang A, Beckmann M, Ni C. Temperature measurement error reduction for MRI-guided HIFU treatment. Int J Hyperthermia 2010;26:347–358.
10. Viallon M, Terraz S, Roland J, Dumont E, Becker CD, Salomir R. Observation and correction of transient cavitation-induced PRFS thermometry artifacts during radiofrequency ablation, using simultaneous ultrasound/MR imaging. Med Phys 2010;37:1491–1506.
11. Streicher MN, Schafer A, Reimer E, Dhital B, Trampel R, Ivanov D, Turner R. Effects of air susceptibility on proton resonance frequency MR thermometry. MAGMA 2012;25:41–47.
12. Sprinkhuizen SM, Bakker CJG, Ippel JH, Boelens R, Viergever MA, Bartels LW. Temperature dependence of the magnetic volume susceptibility of human breast fat tissue: an NMR study. MAGMA 2012;25: 33–39.
13. Sprinkhuizen SM, Konings MK, van der Bom MJ, Viergever MA, Bakker CJG, Bartels LW. Temperature-induced tissue susceptibility changes lead to significant temperature errors in PRFS-based MR thermometry during thermal interventions. Magn Reson Med 2010; 64:1360–1372.
14. Bottomley PA, Foster TH, Argersinger RE, Pfeifer LM. A review of normal tissue hydrogen NMR relaxation-times and relaxation mechanisms from 1–100 Mhz - dependence on tissue-type, NMR frequency, temperature, species, excision, and age. Med Phys 1984;11:425–448.
15. Ye G, Smith PP, Noble JA. Model-based ultrasound temperature visualization during and following HIFU exposure. Ultrasound Med Biol 2010;36:234–249.
16. De poorter J. Noninvasive MRI thermometry with the proton resonance frequency method - study of susceptibility effects. Magn Reson Med 1995;34:359–367.
17. Stollberger R, Ascher PW, Huber D, Renhart W, Radner H, Ebner F. Temperature

monitoring of interstitial thermal tissue coagulation using MR phase images. J Magn Reson Imaging 1998;8:188–196.
18. Bouwman JG, Bakker CJ. Alias subtraction more efficient than conventional zero-padding in the Fourier-based calculation of the susceptibility induced perturbation of the magnetic field in MR. Magn Reson Med 2012;68:621–630.
19. Kohler MO, Mougenot C, Quesson B, Enholm J, Le Bail B, Laurent C, Moonen CT, Ehnholm GJ. Volumetric HIFU ablation under 3D guidance of rapid MRI thermometry. Med Phys 2009;36:3521–3535.
20. Hey S, de Smet M, Stehning C, Grull H, Keupp J, Moonen CTW, Ries M. Simultaneous T1 measurements and proton resonance frequency shift based thermometry using variable flip angles. Magn Reson Med 2012;67:457–463.
21. Yarnykh VL. Actual flip-angle imaging in the pulsed steady state: a method for rapid three-dimensional mapping of the transmitted radiofrequency field. Magn Reson Med 2007;57:192–200.
22. In den Kleef JJ, Cuppen JJ. RLSQ: T1, T2, and rho calculations, combining ratios and least squares. Magn Reson Med 1987;5:513–524.
23. Vanhamme L, van den Boogaart A, Van Huffel S. Improved method for accurate and efficient quantification of MRS data with use of prior knowledge. J Magn Reson 1997;129:35–43.
24. Deoni SC, Rutt BK, Peters TM. Rapid combined T1 and T2 mapping using gradient recalled acquisition in the steady state. Magn Reson Med 2003;49:515–526.
25. Rieke V, Vigen KK, Sommer G, Daniel BL, Pauly JM, Butts K. Referenceless PRF shift thermometry. Magn Reson Med 2004;51:1223– 1231.
26. Vigen KK, Daniel BL, Pauly JM, Butts K. Triggered, navigated, multibaseline method for proton resonance frequency temperature mapping with respiratory motion. Magn Reson Med 2003;50:1003–1010.
27. Schenck JF. The role of magnetic susceptibility in magnetic resonance imaging: MRI magnetic compatibility of the first and second kinds. Med Phys 1996;23:815–850.
28. Durkee JW Jr, Antich PP, Lee CE. Exact solutions to the multiregion time-dependent bioheat equation. I: solution development. Phys Med Biol 1990;35:847–867.
29. Cline HE, Hynynen K, Hardy CJ, Watkins RD, Schenck JF, Jolesz FA. MR temperature mapping of focused ultrasound surgery. Magn Reson Med 1994;31:628–636.
30. Mulay L. Magnetic susceptibility. New York: John Wiley and Sons; 1963.
31. Kuroda K, Oshio K, Chung AH, Hynynen K, Jolesz FA. Temperature mapping using the water proton chemical shift: a chemical shift selective phase mapping method. Magn Reson Med 1997;38: 845–851.
32. Shmatukha AV, Harvey PR, Bakker CJ. Correction of proton resonance frequency shift temperature maps for magnetic field disturbances using fat signal. J Magn Reson Imaging 2007;25:579–587.
33. Kuroda K, Mulkern RV, Oshio K, Panych LP, Nakai T, Moriya T, Okuda S, Hynynen K, Joles FA. Temperature mapping using the water proton chemical shift: self-referenced method with echo-planar spectroscopic imaging. Magn Reson Med 2000;43:220–225.
34. Soher BJ, Wyatt C, Reeder SB, MacFall JR. Noninvasive temperature mapping with MRI using chemical shift water-fat separation. Magn Reson Med 2010;63:1238–1246.

CHAPTER 3

On the influence of water and fat heterogeneity on fat referenced MR thermometry

Baron P, Deckers R, Bouwman JG, Bakker CJG, de Greef M, Viergever MA, Moonen CTW, Bartels LW. On the influence of water and fat heterogeneity on fat referenced MR thermometry. Magn Reson Med. (Submitted)

ABSTRACT

Purpose: To investigate the effect of the aqueous and fatty tissue magnetic susceptibility distribution on absolute and relative temperature measurements as obtained directly from the water/fat frequency difference.

Methods: Absolute thermometry was investigated using spherical phantoms filled with pork and margarine, which were scanned in three orthogonal orientations. To evaluate relative fat referencing, multi-gradient echo scans were acquired before and after heating pork tissue by high intensity focused ultrasound (HIFU). Simulations were performed to estimate the errors that can be expected in human breast tissue.

Results: The sphere experiment showed susceptibility-related errors of 8.4 °C and 0.2 °C for pork and margarine, respectively. For relative fat referencing measurements, fat showed pronounced phase changes of opposite polarity to aqueous tissue. The apparent mean temperature for a numerical breast model assumed to be 37 °C was 47.2 ± 21.6 °C. Simulations of relative fat referencing for a HIFU sonication ($\Delta T = 29.7$ °C) gave a maximum temperature error of 6.6 °C compared to 2.5 °C without fat referencing.

Conclusion: Variations in the observed frequency difference between water and fat are largely due to variations in the water/fat spatial distribution. This effect may lead to considerable errors in absolute MR thermometry. Additionally, fat referencing may exacerbate rather than correct for PRFS-temperature measurement errors.

3.1. Introduction

Magnetic Resonance-guided High Intensity Focused Ultrasound (MR-HIFU) is a technique which combines the noninvasive heating of tissue through delivery of ultrasonic energy into the body with MRI for treatment planning, monitoring, and evaluation of thermal therapy. The ultrasonic energy may be used to non-invasively locally elevate the tissue temperature for applications such as tumor ablation (1) or the realization of mild hyperthermia, which has potential for radiosensitization (2), chemosensitization (3) and for local drug delivery from thermosensitive carriers (4). MR thermometry is used for treatment monitoring during the treatment procedure (5). For tumor ablation, the aim is to ensure that tissue necrosis has occurred at the target zone (typically by elevating the temperature above 56 °C for a few seconds) while preventing damage to healthy tissue. In mild hyperthermia therapy, the tumor tissue is heated up to 40-45 °C for up to 1 hour. For drug delivery, drug release from thermal sensitive carriers typically occurs within a narrow temperature range (41-42 °C (4)).

For all these applications, the commonly employed MR thermometry techniques measure changes in temperature using the temperature dependence of the proton resonance frequency in water (6,7). This temperature dependence stems from the fact that the strength of the hydrogen bonds between water molecules varies with temperature, leading to a temperature dependent screening of the hydrogen nucleus in water molecules by the electron cloud (8).

Due to its relative character, the measurement of temperature based upon the proton resonance frequency shift (PRFS), is prone to several types of errors. First, magnetic field fluctuations not caused by temperature changes, e.g due to field drift (9) or respiration (10), have been shown to corrupt temperature measurements considerably. Second, the relative measurement method requires knowledge of the baseline temperature, which is normally assumed to be 37 °C in human tissue. However, especially during therapeutic sessions requiring multiple sonications, the target tissue temperature may not have cooled down completely to the baseline temperature in between the sonications. When inadequate cooling times are used with relative thermometry techniques, the resulting underestimation of the true temperature remains undetected. Furthermore, thermal dose (11), an important indicator of tissue damage during thermal ablation therapy, requires knowledge of the absolute temperature-time history. Additionally, for mild hyperthermia applications, temperatures should vary within a narrow absolute temperature range to ensure effective hyperthermia (e.g. for drug release) and at the same time avoid tissue damage.

The use of fat signal as a non-temperature dependent resonance has been advocated for solving the problems described above. It has been proposed to use the presence of fat to acquire absolute temperature information directly from the resonance frequency difference between water and fat (12,13), or to use fat as a field probe not sensitive to temperature changes, which can be used to correct PRFS-based measurements for errors due to field variations (14). The first approach will be referred to in this paper as “absolute fat referenced thermometry”, and the second approach as “relative fat referenced thermometry”. Here, the term fat referencing is used for the case in which the water and fat MR signals are assumed to originate from the same voxel. Other authors have referred to this method as self-referencing (14) or using fat as an internal reference (15).

3.1.1. Absolute fat referenced thermometry

In some applications and situations, knowledge of temperature changes only, i.e. relative temperatures, is not sufficient. The baseline temperature in the body may vary depending on the location, individual physiology and pathology (16), as a response to active skin cooling as may be employed to prevent skin burns during thermal therapy (17), or when cumulative

heating is caused by subsequent periods of heating without proper cooling periods in between. Referenced MR thermometry has been proposed as a method for obtaining absolute temperature measurements. The concept is to derive the temperature directly from the resonance frequency difference between the temperature sensitive OH- peak and a reference peak with no temperature sensitivity. In vitro, the use of Ethylene glycol, with CH_2- as the reference component is a well-established method for calibrating the temperature in NMR spectrometers (18). In the brain, the feasibility of measuring the absolute temperature with metabolites such as NAA as reference has been investigated (19). Lastly, deriving the temperature directly from the water-fat resonance frequency difference has previously been proposed (13,14) as a method for obtaining absolute temperature measurements in tissues containing both water and fat. In practice, however, MR thermometry based upon water and fat resonances is not a straightforward task. In the breast, for instance, McDannold et al. have measured a large range in water-fat shift derived temperatures (standard deviation = 14 °C) at constant body temperature (20,21). Possible explanations for this have been proposed, such as spatial variations in pH (20) and water-fat readout chemical shift spatial mismatch (22). Additionally, water and fat reside in different compartments, have different susceptibilities, and thus (even in the same voxel) the hydrogen nuclei in water and fat molecules may experience different nuclear magnetic fields (23).

By simulating the nuclear magnetic field disturbance it is shown in this paper how the water/fat (w/f) distribution and the degree of heterogeneity on the scale of the acquisition voxel influence the measured absolute temperature. Furthermore, we will show that the reported measured temperature variations obtained with fat referenced absolute thermometry in the breast mentioned above (20,21), can largely be explained by the distribution and difference in magnetic susceptibility (about 1 ppm) of water (24) and fat (25).

3.1.2. Relative fat referenced thermometry

An analogous situation occurs for methods with fat acting as a magnetic field probe intended to measure temperature changes using the PRFS method in the presence of time-varying field inhomogeneities. A potential complication is the different change in molecular magnetic field occurring in the water and fat components due to the difference in the magnetic susceptibility temperature dependence of these tissues (13). Because of this, the nuclear field experienced by hydrogen nuclei in water and fat may be different. Notably, Hofstetter et al. (26) measured a larger difference between the fat referenced temperature change and temperature probe readings in pork tissue than in mayonnaise. These findings suggest that the spatial distribution of water and fat and the degree of homogeneity in that distribution play a role here.

In this study we evaluated the performance of relative fat-referencing using simulations and a HIFU heating experiment with the HIFU focal zone centered on the water-fat interface. We show that for a heterogeneous spatial w/f distribution and a typical HIFU heating profile, fat referencing may exacerbate the heat-induced phase errors if the fat is part of the heated region, i.e. with fat acting as the internal reference.

3.2. Methods

3.2.1. The nuclear fields in water and fat

The proton precession frequency ω [rad s^{-1}] is a function of the gyromagnetic ratio γ [rad s^{-1} T^{-1}] and nuclear magnetic field [T]: $\omega = \gamma \cdot B_{nuc}$. This nuclear magnetic field at a certain location r' ($B_{nuc}(r')$) depends on the local electron chemical shift ($\sigma(r')$) and on the magnetic susceptibility distribution (χ) in two ways: directly and locally via the lorentz sphere correction

(-2/3 χ(r')) and indirectly via the macroscopic magnetic field (B_{mac}), which is determined by the susceptibility distribution χ(r) (6):

$$B_{nuc}(r') = \left(1 - \sigma(r') - \frac{2}{3}\chi(r')\right) B_{mac}(\chi(r)) \quad [1]$$

Therefore, the w/f frequency difference is intrinsically dependent on the difference in electron shielding constants and (because water and fat cannot be at the exact same spatial location) on the magnetic susceptibility distribution.

3.2.2. Absolute fat referenced thermometry

To illustrate the influence of the w/f distribution on the estimated absolute temperature (T_{wf}) derived from the water-fat resonance frequency difference ($\Delta\omega_{wf}$), simulations were first performed for simple geometries such as an acquisition for a voxel on a spherical w/f interface and for a voxel containing a dispersion of fat spheres. Then, a more realistic w/f distribution was used, obtained from a 3D breast scan, which required a numerical calculation of the induced nuclear magnetic field. Lastly, we performed an object rotation experiment to validate the role of tissue magnetic susceptibility as a source of variation in T_{wf} for heterogeneous w/f tissues. For this, we made use of the fact known from magnetostatics that the three induced magnetic field perturbations in an object rotated in three orthogonal orientations with respect to the applied magnetic field average to zero.

Absolute thermometry simulations

Voxel on the edge of a fat sphere in water

First simulations were performed for a macroscopically (i.e. on the scale of a voxel) heterogeneous water-fat distribution. For this purpose, spectroscopic acquisitions were simulated of a voxel on the edge of a fat sphere (radius a) embedded in aqueous tissue (see Figure 1a). The susceptibility-induced nuclear magnetic field disturbance (ΔB_{nuc}) was calculated inside the cubic voxel, with edge length L, for 128^3 uniform sampling points inside the voxel using (27):

$$\frac{\Delta B_{nuc,z}}{B_0} = \begin{cases} \frac{\Delta\chi}{3} a^3 \left(2z^2 - x^2 - y^2\right) / \left(x^2 + y^2 + z^2\right)^{5/2} & outside\,sphere \\ 0 & inside\,sphere \end{cases} \quad [2]$$

where (x,y,z) are the spatial coordinates with respect to the center of the voxel, $\Delta\chi = \chi_f - \chi_w = 1.26$ ppm is the magnetic susceptibility difference between fatty (χ_f = -7.79 ppm (25)) and aqueous (χ_w = -9.05 ppm (24)) tissue, and B_0 = 3 T is the main magnetic field strength. For the aqueous tissue, each sampling point contributed to the total summed demodulated voxel signal with amplitude 1 a.u., frequency $\gamma\Delta B_{nuc\_z}$ rad s^{-1} and relaxation rate R_2^* = 40 s^{-1} for echo times TE = 1, 2, … , 24 ms. Because the susceptibility-induced nuclear magnetic field disturbance inside the fat sphere is zero, only the total water signal was fit to one lorentzian peak to determine the influence of magnetic susceptibility on the observed $\Delta\omega_{wf}$ and corresponding observed temperature (i.e. $\Delta T_{wf} = \Delta\omega_{wf}/(-\alpha\gamma B_0)$, where α = 0.01 ppm/°C (8) is the electron screening constant thermal coefficient of water). The influence of the angle between the surface normal and B_0 (θ in Figure 1a) and interface curvature (dimension n = a/L) on ΔT_{wf} were also investigated.

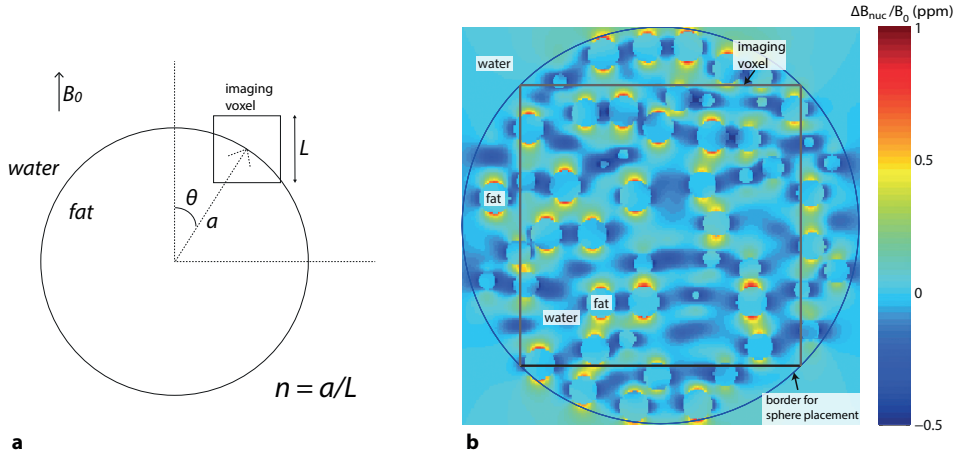

FIG. 1. Simulation of absolute thermometry in an imaging voxel (**a**) on a water/fat interface and (**b**) containing a random distribution of fat spheres embedded in water.

Random fat spheres inside voxel

To model a voxel containing a more homogeneous w/f distribution (on the scale of a voxel), small lipid spheres were randomly dispersed in an aqueous environment. Simulations were performed to investigate the influence of fat fraction (0-21%) on T_{wf}. Fat spheres (r = 10 a.u.) were placed in the largest bounding sphere (R = 128 a.u.) by subsequently adding new fat spheres to the vacant region using a uniformly distributed pseudo-randomization algorithm until the region was completely filled (see Figure 1b). Then the induced nuclear magnetic field disturbance was determined by calculating the summed contribution of each sphere given by eq [2] for 256^3 uniform sampling points. Spectroscopic acquisitions were then simulated for the largest inner cubic voxel (diameter = $256/\sqrt{2}$ a.u.) with signal parameters: $B_0 = 3$ T, $R_2{}^*_w = R_2{}^*_f = 40$ s^{-1}, $A_w = A_f = 1$ a.u., $\omega_w = \gamma \Delta B_{nuc\_z}$ rad s^{-1}, $\omega_f = \gamma(\Delta B_{nuc\_z} - 3.35\times10^{-6}B_0)$ rad s^{-1} by summing the total signal in the voxel for TE = 1, 2, …, 24 ms. The fat fraction was adjusted by varying the gap between the spheres. The influence of magnetic susceptibility on the measured ΔT_{wf} was then obtained by fitting the signal with two lorentzian peaks in the time domain.

Realistic breast anatomy

To study a realistic w/f distribution, simulations were performed of spectroscopic imaging of the female breast. A high resolution (0.63×0.63×0.63 mm^3, matrix = 241×243×224) fat suppressed T_1-w 3D scan of a breast acquired in a volunteer from a previous study (13) was used to create a realistic susceptibility distribution map. Each voxel was automatically labeled (28) as either fibro-glandular tissue, fatty tissue, or air. The difference in magnetic susceptibility between fat and fibro-glandular tissues was set to 1.26 ppm (24,25). The air was assigned the same magnetic susceptibility as the fibro-glandular tissue in order to focus on the w/f distribution and avoid the influence of the gross breast shape on the induced magnetic field. Then the induced nuclear magnetic field disturbance (ΔB_{nuc}) was calculated using a Fourier-based algorithm with B_0 orientated along the z axis (27,29):

$$\Delta B_{nuc} = \left[-\sigma + FT^{-1}\left[\left(\frac{1}{3} - \frac{k_z^2}{k^2} \right) FT(\chi) \right] \right] B_0 \qquad [3]$$

where χ is the magnetic susceptibility spatial distribution, σ the electron shielding constant, and k is the spatial frequency. The theoretical lorentzian MR signal of one spectral peak (either water or fat) was attributed to the fibro-glandular and fat voxels ($T_{baseline}$ = 37 °C, B_0 = 3 T, $\omega_w = \gamma \Delta B_{nuc\_z}$ rad s^{-1}, $\omega_f = \gamma(\Delta B_{nuc\_z} - 3.35\times10^{-6}B_0)$ rad s^{-1}, $R_2{*}_w = R_2{*}_f = 0$ s^{-1}, $A_w = A_f = 1$ a.u.) and spectroscopic imaging (TE= 1,2,…,24 ms, transverse slice) was simulated with down sampled resolution (in-plane = 5×5 mm^2 , slice thickness = 10 mm). In voxels containing both water and fat, $\Delta\omega_{wf}$ was obtained with a two peak lorentzian fitting model, and used to calculate apparent absolute temperature maps.

To verify the validity of the field calculations, we investigated for the numerical breast model whether the influence of the magnetic susceptibility distribution on the resulting magnetic field is completely removed, when the induced 3D magnetic field disturbance maps of an object in three orthogonal orientations (x,y,z) with respect to B_0 are averaged, leaving only the electron shielding constant (i.e.):

$$\Delta B_{av,nuc} = \frac{1}{3}\left[-\sigma + FT^{-1}\left[\left(\frac{1}{3}-\frac{k_x^2}{k^2}\right)FT(\chi)\right] - \sigma + FT^{-1}\left[\left(\frac{1}{3}-\frac{k_y^2}{k^2}\right)FT(\chi)\right] - \sigma + FT^{-1}\left[\left(\frac{1}{3}-\frac{k_z^2}{k^2}\right)FT(\chi)\right]\right]B_0 = -\sigma B_0 \quad [4]$$

where $k^2 = k_x^2 + k_y^2 + k_y^2$.

Absolute thermometry experiments

To experimentally investigate the influence of the w/f distribution on the T_{wf}, spectroscopic scans were acquired of a more homogeneous and a more heterogeneous w/f mixture with the object in three orthogonal orientations with respect to the direction of B_0. A spherical holder (r= 4 cm) was in one experiment filled completely with margarine (40% fat, homogeneous distribution) and in a subsequent experiment completely filled with pork meat (Figure 2a,

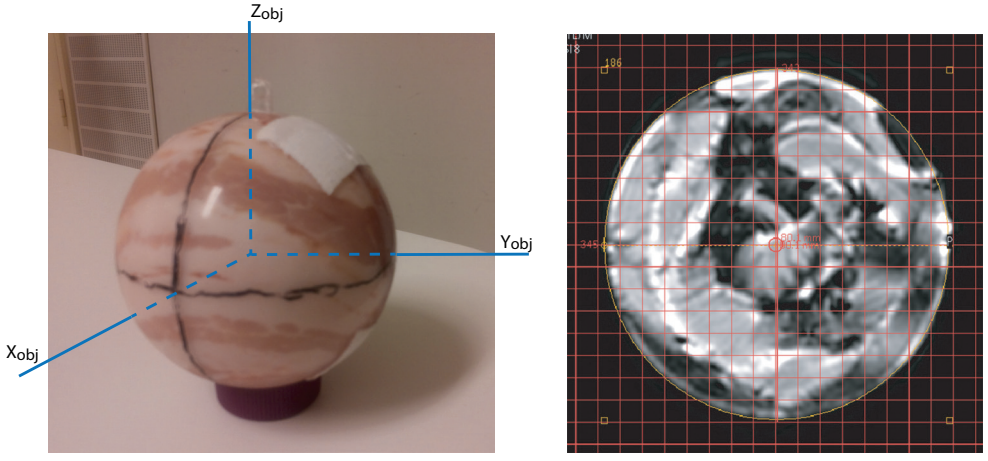

FIG. 2. (**a**) Pork sphere with the object coordinate axes fixed to the sphere and (**b**) grid of the 2D spectroscopic acquisition scans.

heterogeneous distribution of muscle and fat) and placed at the isocenter inside the bore of a 3-T MRI scanner (Achieva, Philips Healthcare, Best, The Netherlands.) A sphere was used to remove the influence of the shape of the object itself on the induced field inside the object. Prior to the experiment the samples were stored at room temperature for at least four hours, and the MR room temperature was measured with a digital thermometer (Hanna instruments, Rhode Island, USA). A 3D reference coordinate frame (x_{obj}, y_{obj}, z_{obj}) was assigned, fixed to the sphere, with the origin located in its center. In three orthogonal orientations $\{z_{obj} \parallel B_0, y_{obj} \parallel B_0, x_{obj} \parallel B_0\}$, a 2D spectroscopic scan was acquired. (PRESS, FOV = 250×250 mm^2, slice thickness = 10 mm, $N_x \times N_y$ = 50×50, TR = 400 ms, TE = 30 ms, BW = 1 kHz, number of samples =256) with the slice intersecting the center of the sphere such that the same region was imaged for each object orientation (Figure 2b). One volumetric shimming procedure was performed containing the whole sphere, prior to the experiment. For each voxel $\Delta\omega_{wf}$ was determined by fitting a two peak model to the spectral time signal using in-house software developed in MATLAB (MathWorks, Natick, MA). The measured absolute temperature (°C) was calculated as (13):

$$T_{wf}\left[°C\right] = 37.0\left[°C\right] + \frac{\left(\Delta\omega_{wf} / \left(\gamma B_0\right) - 3.35\left[ppm\right]\right)}{-0.01\left[\frac{ppm}{°C}\right]} \quad [5]$$

where 3.35 ppm is the commonly used chemical shift between water and fat at the reference temperature 37 °C without considering the influence of magnetic susceptibility. The temperature map obtained by averaging T_{wf} in the three orientations was compared to the individual temperature maps. However, because averaging itself may decrease the temperature variation, a cumulative distribution function was used to compare the average map obtained from three orthogonal orientations with all voxel- wise temperature combinations of the three individual orientations.

3.2.3. Relative fat reference thermometry

For measuring changes in temperature, fat referenced proton PRFS thermometry offers an advantage with its general applicability for compensating magnetic field disturbances of various origins (14,15,26,30-33). One source of magnetic field disturbance originates from heat-induced tissue magnetic susceptibility changes (13). This section describes the experiments that were performed to investigate the influence of heat-induced tissue magnetic susceptibility changes of fatty and aqueous tissue on the effectiveness of fat referenced thermometry.

Relative thermometry simulations

Simulations were performed of fat referenced PRFS thermometry of a voxel on the tumor/fat boundary during a HIFU sonication (Figure 3a). Fat referencing may for example be achieved by using an MR pulse sequence with alternating water- and fat- selective pulses (30). The geometry was defined as a spherical tumor with a diameter of 10 mm embedded in a sphere of fat with a diameter of 25.4 mm. The isotropic voxel size was 0.1 mm and the total calculation matrix size was 256×256×256. A 3D Gaussian HIFU power distribution (amplitude: 5×10^6 W/m^3, kernel width: 2 mm in all directions) was applied for 40 s to the lower edge of the tumor/fat boundary. The temporal temperature evolution was simulated with in-house developed 3D finite-difference simulation software (MATLAB; MathWorks, Natick, MA) using the following tissue properties for fat and tumor tissue, respectively:

density: 888 and 1000 kg/m^3 (34,35), specific heat capacity: 2387 and 3600 J/(kg K) (36), thermal conductivity: 0.217 and 0.36 W/(mK) (36,37).

From the temperature change, the field disturbance was calculated using the susceptibility temperature coefficients of 0.002 ppm/°C (6) for aqueous (tumor) tissue and 0.0055 ppm/°C (38) for fat tissue. On the water/fat boundary, fat referenced imaging was simulated for a 1×1×1 mm^3 voxel. Every sampling point (N = 10^3) was assumed to contribute a signal magnitude of one and the relaxation terms (and the influence of temperature changes thereon) were ignored. The fat referenced temperature change was derived ($\Delta T_{wf} = \Delta\varphi/\alpha\gamma B_0 TE$) from the corrected phase change ($\Delta\varphi = \Delta\varphi_{PRFS} - \Delta\varphi_{fat}$), where $\Delta\varphi_{PRFS}$ is the induced phase change including field disturbance in the tumor compartment of the voxel, and $\Delta\varphi_{fat}$ is the total phase change from the fat part of the voxel. These measurements were compared to the average temperature in the voxel. Because of the symmetry in geometry, only two main magnetic field orientations were investigated (label 1 and 2 in Figure 3a).

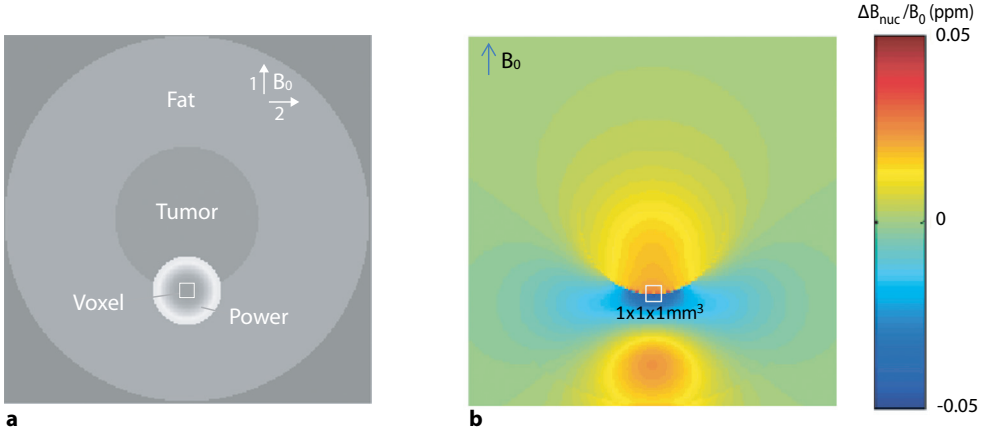

FIG. 3. (**a**) Intersection of the simulation geometry showing the spherical tumor embedded in fat tissue. (**b**) Field disturbance change for the maximum temperature change. The location of the imaging voxel, power distribution, and B_0 field orientations 1 and 2 are also shown.

Relative thermometry experiments

To investigate the effectiveness of fat referencing on a fat/muscle interface a HIFU experiment was performed. Pork tissue was placed in the breast cup of a prototype dedicated MR-HIFU breast platform (Sonalleve Breast MR-HIFU, Philips Healthcare, Vantaa, Finland). The section of the fat/muscle interface that was parallel to the B_0 field was sonicated with 100 W for 25 s (Figure 4). Prior to the sonication and 30 s after the end of the sonication, multi-gradient echo scans were acquired repeatedly every 12 s. TE = 2.3, 4.6, … ,27.6 ms, flip angle = 65°, TR = 38 ms, matrix = 80×80, FOV = 160×160 mm^2, ST = 6 mm. For the voxels with partial w/f volume, the complex signal was fit with a two peak lorentzian model to obtain the peak frequencies of water and fat. From the change in $\Delta\omega_{wf}$ the fat referenced change in temperature was determined. The fat referenced temperature change was then compared to the temperature change obtained from the field-drift corrected shift in the water frequency component of the same voxel. The field drift was corrected by subtracting the mean phase change measured in the unheated regions.

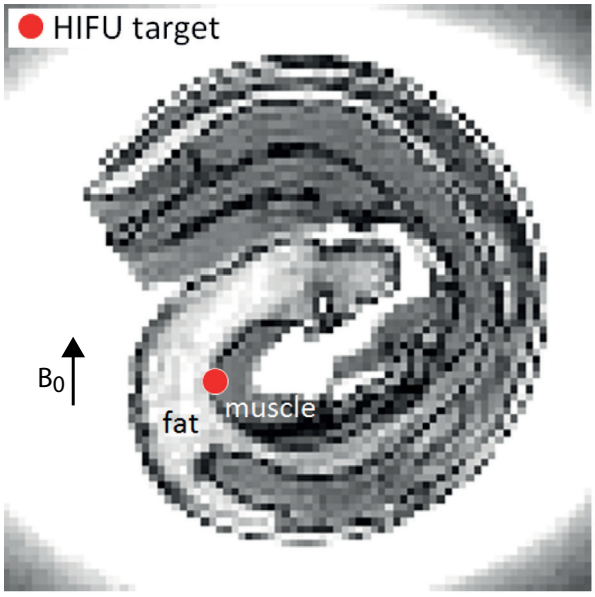

FIG. 4. Location of the HIFU target on the fat/muscle interface.

3.3. Results

3.3.1. Absolute fat referenced thermometry

Figure 5a shows the influence of interface normal angle (θ in Figure 1a) and sphere-to-voxel dimension (n) on the temperature measurement offset (ΔT_{wf}) for a voxel on the w/f interface. The influence of orientation on ΔT_{wf} is larger for flatter surfaces (higher value of n). From equation 2 it can be seen that for a flat surface (i.e. $n \to \infty$) ΔT_{wf} converges to $(\Delta\chi/3)\left(3\cos\theta^2 - 1\right)/-0.01$ (the black line in Figure 5a). When θ is equal to the magic angle ≈ 54.7° (vertical line in Figure 5a) the field disturbance is the smallest and ΔT_{wf} is closer to 0 °C. For the homogeneous w/f distribution (Figure 5b), ΔT_{wf} increased linearly with increasing volume fat percentage by 0.09 °C per percent. Figure 6a shows the simulation of the measured absolute temperature (T_{wf}) in the breast. For the indicated ROI, the mean T_{wf} was 47.2 ± 21.6 °C (N = 180 after removing one outliers > 3 × standard deviations from the average). Simulation of the average temperature measurement calculated for three orthogonally applied B_0 field directions (Figure 6b) gave a mean ΔT_{wf} of 0.7 ± 5.9 °C (N = 180).

For margarine (Figure 7: upper panel), the absolute temperature measured for $x_{obj} \| B_0$ was 18.0 ± 1.3 °C. The mean temperature of the average of the three orientations was 18.7 ± 0.7 °C. For pork (Figure 7: lower panel), the absolute temperature measured for $x_{obj} \| B_0$ was 19.9 ± 11.9 °C. The mean temperature of the average of the three orientations was 18.4 ± 5.1 °C. The measured MR room temperature was 21.3 °C. Figure 8 shows the cumulative distribution function of T_{wf} for the average of the three orthogonal orientations compared to the average of all temperature combinations of the three individual orientations. For margarine (Figure 8a) the 10th to 90th percentile interval of T_{wf} was 1.5 °C for all combinations and 1.3 °C for the mean image (i.e. a decrease of 0.3 °C). For pork (Figure 8b) the 10th to 90th percentile interval of T_{wf} was 18.6 °C for all combinations and 10.2 °C for the mean image (i.e. a decrease of 8.4 °C).

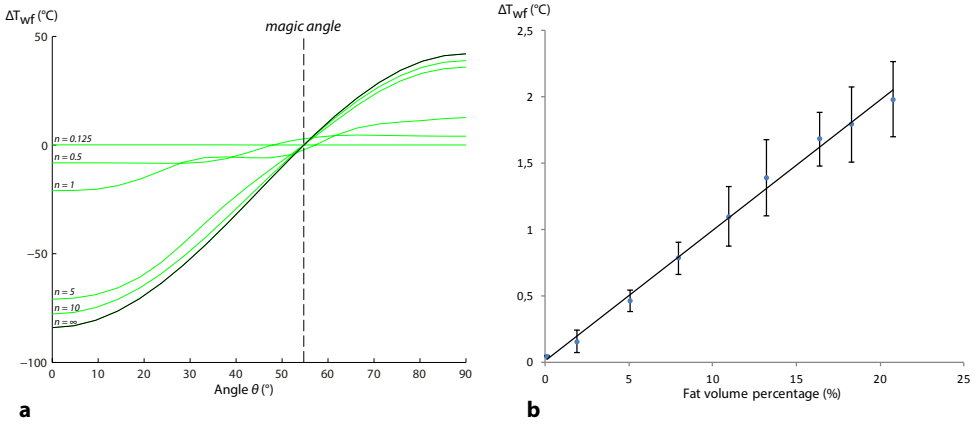

FIG. 5. (**a**) Influence of surface normal orientation (θ) and n=a/L on the measured temperature T_{wf} (**b**) Influence of fat volume percentage on the measured temperature for a homogeneous mixture.

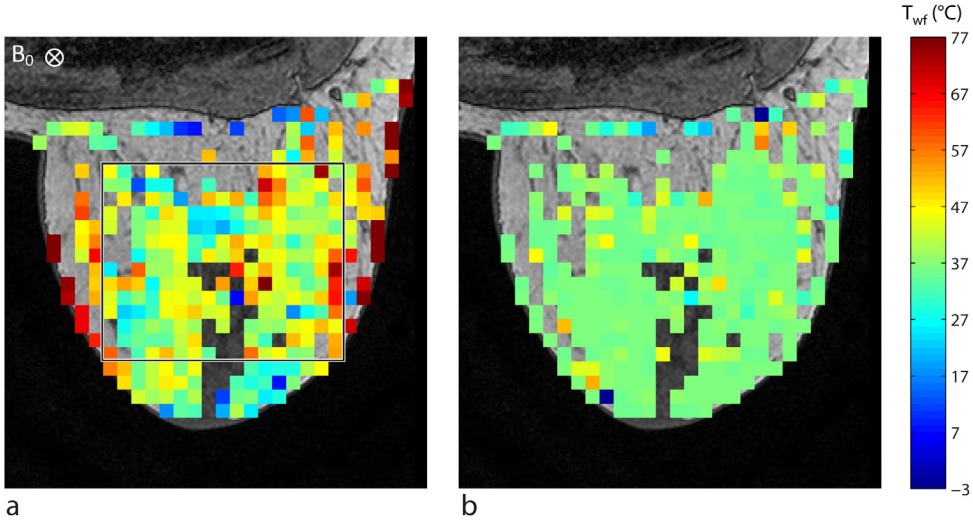

FIG. 6. (**a**) The simulated apparent temperature T_{wf} in the breast and (**b**) after averaging the temperature obtained individually from three orthogonally applied B_0 fields. (The rectangle marks the ROI).

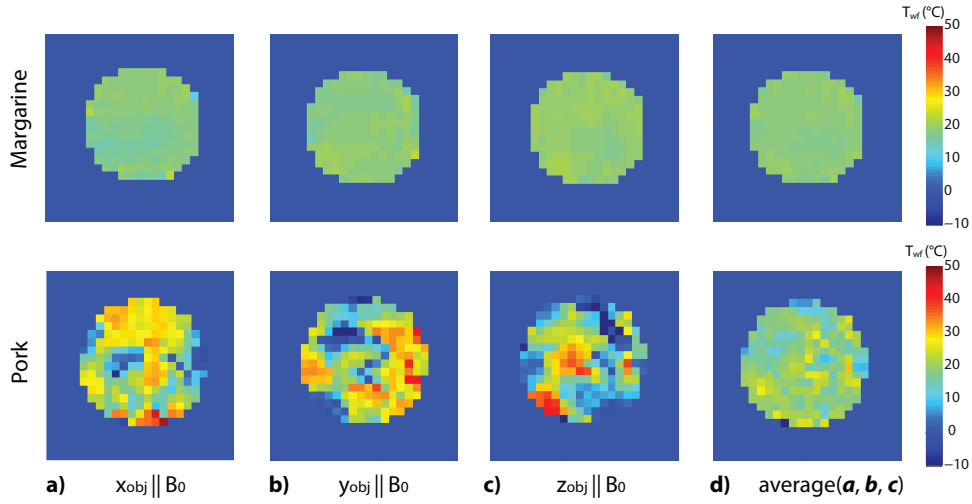

FIG. 7. (**a-c**) The absolute temperature measured for a sphere of margarine and pork for the three object orientations and (**d**) the average of the three orientations.

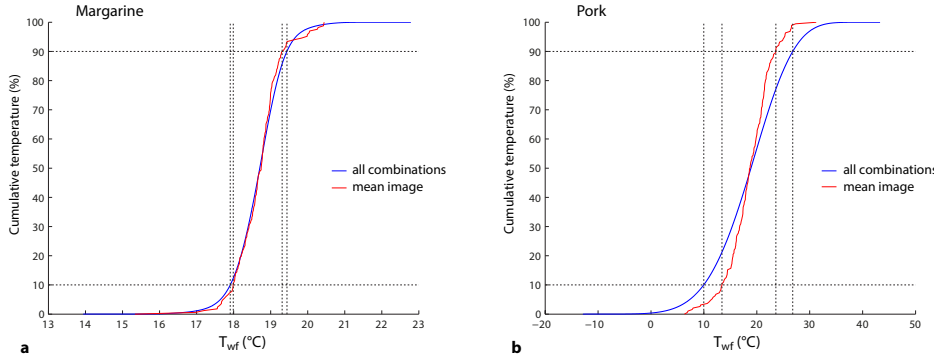

FIG. 8. Cumulative distribution functions of the measured absolute temperature for the average of all temperature combinations (blue line) and for the average of the three orientations (red line) measured for (**a**) margarine and (**b**) pork tissue.

3.3.2. Relative fat referenced thermometry

Figure 3b shows the nuclear magnetic field disturbance change after 20 s of heating for the magnetic field orientation perpendicular to the tumor/fat interface. Figure 9 shows the results of the fat referenced simulations. The true maximum temperature change was 29.7 °C. For B_0 parallel to the interface (Figure 9a) the maximum temperature change for the PRFS-based thermometry and fat referenced method was 30.9 °C and 33.0 °C, respectively. For B_0 perpendicular to the interface (Figure 9b) the maximum temperature change for PRFS-based thermometry and fat referencing was 27.2 °C and 23.1 °C, respectively. The average temperature change of the three orthogonal orientations (two parallel and one perpendicular) for fat referencing was within 10^{-3} °C from the true temperature change.

For the HIFU sonication on the muscle/fat boundary, the magnetic field change derived from the phase change (Figure 10a-b) showed the opposite polarity in the fat as in the

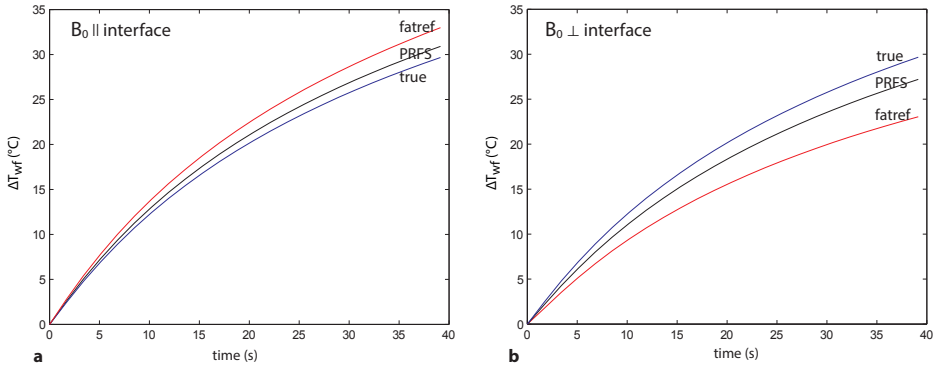

FIG. 9. The true (blue), PRFS (black) and fat referenced (red) temperature change as measured in the voxel shown in Figure 2 for B_0 orientated (**a**) parallel and (**b**) perpendicular to the tumor/fat interface.

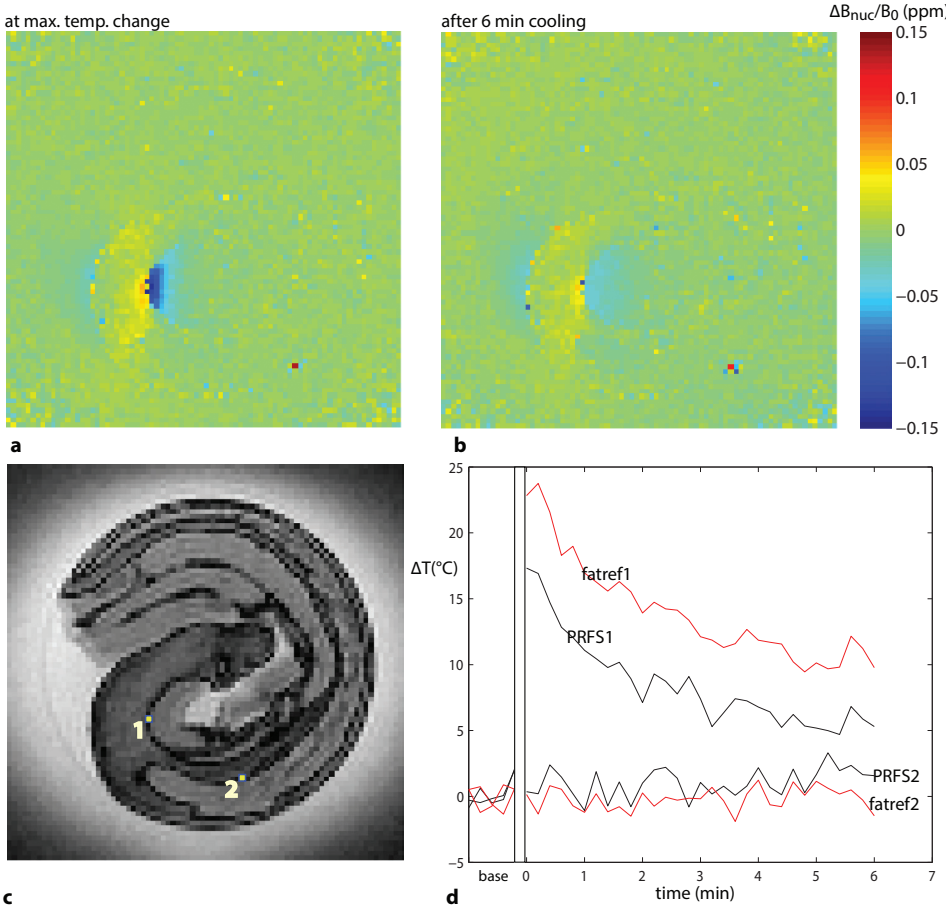

FIG. 10. Nuclear magnetic field change map at (**a**) the measured maximum temperature change and (**b**) after 6 minutes cooling. (**c**) Two voxel locations in a heated (label 1) and unheated (label 2) region. (**d**) The temperature change measured at the two voxels in Figure 9c on the muscle/fat interface during the cool-down period after a HIFU sonication. Fat referencing is compared with field drift corrected PRFS for the same voxel.

muscle. For the voxel in the heated region (Figure 10c label 1) the maximum fat referenced temperature change measured was 23.7 °C (Figure 10d). For the same voxel, the maximum (field drift corrected) PRFS temperature change measured was 17.3 °C. During the cool down period, the offset between the fat referenced measurement and (PRFS measurement decreased from 6.4 °C to 4.5 °C. As control, a voxel in the unheated region was also measured (Figure 10c label 2). For this voxel the measured (field drift corrected) PRFS temperature and fat referenced temperature change remained around 0 °C (Figure 10d).

3.4. Discussion

Measuring absolute temperature in vivo would complement existing MR thermometry methods which are mainly concerned with measuring changes in temperature. However, we have shown that absolute thermometry based on the w/f frequency difference is prone to errors when the spatial variation in magnetic susceptibility is not taken into account. The simulations in the breast and the margarine and pork rotation experiments show that local magnetic field inhomogeneity plays an important role, largely explaining the temperature variations measured by McDannold et al. in the breast (20,21).

Note, that one limitation of the rotation experiment is the limited spatial resolution. Whereas equation [4] requires an analytical solution for the magnetic field disturbance, discretization resulted in some residual temperature variations after averaging ΔT_{wf}, as was seen in Figure 6b. For the in vivo situation, the lipids and aqueous tissues are in itself separate microscopic entities, making the measurements inherently subject to errors from local magnetic field variations. An advantage of internal referencing is the close spatial proximity of the component used to probe the magnetic field (i.e. fat) and the temperature-sensitive component (i.e. water). New techniques such as intermolecular multiple quantum MRI may show insensitivity to susceptibility changes of water and fat (39), but are sensitive to variations in iron concentration (40) and have low SNR (39). For special cases of water/fat distributions such as randomly dispersed fat spheres in water, the simulation shows a water/fat shift independent of B_0 orientation but with a slight dependence on fat fraction. Although this is consistent with brain temperature measurements, in which an increase in the observed temperature was found for larger protein content (41), magnetic susceptibility differences would have to be confirmed as the origin of this effect. Additionally, the difference in pH between margarine and pork may also have influenced the chemical shift of the water proton (42). In the absolute thermometry experiments, a difference was found in the probe temperature measurement (21.3 °C) and the absolute temperature measured in margarine (18.7 °C) and pork (18.4 °C) after reducing the influence of the w/f distribution. This might have been expected because equation [5] does not take the magnetic susceptibility distribution into account.

In this study lorentzian line shapes were used for the peak fitting although more complex spectra are expected. Spectral characteristics have previously been used to characterize properties of small objects (43). Whether other spectral analysis techniques could probe the susceptibility-independent w/f shift is an interesting question that deserves further investigation. In this work it was assumed that the underlying geometric magnetic susceptibility distribution was unknown and therefore a simple line shape was used to fit the spectra. Furthermore, practical echo times were used as may be acquired with a multi gradient echo sequence. The feasibility of absolute thermometry in homogeneous tissues such as bone marrow has previously been investigated by other authors (40,44,45). Additionally, relaxation based techniques may be explored for absolute thermometry, especially in adipose tissue

which is assumed to be less sensitive to heat-induced coagulation and edema formation than aqueous tissues. Beyond the implications for absolute thermometry, the local susceptibility induced source of w/f frequency differences may be added to the list of confounding factors regarding w/f separation (46). How the fitting protocol may influence the obtained T_{wf} was not considered here (for example: the selected echo times, inclusion of multiple fat peaks, model fitting algorithm and robustness to noise, line shape parameter constraints, or modeling of eddy currents or J-coupling.)

For voxels containing both water and fat, fat referenced thermometry has been explored for measuring temperature change mainly for homogeneous w/f distributions (14,15,30-33). The technique has been shown to work better in homogeneous w/f distributions than heterogeneous ones (26). With simulations and a HIFU experiment we have shown that this is largely due to differences in the magnetic susceptibility temperature dependence of aqueous and adipose tissues. For the geometry and HIFU heating profile used in the study, the internal reference experiences another change in macroscopic magnetic field than the aqueous component. The heat-induced magnetic susceptibility changes have been shown to result in PRFS thermometry errors in aqueous tissue (13). This work shows that fat-referencing may not reduce this effect but even exacerbate it because of the opposite polarity in the change in magnetic field experienced by the water and fat components. The simulations demonstrated that fat referencing either overestimated or underestimated the actual temperature change, depending on the orientation of the interface with respect to the B_0 field. The HIFU experiment further validated this; for the interface parallel to the B_0 field the fat referenced temperature change was higher than the field drift corrected PRFS-based temperature change. This difference is expected to decrease as the total temperature change decreases. In the experiment only a slight decrease in offset was found likely because of the long cooling time of fatty tissue (47). The nuclear magnetic field change map (Figure 9b) confirmed pronounced phase changes in fat even after 6 minutes of cooling. A consequence of these findings is that fat referencing for heterogeneous water/fat distributions may be suboptimal if fat is part of the heated region.

In conclusion, this study has shown that the variation in observed absolute temperatures for heterogeneous w/f tissues may largely be explained by the difference in magnetic susceptibility between aqueous and fatty tissues. Analogously, the simulations and experiments have illustrated why relative fat referencing may not always correct for field disturbances originating from heat-induced magnetic susceptibility changes.

3.5. Acknowledgements

This research was performed within the framework of CTMM, the Center for Translational Molecular Medicine, project VOLTA.

3.6. References

1. ter Haar G. Ultrasound focal beam surgery. Ultrasound in medicine & biology 1995;21(9):1089-1100.
2. Raaphorst GP, Szekely JG. Thermal Enhancement of Cellular Radiation-Damage - a Review of Complementary and Synergistic Effects. Scanning Microscopy 1988;2(1):513-535.
3. Issels RD, Lindner LH, Verweij J, Wust P, Reichardt P, Schem BC, Abdel-Rahman S, Daugaard S, Salat C, Wendtner CM, Vujaskovic Z, Wessalowski R, Jauch KW, Durr HR, Ploner F, Baur-Melnyk A, Mansmann U, Hiddemann W, Blay JY, Hohenberger P. Neo-adjuvant chemotherapy alone or with regional hyperthermia for localised high-risk soft-tissue sarcoma: a randomised phase 3 multicentre study. Lancet Oncol 2010;11(6):561-570.
4. Grull H, Langereis S. Hyperthermia-triggered drug delivery from temperature-sensitive liposomes using MRI-guided high intensity focused ultrasound. J Control Release 2012;161(2):317-327.
5. Rieke V, Butts Pauly K. MR thermometry. Journal of magnetic resonance imaging : JMRI 2008;27(2):376-390.
6. De Poorter J. Noninvasive MRI thermometry with the proton resonance frequency method: study of susceptibility effects. Magn Reson Med 1995;34(3):359-367.
7. Ishihara Y, Calderon A, Watanabe H, Okamoto K, Suzuki Y, Kuroda K, Suzuki Y. Precise and Fast Temperature Mapping Using Water Proton Chemical-Shift. Magn Reson Med 1995;34(6):814-823.
8. Hindman JC. Proton Resonance Shift of Water in Gas and Liquid States. J Chem Phys 1966;44(12):4582.
9. Depoorter J, Dewagter C, Dedeene Y, Thomsen C, Stahlberg F, Achten E. The Proton-Resonance-Frequency-Shift Method Compared with Molecular-Diffusion for Quantitative Measurement of 2-Dimensional Time-Dependent Temperature Distribution in a Phantom. J Magn Reson Ser B 1994;103(3):234-241.
10. Peters NH, Bartels LW, Sprinkhuizen SM, Vincken KL, Bakker CJ. Do respiration and cardiac motion induce magnetic field fluctuations in the breast and are there implications for MR thermometry? Journal of magnetic resonance imaging : JMRI 2009;29(3):731-735.
11. Sapareto SA, Dewey WC. Thermal dose determination in cancer therapy. Int J Radiat Oncol Biol Phys 1984;10(6):787-800.
12. Kuroda K. Non-invasive MR thermography using the water proton chemical shift. Int J Hyperther 2005;21(6):547-560.
13. Sprinkhuizen SM, Konings MK, van der Bom MJ, Viergever MA, Bakker CJ, Bartels LW. Temperature-induced tissue susceptibility changes lead to significant temperature errors in PRFS-based MR thermometry during thermal interventions. Magn Reson Med 2010;64(5):1360-1372.
14. Kuroda K, Mulkern RV, Oshio K, Panych LP, Nakai T, Moriya T, Okuda S, Hynynen K, Jolesz FA. Temperature mapping using the water proton chemical shift: self-referenced method with echo-planar spectroscopic imaging. Magn Reson Med 2000;44(1):167.
15. Pan X, Li C, Ying K, Weng D, Qin W, Li K. Model-based PRFS thermometry using fat as the internal reference and the extended Prony algorithm for model fitting. Magn Reson Imaging 2010;28(3):418-426.
16. Sudharsan NM, Ng EY, Teh SL. Surface Temperature Distribution of a Breast With

and Without Tumour. Comput Methods Biomech Biomed Engin 1999;2(3):187-199.
17. Wijlemans J, de Greef M, Schubert G, van den Bosch M, Moonen C, Ries M. Near-field management during MR-HIFU ablation in highly perfused organs.In Proceedings of the 23th Annual Meeting of the ISMRM, Milan, Italy, 2014. p. 2340.
18. Ammann C, Meier P, Merbach AE. A Simple Multi-Nuclear NMR Thermometer. J Magn Reson 1982;46(2):319-321.
19. Kuroda K, Takei N, Mulkern RV, Oshio K, Nakai T, Okada T, Matsumura A, Yanaka K, Hynynen K, Jolesz FA. Feasibility of internally referenced brain temperature imaging with a metabolite signal. Magnetic resonance in medical sciences : MRMS : an official journal of Japan Society of Magnetic Resonance in Medicine 2003;2(1):17-22.
20. McDannold N, Barnes AS, Rybicki FJ, Oshio K, Chen NK, Hynynen K, Mulkern RV. Temperature mapping considerations in the breast with line scan echo planar spectroscopic imaging. Magn Reson Med 2007;58(6):1117-1123.
21. McDannold N, Hynynen K, Oshio K, Mulkern RV. Temperature monitoring with line scan echo planar spectroscopic imaging. Med Phys 2001;28(3):346-355.
22. Simonis FF, Petersen ET, Bartels LW, Lagendijk JJ, van den Berg CA. Compensating for magnetic field inhomogeneity in multigradient-echo-based MR thermometry. Magn Reson Med 2014.
23. Baron P, De Greef M, Deckers R, Bakker CJG, Bouwman JG, Bartels LW. Influence of Magnetic Susceptibility on Absolute Temperature as Measured Directly from the Water/fat Frequency Shift.;In Proceedings of the 23th Annual Meeting of the ISMRM, Milan, Italy, 2014. p. 3678.
24. Schenck JF. The role of magnetic susceptibility in magnetic resonance imaging: MRI magnetic compatibility of the first and second kinds. Med Phys 1996;23(6):815-850.
25. Hopkins JA, Wehrli FW. Magnetic susceptibility measurement of insoluble solids by NMR: magnetic susceptibility of bone. Magn Reson Med 1997;37(4):494-500.
26. Hofstetter LW, Yeo DT, Dixon WT, Kempf JG, Davis CE, Foo TK. Fat-referenced MR thermometry in the breast and prostate using IDEAL. Journal of magnetic resonance imaging : JMRI 2012;36(3):722-732.
27. Salomir R, De Senneville BD, Moonen CTW. A fast calculation method for magnetic field inhomogeneity due to an arbitrary distribution of bulk susceptibility. Concept Magn Reson B 2003;19B(1):26-34.
28. Noorda YH, Kabus S, Bartels LW, Pluim JPW. Segmentation of the Inner Breast Structures in 3D MRI. In Proceedings of the 14th International Conference on Medical Image Computing and Computer Assisted Intervention (MICCAI), Toronto, Canada, 2011. p. 65.
29. Bouwman JG, Bakker CJ. Alias subtraction more efficient than conventional zero-padding in the Fourier-based calculation of the susceptibility induced perturbation of the magnetic field in MR. Magn Reson Med 2012;68(2):621-630.
30. Shmatukha AV, Harvey PR, Bakker CJ. Correction of proton resonance frequency shift temperature maps for magnetic field disturbances using fat signal. J Magn Reson Imaging 2007;25(3):579-587.
31. Li C, Pan X, Ying K, Zhang Q, An J, Weng D, Qin W, Li K. An internal reference model-based PRF temperature mapping method with Cramer-Rao lower bound noise performance analysis. Magn Reson Med 2009;62(5):1251-1260.
32. Soher BJ, Wyatt C, Reeder SB, MacFall JR. Noninvasive temperature mapping with

MRI using chemical shift water-fat separation. Magn Reson Med 2010;63(5):1238-1246.
33. Taylor BA, Elliott AM, Hwang KP, Shetty A, Hazle JD, Stafford RJ. Measurement of temperature dependent changes in bone marrow using a rapid chemical shift imaging technique. Journal of magnetic resonance imaging : JMRI 2011;33(5):1128-1135.
34. Farvid MS, Ng TW, Chan DC, Barrett PH, Watts GF. Association of adiponectin and resistin with adipose tissue compartments, insulin resistance and dyslipidaemia. Diabetes Obes Metab 2005;7(4):406-413.
35. Urbanchek MG, Picken EB, Kalliainen LK, Kuzon WM. Specific force deficit in skeletal muscles of old rats is partially explained by the existence of denervated muscle fibers. J Gerontol a-Biol 2001;56(5):B191-B197.
36. Henriques FC, Moritz AR. Studies of Thermal Injury .1. The Conduction of Heat to and through Skin and the Temperatures Attained Therein - a Theoretical and an Experimental Investigation. Am J Pathol 1947;23(4):530-549.
37. Cohen ML. Measurement of the thermal properties of human skin. A review. The Journal of investigative dermatology 1977;69(3):333-338.
38. Sprinkhuizen SM, Bakker CJ, Ippel JH, Boelens R, Viergever MA, Bartels LW. Temperature dependence of the magnetic volume susceptibility of human breast fat tissue: an NMR study. Magma 2012;25(1):33-39.
39. Jenista ER, Branca RT, Warren WS. Absolute temperature imaging using intermolecular multiple quantum MRI. Int J Hyperthermia 2010;26(7):725-734.
40. Davis RM, Warren WS. Intermolecular zero quantum coherences enable accurate temperature imaging in red bone marrow. Magn Reson Med 2014: doi: 10.1002/mrm.25372.
41. Corbett RJ, Laptook AR, Tollefsbol G, Kim B. Validation of a noninvasive method to measure brain temperature in vivo using 1H NMR spectroscopy. J Neurochem 1995;64(3):1224-1230.
42. Lutz NW, Kuesel AC, Hull WE. A H-1-NMR Method for Determining Temperature in Cell-Culture Perfusion Systems. Magn Reson Med 1993;29(1):113-118.
43. Seppenwoolde JH, van Zijtveld M, Bakker CJ. Spectral characterization of local magnetic field inhomogeneities. Phys Med Biol 2005;50(2):361-372.
44. Lam MK, De Greef M, Deckers R, Bartels LW. Feasibility of absolute MR thermometry in bone marrow for MR-guided HIFU of bone metastases.;12th International Symposium on Therapeutic Ultrasound, Heidelberg, Germany, 2012. A-107.
45. Sprinkhuizen SM, Tromp HA, Bakker CJG, Workum JD, Leeuw Hd, Viergever MA, Bartels LW. A novel application for MR Thermometry: Post Mortem Interval estimation in forensic medicine.;In Proceedings of the 17th Annual Meeting of the ISMRM, Honolulu, Hawaii, 2009. p. 4394.
46. Karampinos DC, Yu H, Shimakawa A, Link TM, Majumdar S. Chemical shift-based water/fat separation in the presence of susceptibility-induced fat resonance shift. Magn Reson Med 2012;68(5):1495-1505.
47. Baron P, Ries M, Deckers R, de Greef M, Tanttu J, Kohler M, Viergever MA, Moonen CT, Bartels LW. In vivo T2 -based MR thermometry in adipose tissue layers for high-intensity focused ultrasound near-field monitoring. Magn Reson Med 2014;72(4):1057-1064.

3

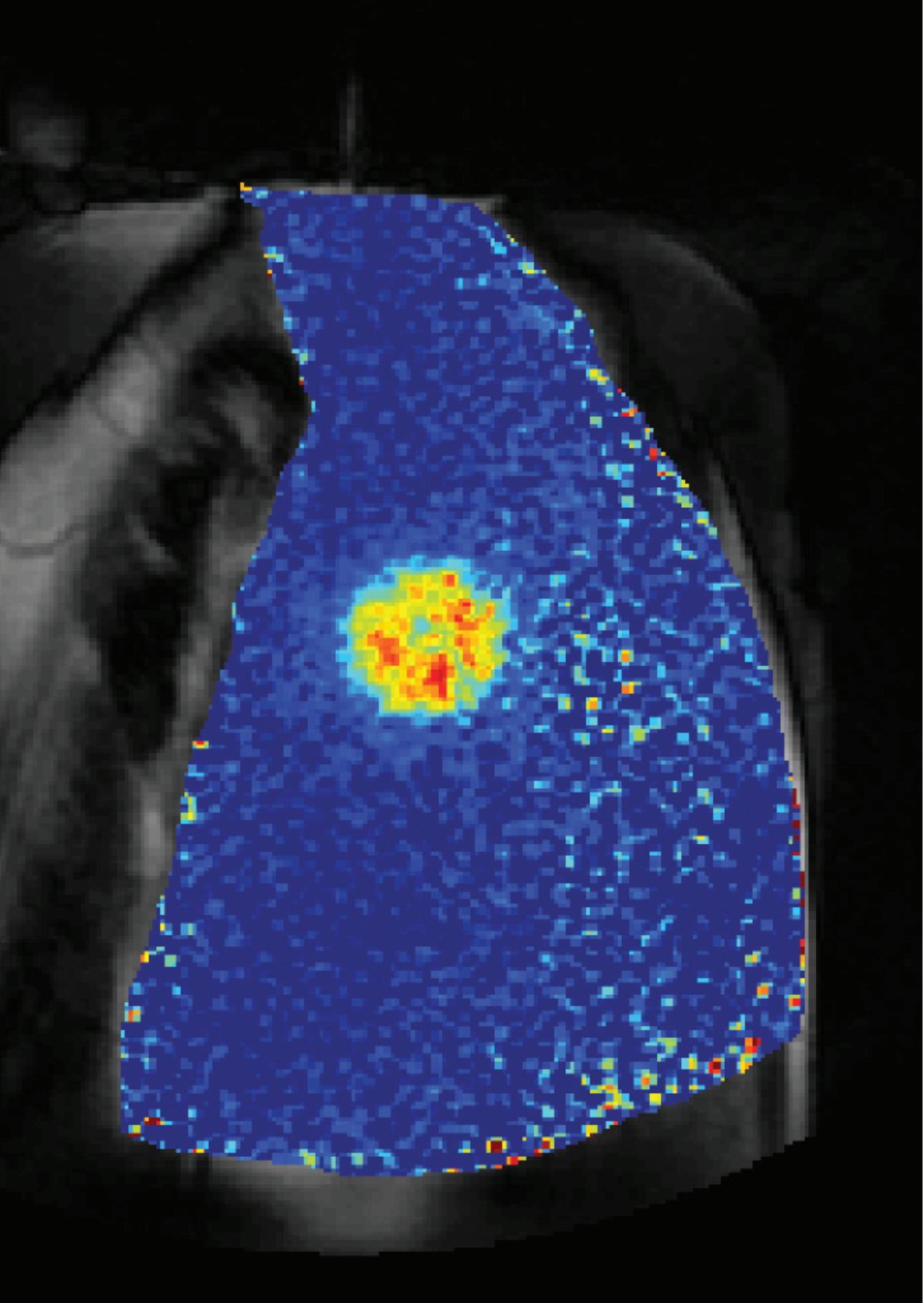

CHAPTER 4

In vivo T_2-based MR thermometry in adipose tissue layers for High Intensity Focused Ultrasound near-field monitoring

Published as:

Baron P, Ries M, Deckers R, Greef M, Tanttu J, Kohler M, Viergever MA, Moonen CTW, Bartels LW. In Vivo T2-Based MR Thermometry in Adipose Tissue Layers for High-Intensity Focused Ultrasound Near-Field Monitoring. Magn Reson Med 2014;72(4):1057-1064.

ABSTRACT

Purpose: During MR-guided high-intensity focused ultrasound (HIFU) therapy, ultrasound absorption in the near field represents a safety risk and limits efficient energy deposition at the target. In this study, we investigated the feasibility of using T_2 mapping to monitor the temperature change in subcutaneous adipose tissue layers.

Methods: The T_2 temperature dependence and reversibility was determined for fresh adipose porcine samples. The accuracy was evaluated by comparing T_2-based temperature measurements with probe readings in an ex vivo HIFU experiment. The in vivo feasibility of T_2-based thermometry was studied during HIFU ablations in the liver in pigs and of uterine fibroids in human patients.

Results: T_2 changed linearly and reversibly with temperature with an average coefficient of 5.2 ± 0.1 ms/°C. For the ex vivo HIFU experiment, the difference between the T_2-based temperature change and the probe temperature was <0.9 °C. All in vivo experiments showed temperature-related T_2 changes in the near field directly after sonications. As expected, considerable intersubject variations in the cooling times were measured in the in vivo porcine experiments.

Conclusions: The reversibility and linearity of the T_2-temperature dependence of adipose tissue allows for the monitoring of the temperature in the subcutaneous adipose tissue layers.

4.1. Introduction

There is growing interest in the use of noninvasive techniques for the treatment of both benign and malignant tumors (1). MR-guided high-intensity focused ultrasound (MR-HIFU) is a minimally invasive modality that has shown substantial promise for thermal therapy because it combines excellent soft tissue imaging (2), real-time temperature mapping (3), and noninvasive local heat deposition (4).

However, the advantage of energy delivered noninvasively by an extracorporal transducer is accompanied by several practical complications. The necessity to deliver the ultrasonic energy through cutaneous, subcutaneous, and intermediary tissue layers before it reaches the target area leads to ultrasound energy absorption in the near field (5). This absorption causes a moderate temperature rise in these intermediate tissue layers, which is generally undesirable. For extended high-power sonications, the near-field heating can even lead to irreversible tissue damage outside the desired ablation area (6). As a consequence, the requirement to mitigate the risk of near-field tissue damage for therapeutic HIFU applications leads to limitations of the lesion volume that can be ablated in a single uninterrupted ablation (5,7). Larger lesion volumes have to be split into subvolumes, which are subsequently treated once the interstitial and subcutaneous tissue layers have cooled down sufficiently. This increases overall treatment time to unacceptable durations. The duration of the required cool-down period is in practice decisive for both patient safety and the overall duration of the intervention.

Unfortunately, the composition and the thickness of the tissue layers between the HIFU transducer and the target area display substantial variations between subjects. In particular, adipose tissue in the near field represents a practical limitation to the sonication rate due to its lower specific heat capacity (8), lower heat conductivity (8,9), and lower perfusion (10) than other tissues in the near field. As a consequence, the duration of the cool-down period is generally chosen rather conservatively in order to assure patient safety, which leads to a long overall duration of the HIFU intervention (11).

A potential solution would be to monitor the cool-down process of each sonication cycle in near real-time and to adapt the required delay between the sonication cycles. However, although proton resonance frequency shift (PRFS) thermometry is the method of choice in water-containing tissues including the tumor area itself, PRFS thermometry in adipose tissues is practically impossible (12). PRFS thermometry could be performed in muscle tissue, but measuring the accumulation of heat over a long period would be difficult because of field drift and respiration-induced magnetic field changes. Monitoring the temperature in the near field adipose tissue allows the use of relaxation time-based methods, which are more robust. T_1-based thermometry has been suggested in the past as a suitable candidate for noninvasive thermometric measurements in adipose tissue (13). An alternative is provided by thermometric measurements based on the temperature dependence of the T_2 relaxation time in adipose tissue (14). In aqueous tissues, T_2-based thermometry has several disadvantages compared with PRFS thermometry, including nonreversibility (15) and nonlinear behavior (15). This led to the tendency to discard T_2-based thermometry for MR guidance of noninvasive thermal therapies in clinical applications.

The possibility of performing reliable T_2-based thermometric measurements in adipose tissue has, to our knowledge, not yet been systematically investigated. How adipose tissue responds to heating is not well known (e.g., with regard to edema formation). Accordingly, the purpose of this study was to investigate the possibility of accurate, precise, and reproducible thermometric measurements using rapid T_2 mapping in adipose tissue layers.

This study encompasses ex vivo experiments to assess the precision and accuracy of the

method and in vivo experiments with HIFU ablations in a porcine model, which demonstrate the ability to monitor the near-field heating process. We will also show clinical data from uterine fibroid ablations in patients to demonstrate the clinical feasibility and the usefulness of the approach for heat management.

4.2. Methods

The study was part of a larger project concerned with technical developments of MR-HIFU techniques for clinical applications in the liver. After the in vivo porcine near-field experiments had been performed, the pigs were sacrificed, and the abdominal adipose tissue was immediately used for the calibrations and the ex vivo HIFU experiment described herein.

4.2.1. Animals

All animal experiments were approved by the animal ethics committee at our institution. Experiments were performed in five female pigs with an average weight of 70 kg. After intravenous administration of analgesic meloxicam (0.4 mg/kg), general anesthesia was induced with ketamine (13 mg/kg). During the experiments, the pigs were intubated and sufentanil (0.0113 mg/kg h), midazolam (1 mg/kg h), and nimbex (0.09 mg/kg h) were administered as an infusion. The animals were mechanically ventilated at a rate of 14 breaths per minute. Carbon dioxide concentration and arterial blood pressure were monitored continuously during the experiment.

4.2.2. Ex vivo adipose porcine T_2 temperature calibration

The first series of experiments were performed to investigate the temperature dependence of T_2 in subcutaneous adipose tissue and the intersubject variations. For this, five samples of subcutaneous adipose porcine tissue from five different pigs were obtained directly post mortem. The samples were placed in a 50-mL cylindrical holder, which was installed inside a temperature-stabilized closed circuit water bath (Fig. 1). The water bath was placed inside the bore of a 1.5T MRI scanner (Achieva, Philips Healthcare, Best, The Netherlands) and two laterally installed surface receive coils were used for signal detection.

The samples were first slowly heated and then allowed to cool down. T_2 maps were acquired at constant temperature steps first during the heating phase and then during the cooling phase. For five samples, this was done at four temperature points in the range of 25

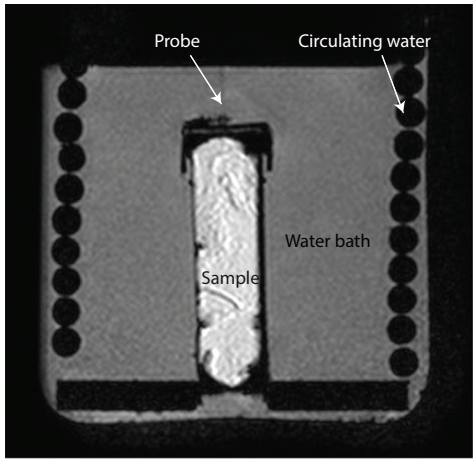

FIG. 1. MR image showing the T_2 temperature calibration measurement set-up. The water bath contains a holder for a sample tube. The sample tube contains subcutaneous adipose tissue with a fiber optic probe inserted. The water in the bath is heated and cooled by the water circulated in the inserted spiral tubing.

°C - 45 °C, and for one sample the range was extended to 25 °C - 74 °C. The actual sample temperature was independently recorded with a fiber-optic probe (Luxtron, LumaSense, Santa Clara, California, USA).

To ensure a homogenous temperature distribution, constant in time, T_2 maps were acquired after the temperature probe reading had been stable for at least 15 minutes. One coronal slice was acquired using the following parameters: dual echo turbo spin echo (TSE); effective echo time (TE) = 38 ms (TE_1) and 180 ms (TE_2); pulse repetition time = 2000 ms; TSE factor = 40; interecho spacing = 4.8 ms; readout bandwidth = 352 Hz/pixel; slice-selective refocusing pulses with angle = 160°; matrix = 180 × 160; field of view = 450 × 450 mm^2; reconstructed voxel size = 1.75 × 1.75 × 5 mm^3 with spectral presaturation with inversion recovery (SPIR) (16) water suppression and a duration of 16 s per image. A full preparation scan, including shimming and demodulation frequency (f_0) determination, was performed prior to each acquisition. For all images, native in-plane resolution was 2.50 × 2.81 mm^2, interpolated to 1.75 × 1.75 mm^2. The T_2 maps were calculated by assuming monoexponential decay of the modulus signal so that T_2 could be calculated based on measurements at two TEs from

$$T_2 = \frac{TE_2 - TE_1}{\ln(S(TE_1)/S(TE_2))} \quad [1]$$

where S(TE) is the modulus of the signal at TE. Although the apparent T_2 values obtained will include influences from T_1-relaxation and J-coupling, as further discussed in the Discussion, we refer to them as T_2 values hereafter. To increase the signal-to-noise ratio (SNR), the number of signal averages was four and the values of 16 voxels of the T_2 maps in the center of the sample were averaged. The total acquisition time for the four averages was 64 s.

If the adipose subcutaneous layer would be thick enough to contain the whole imaging slice, SPIR water suppression would probably not be necessary. This would increase the acquisition speed. Furthermore, the sequence without water suppression may be more robust for quantitative measurements, especially when the region of interest is far from the magnet isocenter. Therefore, the influence of using SPIR water suppression was also investigated. For two samples, T_2 maps were acquired with and without SPIR water suppression for every temperature. The other scan parameters were kept the same.

For turbo spin echo sequences, imperfect refocusing flip angles may lead to stimulated echoes and related T_1- contamination (17). To determine the influence of refocusing flip angle on the measured T_2 temperature coefficient, temperature calibration experiments were performed for the temperature range of 25 °C - 45 °C using SPIR water suppression and a series of scans with refocusing angles 120°, 140°, 160°, and 180°. The range of refocusing angles was chosen based on prior knowledge of typical B_1 variation measured in volunteers on the MR-HIFU table.

4.2.3. Ex vivo porcine HIFU experiment

To verify the accuracy of the measured temperature change in the near field during a HIFU sonication, an ex vivo experiment was performed. Directly after a pig from the in vivo experiments had been sacrificed, a section of the subcutaneous adipose tissue that had not been sonicated was removed and kept at room temperature. The HIFU membrane (which serves as the transparent ultrasound (US) window enclosing the tank containing the transducer) was first covered by a gel pad and then by the adipose tissue layer (Fig. 2). This was covered with a cylindrical block of agar gel (2% agar, 2% silica), which served as the sonication target. All surface interfaces were filled with water to ensure adequate acoustic

coupling. The perpendicular distance from the imaging slice to the center of the focus was 43.3 mm. During sonication, coronal dynamic T_2 maps were acquired in the adipose tissue using the same T_2 mapping protocol that was used for the calibration experiments with water suppression. A full preparation scan was performed once prior to the dynamic acquisition series and the temporal resolution of the dynamic scans was 16 s per T_2 map. Furthermore, the temperature in the adipose tissue in the center of the cross section of the beam path and the adipose tissue was monitored with a fiber-optic probe (Luxtron LumaSense) sampling at a frequency of 1 Hz.

The experiment was performed on a clinical 1.5T MR-HIFU system (Sonalleve, Philips Healthcare, Vantaa, Finland) applying 10 W of acoustic power for 1000 s, using an 8-mm-diameter volumetric sonication protocol (18). The MR-HIFU system had a dedicated two-element coil integrated into the acoustic window of the MR-HIFU tabletop combined with a dedicated three element surface coil positioned dorsally. The temperature change was calculated for every voxel based on the average of the calibrated T_2 temperature coefficients of the five samples measured with water suppression. The temperature change of one voxel at the center of the cross-section of the beam path and the adipose tissue (Fig. 2) was compared with the fiber optic probe readings.

For the two TEs, SNR values in the adipose tissue were calculated using (19):

$$SNR_{TE} = 0.66\frac{I_{TE}}{\sigma_{TE}} \quad [2]$$

where I_{TE} is the magnitude of a voxel in adipose tissue (prior to sonication) and σ_{TE} is the standard deviation (SD) of the magnitude values of a region of interest (area 3.1 cm^2) placed in the air.

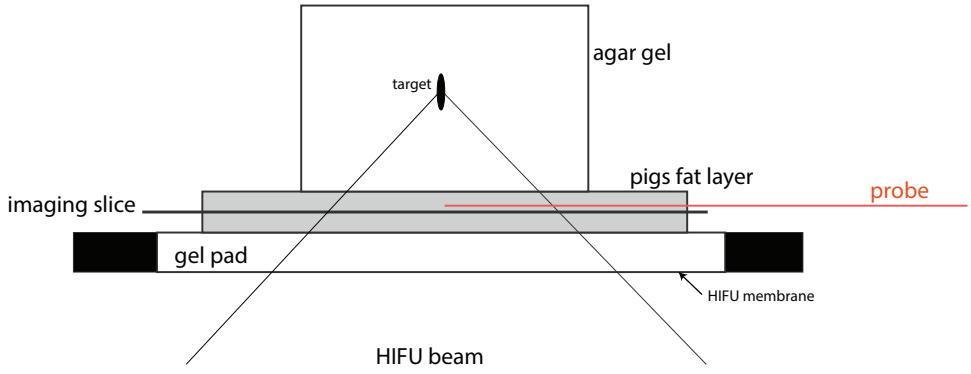

FIG. 2. Schematic of the ex vivo HIFU experiment set-up, showing the locations of the imaging slice and probe.

4.2.4. In vivo porcine HIFU experiment

To investigate the in vivo feasibility of T_2-based thermometry in adipose tissue, the temperature changes in the subcutaneous adipose tissue layer of five pigs were monitored during liver sonications. Figure 3a shows a sagittal planning view with the ultrasound target area, beam path, and transducer overlaid onto a T_2-weighted image. The pigs were lying in the prone position (hind legs first) and they were sedated and mechanically ventilated. The pig's abdominal skin was shaved for optimal acoustic coupling between the skin and gel pad. The acoustic power ranged from 300 to 450 W and the sonication duration was between 20 and 30 s. The applied power levels and durations had previously been found sufficient to give

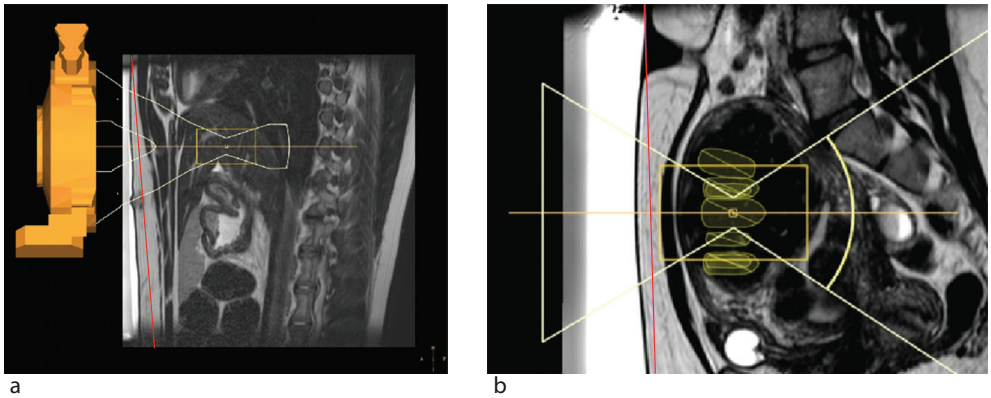

FIG. 3. In vivo sonication of (**a**) porcine liver and (**b**) uterine fibroid. Both images show sagittal slices with the beam cone drawn as an overlay. The orange line gives the location of the T_2 mapping slice.

a lethal thermal dose in a defined region in the pig liver in vivo (20). Volumetric sonication cells with a diameter of 8 mm were positioned to target the liver. During sonication, dynamic T_2 maps with a temporal resolution of 16 s were acquired in the subcutaneous fat layer. The T_2 mapping protocol was the same as for the calibration experiments with water suppression.

The T_2 change was converted to temperature change using the average calibrated T_2 temperature coefficient found. To characterize the rate of cooling in every heated voxel, the measured temperature change over time during the cool-down period was fit with a monoexponential decay function. The optimal least-squares fit (Levenberg-Marquardt algorithm) for the exponential time constant was called the cooling time constant. All data were processed using MATLAB (MathWorks, Natick, Massachusetts, USA). SNR values were also measured as was done for the ex vivo HIFU experiment.

4.2.5. Monitoring during a uterine fibroid HIFU treatment

The clinical feasibility of T_2-based thermometry was evaluated during a standard clinical uterine fibroid MRHIFU treatment in nine patients (Fig. 3b). Informed consent had been given by all patients. Furthermore, the potential for measuring accumulative heat build-up for multiple sonications was explored. For three patients, T_2 maps were acquired dynamically after the first sonication for an average duration of 15 min to obtain an estimate for the cooling time constant. For one patient, T_2 maps were acquired prior to treatment and 0.5 to 1.5 min after five therapeutic sonications (acoustic powers: 110-120 W; durations: 57 s to 1 min 12 s). For all nine patients one T_2 map was acquired before the first sonication, and at least one T_2 map was acquired after the first sonication so that the temperature increase directly after the first sonication could be estimated. Additionally, the mean subcutaneous adipose tissue T_2 value of the nine patients was measured before the first sonication. For this measurement, a region of interest with an area of 27.6 cm^2 (30 × 30 pixels) was used. The T_2 mapping protocol was the same as the one used for the ex vivo calibration experiments acquired without SPIR water suppression but with one signal average when applied in patients to reduce the scan duration. For all patients, the subcutaneous adipose tissue was thick enough to fully contain the 5-mm imaging slice. The temperature change maps were calculated based on the difference with the T_2 map acquired prior to the first sonication, and by using the average T_2 temperature coefficient found for the adipose porcine samples without SPIR water suppression. SNR values were also measured in a similar way as for the ex vivo HIFU experiment.

4.3. Results

4.3.1. Adipose porcine T_2 temperature calibration

For the five subcutaneous pig fat samples measured in the smaller temperature range (25 ºC - 45 °C), the measured T_2 was found to change linearly ($R^2 > 0.99$) with temperature, as shown in Figure 4a. The mean (± SD) of the T_2 temperature coefficient was 5.17 ± 0.1 ms/ºC (minimum: 5.01 ms/ºC; maximum: 5.29 ms/ºC). The SD of the T_2 values in the region of interest generally increased with temperature from 1.7 ms at 25 ºC to 7.0 ms at 45 °C. These results correspond with temperature variations of 0.3 ºC at 25 °C and 1.3 ºC at 45 °C, calculated using the mean T_2 temperature coefficient. The linear regression equations for the five samples are shown in Table 1. For the two samples comparing the use of water suppression (Fig. 4b), a larger T_2 temperature coefficient was found using SPIR water suppression (5.08 ms/ºC) than without water suppression (3.77 ms/ºC). For the sample measured in the larger temperature range (25 °C - 74 °C; Fig. 4c), T_2 changed exponentially with temperature for the acquisitions both with ($R^2 > 0.99$) and without ($R^2 > 0.99$) SPIR water suppression. All measurements showed reversible T_2 changes after the samples had been heated. For the temperature calibration experiments with refocusing angles ranging from 120º to 180º, the difference in measured T_2 temperature coefficients was <0.15 ms/ºC.

Table 1. Linear regression lines for the individual calibration experiments and the mean T_2 temperature coefficients.

Sample nr	With SPIR WS (ms)	R^2	No SPIR WS (ms)	R^2
1	T_2 = (5.01±0.14)T + (18.80±4.67)	0.995	T_2 = (4.00±0.10)T + (30.42±3.31)	0.998
2	T_2 = (5.15±0.14)T + (13.31±4.91)	0.995	T_2 = (3.54±0.08)T + (42.21±2.82)	0.998
3	T_2 = (5.12±0.13)T + (15.33±4.56)	0.995		
4	T_2 = (5.28±0.15)T + (10.44±5.04)	0.995		
5	T_2 = (5.29±0.13)T + (17.99±4.31)	0.997		
Mean coeff.	$\Delta T_2/\Delta T$ = 5.17±0.12 ms/°C		$\Delta T_2/\Delta T$ = 3.77±0.33 ms/°C	

T, temperature in degrees Celsius

4.3.2. Ex vivo porcine HIFU experiment

Figure 5a shows the maximum temperature change for the ex vivo near-field HIFU experiment. For this experiment, the temperature change was calculated based on the average of the calibrated T_2 temperature coefficients of the five samples with water suppression (5.17 ms/ºC). The correspondence between probe temperature and T_2- based thermometry of one voxel at the probe location is shown in Figure 5b. The average probe temperature before heating was taken as the baseline temperature for T_2-based thermometry. During the entire sonication, the difference between the probe temperature and the T_2- based temperature change was <0.9 °C. The SNR values ranged from 200 to 630 for TE_1 and 80 to 260 for TE_2.

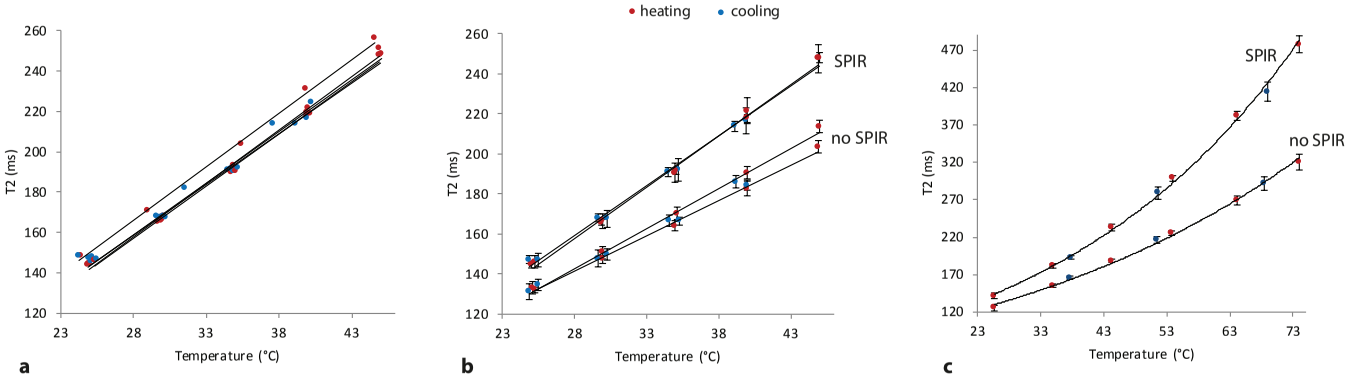

FIG. 4. Calibration curves showing the T_2 measurements during heating (red dots) and subsequent cooling (blue dots) for: (**a**) five pig samples measured with SPIR water suppression, (**b**) two pig samples measured with and without SPIR water suppression, and (**c**) one sample measured with a larger temperature range.

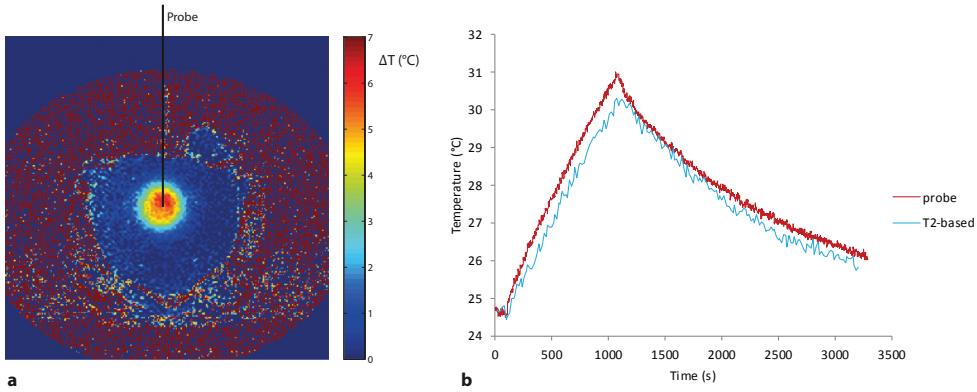

FIG. 5. (**a**) Coronal slice of ex vivo adipose tissue sample showing the maximum temperature change in the near field and the location of the probe. The temperature change was computed from the average T_2- temperature coefficient as measured in the calibration experiments. (**b**) Correspondence between probe temperature and T_2-based thermometry of one voxel in the near field, for a 10W, 1000s sonication.

4.3.3. In vivo porcine HIFU experiment

In the porcine adipose tissue, temperature-induced changes in T_2 were observed for all five pigs during in vivo ablations of liver tissue. The mean ± SD cooling time constant for the five pigs was 241 ± 74 s (range: 168 - 359 s). Examples for two pigs (Pig I and Pig II) are shown in Figure 6. The maximum temperature changes were 9.2 ℃ for Pig I and 12.6 ℃ for Pig II (Fig. 6a, 6d). The temperature change exhibited a heterogeneous spatial distribution, with a clear depressed region in the center of the beam path. Pig I generally had higher cooling time constants than Pig II (Fig. 6b, 6e). The mean ± SD cooling time constant of the heated region was 359 ± 83 s for Pig I and 168 ± 59 s for Pig II. Figure 6c and 6f show example graphs of the temperature change versus time for individual voxels. The SNR values ranged from 50 to 350 for TE_1 and 20 to 150 for TE_2.

4.3.4. Monitoring during a uterine fibroid HIFU treatment

For all nine patients undergoing uterine fibroid treatment, T_2 difference maps showed clear intensity changes in the adipose region from the last applied US sonication. The mean ± SD T2 value before the first sonication in the fat layer was 150.7 ± 3.9 ms (n = 9). The temporal resolution was sufficient to measure heat accumulation and cooling time constants. From the average cooling time constant of 10 min (n = 3), the temperature increase directly after the first therapy sonication was estimated by means of exponential extrapolation and ranged from 2 °C to 15 °C in the nine patients. Figure 7 shows the temperature evolution for the one patient that had received five therapy sonications, overlaid on the T_2 reference map obtained before the first therapy sonication. The cumulative effects of the overlapping areas of the US cones are clearly visible. Arc-like structures are also visible. The SNR values ranged from 150 to 500 for TE_1 and 60 to 230 for TE_2.

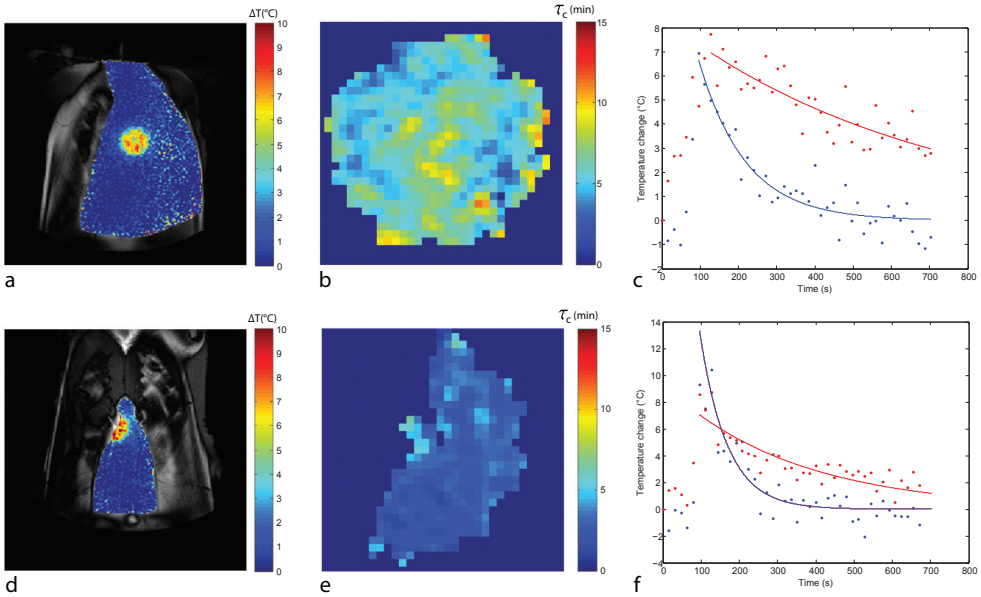

FIG. 6. The upper panels show the results for Pig I and the lower panels for pig II. (**a,d**) Peak temperature maps overlaying a T_2-w background image. (**b,e**) Zoomed-in regions showing the time constant maps for the cooling phase. (**c,f**) Temperature change versus time for the voxels with the longest and shortest cooling times. Dots are the T_2- based measurements and lines the mono-exponential fits.

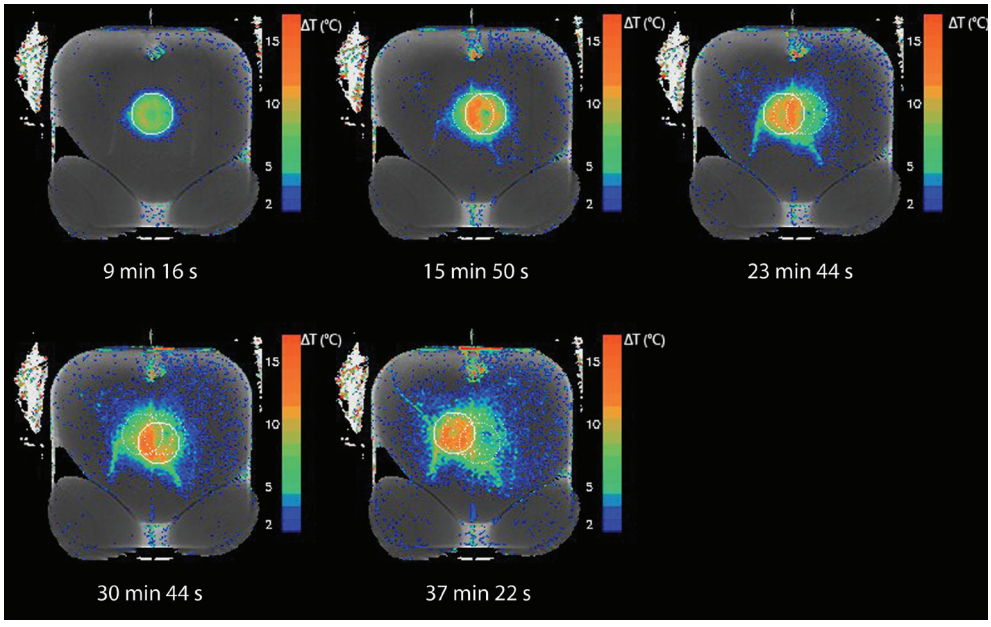

FIG. 7. Example of a T_2 reference map with T_2 difference based temperature overlay showing near-field heating in the subcutaneous adipose tissue layer after five consecutive volumetric sonications during a uterine fibroid treatment in a human patient. The intersection of the beam cone with the imaging slice during the latest sonication is shown as a solid circle. The sonications before that are shown as dotted circles. The time difference between the new T_2 measurement and the reference T_2 map is given.

4.4. Discussion

In the temperature range 25 °C - 45 ºC, a linear T_2 temperature dependence of adipose tissue was observed. The mean T_2 temperature coefficient of 5.17 ms/ºC had a high subject-to-subject reproducibility with an SD of 0.12 ms/ºC. This allowed us to continuously monitor the temperature change in the subcutaneous tissue layers in near real-time during cool-down experiments.

Reversible T_2 changes were found in the temperature range from 25 °C to 74 °C for the sequences implemented both with and without SPIR water suppression. Triglycerides, the signals of which predominantly constitute the signal from adipose tissue, are known to undergo reversible phase transitions (21). The reversible T_2 changes we found are consistent with the results of Kuroda et al. (22), who showed reversible T_2 changes for the CH_2 and CH_3 components of adipose tissue from 20 °C to 60 °C.

We took care to measure the T_2 temperature dependence in adipose tissue that was harvested directly postmortem. In prior experiments we had found a difference between the T_2 temperature coefficients of fresh and refrigerated samples; furthermore, the refrigerated samples displayed hysteresis in the T_2 values after heating. For clinical applications, the T_2 temperature coefficients and inter-subject variations will need to be evaluated. This would require fresh human adipose tissue samples, which would have to be obtained directly post-mortem or obtained from fat reduction surgery; this was outside the scope of the present study.

Furthermore, since the employed multiecho imaging sequence is also intrinsically T_1-weighted, sequence modifications affecting the TE, interecho spacing, refocusing pulse slice profile, or k-space sampling scheme can be expected to modify the observed T_2 temperature dependence (23–26). Moreover, because we are dealing with adipose tissue, J-coupling between fatty acid groups may influence the measured T_2 value depending on the chosen interecho spacing (17). These issues were avoided by using the same protocol for the calibrations as for the temperature monitoring in the near field.

Equation 1 was used as the basic relaxation model for characterizing the signal change between two echo times. Further research may investigate the actual T_1 and T_2 contrast contributions from the different fatty acid components. Although the same protocol was used for the calibrations as for the near-field measurements, the B_1 field as well as the adipose fatty acid composition ratios may vary depending on the application. Regarding the B_1 variation, the calibration experiments revealed little variation in the T_2 temperature coefficient. Therefore, this would not limit the application of the proposed technique. Variation in adipose tissue fatty acid composition has been shown to give rise to temperature errors in T_1- based thermometry when this effect is neglected (22). However, the small intersubject variation in the T_2 temperature coefficients we found (Table 1) suggest little influence from this variation in the porcine samples investigated. This last issue would also have to be investigated for human subcutaneous adipose tissue.

Differences between the T_2 temperature coefficient and T_2 offset values were found between the sequences with and without SPIR water suppression. This may be explained by the suppression of the CH=CH peak (5.4 ppm) in the fat spectrum, which is close to the frequency of water (4.7 ppm). The difference may also be due to the suppression of signal coming from water containing structures in the fat layer such as the cell cytoplasm, the interstitial space, or mixed-in regions of aqueous tissue. Our observations may favor the use of water suppression to obtain consistent T_2 values. No water suppression was used for the uterine fibroid patients, as these measurements were performed prior to the comparison study.

For the ex vivo HIFU experiment, a slightly larger temperature change was recorded with the probe than based on the T_2 maps (Fig. 5b). This may be due to ultrasound absorption in the fiber tip. The ultrasound absorption would lead to local heating, overestimating the temperature change when compared with the T_2-based temperature maps, which represent a larger 2.50 × 2.81 × 5 mm^3 volume. The maximum temperature change showed large spatial heterogeneities for the in vivo pig experiments. This can be explained by the spatially varying fat thickness, which influences the amount of US energy absorbed as well as the local thermal properties in the near field. Additionally, the temperature change maps show a clear depressed region in the center of the beam path. The intensity of the ultrasound waves is lower there because the used transducer array has no transmitting elements in the center.

Noise limits voxel-wise interpretation of the cooling time constant maps, but on a larger scale, a heterogeneous spatial distribution of cooling time constants was observed. Large variations in cooling time constants were found both intra-subject and inter-subject in the porcine experiments. The cooling time will depend on factors such as the spatial distribution of absorbed acoustic power and tissue perfusion. The cooling time can be expected to be geometry- and subject-specific, which underlines the need for individual observation of the cool-down process to avoid cumulative heating of subcutaneous tissue and to ensure time-efficient therapy sessions, by avoiding long waiting times between subsequent sonications. The sequence used in this study to acquire T_2 maps had an acquisition time of 16 s. This was fast enough to monitor the cool-down process in adipose tissue, which is slow due to its thermal properties (as mentioned in the Introduction). This would also not be an issue during most HIFU treatments, because other scans are often not required in the cooling period in between subsequent sonications.

For the uterine fibroid treatment illustrated in Figure 7, a maximum temperature change of 15 °C was measured. With a body temperature of 37 °C, the absolute temperature would be more than 50 °C, which means that within the duration of a typical sonication, the lethal thermal dose could be reached in adipose tissue (27). Although the adipose tissue layer was rather close to the skin, and the lethal thermal dose for skin is lower than for fat (27), no skin burns were found in all nine patients undergoing the uterine fibroid treatment. Additionally, the posttreatment T_2-weighted images revealed no edema formation in the subcutaneous tissue layers. One possible explanation for this observation may be a lower initial temperature than 37 °C due to the cooling effect of the gel pad, which is in direct contact with the skin. Also, the T_2 temperature dependence in porcine subcutaneous adipose samples may be different than that for human samples. Furthermore, the clinically relevant thermal dose safety limit for adipose tissue would have to be explored further.

It is in principle also possible to use the presented method to monitor the heating process in adipose tissue during sonications. Although quantitative T_2 measurements are >10 times slower than PRFS measurements of comparable resolution, the approach is still suitable for near-field monitoring, since the lower power density leads to a slower temperature increase compared with that in the beam focus. However, it complicates simultaneous observation of the temperature increase in the focal area, which limits volume coverage or scan time. Ideally, a combined PRFS-T_2 mapping sequence may be used in which PRFS thermometry monitors the rapid temperature changes in the focal point, and T_2 thermometry monitors the slow heat build-up in the near field, so as to shorten the required resonication delay.

In conclusion, we have shown that thermometry based on T_2 mapping allows monitoring of the near field temperature in adipose tissue during the cool-down period. One drawback is the need for tissue- and imaging protocol-specific calibrations. The feasibility of the method in in vivo pig and human experiments was proven, and the method was quantitatively verified in an ex vivo HIFU experiment. Furthermore, it was possible to measure the heat accumulation over a longer period of time.

4.5. Acknowledgments

We thank Gerald Schubert for technical support, Joost Wijlemans for help in setting up and performing animal experiments, and Marlijne Ikink for help in performing near-field thermometry during patient treatment procedures.

4.6. References

1. Hynynen K. MRIgHIFU: a tool for image-guided therapeutics. J Magn Reson Imaging 2011;34:482–493.
2. Taylor DG, Bore CF. A review of the magnetic-resonance response of biological tissue and its applicability to the diagnosis of cancer by NMR radiology. J Comput Tomogr 1981;5:122–134.
3. Quesson B, de Zwart JA, Moonen CTW. Magnetic resonance temperature imaging for guidance of thermotherapy. J Magn Reson Imaging 2000;12:525–533.
4. ter Haar GR. High intensity focused ultrasound for the treatment of tumors. J Card 2001;18:317–322.
5. Damianou C, Hynynen K. Focal spacing and near-field heating during pulsed high-temperature ultrasound therapy. Ultrasound Med Biol 1993;19:777–787.
6. Kopelman D, Papa M. Magnetic resonance-guided focused ultrasound surgery for the noninvasive curative ablation of tumors and palliative treatments: a review. Ann Surg Oncol 2007;14:1540–1550.
7. Mougenot C, Kohler MO, Enholm J, Quesson B, Moonen C. Quantification of near-field heating during volumetric MR-HIFU ablation. Med Phys 2011;38:272–282.
8. Henriques FC, Moritz AR. Studies of thermal injury. I. The conduction of heat to and through skin and the temperatures attained therein. A theoretical and an experimental investigation. Am J Pathol 1947;23:530–549.
9. Cohen ML. Measurement of the thermal properties of human skin. A review. J Invest Dermatol 1977;69:333–338.
10. ESHO Task Group Committee. Treatment planning and modeling in hyperthermia: a task group report of the European Society for Hyperthermic Oncology. Rome: Tor Vergata; 1992.
11. Kim YS, Keserci B, Partanen A, Rhim H, Lim HK, Park MJ, Kohler MO. Volumetric MR-HIFU ablation of uterine fibroids: role of treatment cell size in the improvement of energy efficiency. Eur J Radiol 2012;81:3652–3659.
12. De poorter J. Noninvasive MRI thermometry with the proton resonance frequency method-study of susceptibility effects. Magnet Reson Med 1995;34:359–367.
13. Cline HE, Hynynen K, Hardy CJ, Watkins RD, Schenck JF, Jolesz FA. MR temperature mapping of focused ultrasound surgery. Magnet Reson Med 1994;31:628–636.
14. Gandhi S, Daniel BL, Butts K. Temperature Dependence of Relaxation Times in Bovine Adipose Tissue. In Proceedings of the 6th Annual Meeting of ISMRM,

Sydney, Australia, 1998. p. 701.
15. Graham SJ, Bronskill MJ, Henkelman RM. Time and temperature dependence of MR parameters during thermal coagulation of ex vivo rabbit muscle. Magnet Reson Med 1998;39:198–203.
16. Kaldoudi E, Williams SC, Barker GJ, Tofts PS. A chemical shift selective inversion recovery sequence for fat-suppressed MRI: theory and experimental validation. Magn Reson Imaging 1993;11:341–355.
17. Constable RT, Anderson AW, Zhong J, Gore JC. Factors influencing contrast in fast spin-echo MR imaging. Magn Reson Imaging 1992;10: 497–511.
18. Kohler MO, Mougenot C, Quesson B, Enholm J, Le Bail B, Laurent C, Moonen CTW, Ehnholm GJ. Volumetric HIFU ablation under 3D guidance of rapid MRI thermometry. Med Phys 2009;36:3521–3535.
19. Gudbjartsson H, Patz S. The Rician distribution of noisy MRI data. Magn Reson Med 1995;34:910–914.
20. Wijlemans J, van den Bosch Mvd, de Greef M, Bartels LW, Moonen C, Ries M, Schubert G, Kohler M, Ylihautala M. In-vivo evaluation of volumetric magnetic resonance-guided high-intensity focused ultrasound (MR-HIFU) ablation in porcine liver. In Proceedings of the 13th International Symposium on Therapeutic Ultrasound, Shanghai, China, 2013. p. 138.
21. Graham SJ, Stanisz GJ, Kecojevic A, Bronskill MJ, Henkelman RM. Analysis of changes in MR properties of tissues after heat treatment. Magn Reson Med 1999;42:1061–1071.
22. Kuroda K, Iwabuchi T, Obara M, Honda M, Saito K, Imai Y. Temperature dependence of relaxation times in proton components of fatty acids. Magn Reson Med Sci 2011;10:177–183.
23. Hennig J. Multiecho imaging sequences with low refocusing flip angles. J Magn Reson 1988;78:397–407.
24. Glover G, Tkach J, Shimakawa A. Reduction of non-equilibrium effects in RARE sequences. In Book of abstracts: Society of Magnetic Resonance in Medicine 1991. Berkeley, California: Society of Magnetic Resonance in Medicine, 1991. p. 1242.
25. Le Roux P, Hinks RS. Stabilization of echo amplitudes in FSE sequences. Magn Reson Med 1993;30:183–190.
26. Norris DG. Ultrafast low-angle RARE: U-FLARE. Magn Reson Med 1991;17:539–542.
27. Dewey WC. Arrhenius relationships from the molecule and cell to the clinic. Int J Hyperthermia 2009;25:3–20.

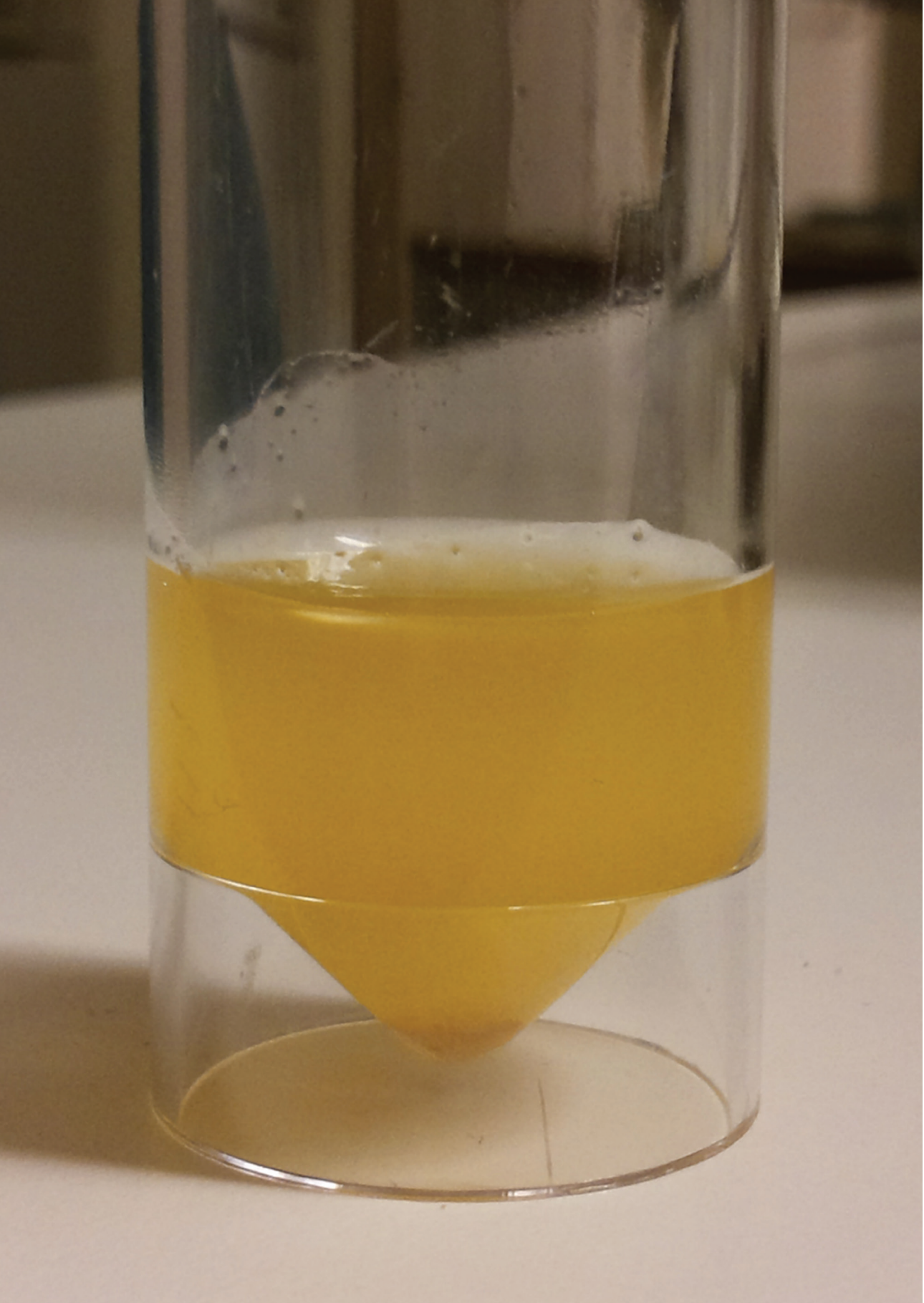

CHAPTER 5

The T_1 and T_2 temperature dependence of female human breast adipose tissue at 1.5 T: Groundwork for monitoring thermal therapies in the breast

ABSTRACT

Purpose: To investigate T_1 and T_2 temperature dependence of female breast adipose tissue at 1.5T in order to evaluate the applicability of relaxation-based MR thermometry in fat for monitoring of thermal therapies in the breast.

Methods: Relaxation times T_1, T_2, and T_{2TSE} (the apparent T_2 measured using a turbo spin echo readout sequence) were measured in seven fresh adipose breast samples for temperatures from 25 to 65 °C. Spectral water suppression was used to reduce the influence of residual water signal. The temperature dependence of the relaxation times was characterized. The expected maximum temperature measurement errors based on average calibration lines were calculated. Additionally, the heating-cooling reversibility was investigated for two samples.

Results: The T_1 and T_{2TSE} temperature (T) dependence could be well fit with an exponential function of 1/T. A linear relationship between T_2 and temperature was found. The temperature coefficients (mean ± inter-sample standard deviation) of T_1 and T_{2TSE} increased from 25 °C ($dT_1/dT = 5.35 \pm 0.08$ ms/°C, $dT_{2TSE}/dT = 3.82 \pm 0.06$ ms/°C) to 65 °C ($dT_1/dT = 9.50 \pm 0.16$ ms/°C, $dT_{2TSE}/dT = 7.99 \pm 0.38$ ms/°C). The temperature coefficient of T_2 was 0.90 ± 0.03 ms/°C. The temperature-induced changes in the relaxation times were found to be reversible after heating to 65 °C.

Conclusion: Given the small inter-sample variation of the temperature coefficients, relaxation-based MR thermometry appears feasible in breast adipose tissue, and may be used as an adjunct to PRFS thermometry in aqueous tissue (glandular +tumor).

5.1. Introduction

There is increased interest in the application of minimally invasive thermal therapies for breast cancer. These therapies include thermal ablation (1) techniques, in which the aim is to achieve high temperatures (commonly above 56 °C) in order to cause necrosis of the tumor tissue. The energy in ablation therapies may be delivered with radiofrequency (2), lasers (3), or focused ultrasound (4). Additionally, the application of mild hyperthermia (with temperatures slightly above body temperature) has drawn attention for radio- and chemo- sensitization (5,6), or for drug release from thermosensitive carriers (7). Compared to conventional surgery, minimally invasive techniques are expected to have less complications and better cosmetic results. MRI, with its excellent soft tissue imaging capabilities (8), may be combined with these thermal therapies and be used for treatment planning, guidance, and evaluation. An advantage of MRI is that it allows for temperature mapping. Reliable MR temperature monitoring during thermal therapies facilitates sufficient thermal dose deposition at the tumor site and helps avoid unwanted heating of tissue outside the target area. The proton resonance frequency shift (PRFS) is the most commonly used MR temperature monitoring technique. PRFS MR thermometry uses the temperature dependence of the electron screening constant of the hydrogen nuclei (protons) in water molecules (9), and can therefore be used in aqueous tissues. A temperature increase leads to an increase in shielding of the water hydrogen proton by the electron cloud (because of less strong hydrogen bonding (10)) and to a subsequent decrease in the nuclear magnetic field experienced by the protons. A change in the nuclear field yields a corresponding shift in the proton resonance frequency, which can be measured with phase mapping or spectroscopy techniques. An advantage of PRFS thermometry is the almost tissue type-independent thermal coefficient for the screening constant of hydrogen nuclei in water, even after coagulation (11).

However, for monitoring thermal therapy in the breast or other organs that contain a mixture of water and fat, temperature monitoring in adipose tissues is also desirable. Although breast tumor tissue and glandular tissue both are aqueous tissues, breast tumors are often embedded in adipose tissue, and in the margins outside the tumor visible on MRI tumor cells may also be present (12). Due to the fact that adipose tissue has a lower specific heat capacity (13) and lower heat conductivity (13,14) compared to other tissues in the breast, unwanted heat accumulation may especially occur in adipose tissue when ablating breast tumors. Additionally, temperature monitoring in the -often fatty- tumor margins, is required to ensure that a lethal thermal dose is reached there. However, PRFS thermometry is complicated in adipose tissue due to the very low water content and the absence of hydrogen bonding between fat molecules. As an alternative method for measuring temperatures in adipose tissue, MR thermometry based on the temperature dependence of T_1 and T_2 relaxation times has been proposed (15). At 0.2 T, the T_1 of porcine fat increased with temperature and was reversible during the cooling phase after heating to above 43 °C (16). At 0.5 T both T_1 and T_2 of bovine adipose tissue were shown to increase with temperature (15). At 1.5 T, the T_1 of porcine adipose tissue was found to increase linearly with temperature (17), and at 3T the same was observed for the T_1 of human breast adipose tissue (18,19). The apparent T_2 of porcine adipose tissue increased with temperature and was reversible after heating (20). Additionally, the change in T_1 -weighting has been used for thermometry in rabbit fatty tissue at 1.5 T (21). However, there is limited data available regarding the temperature dependence of human breast adipose tissue at 1.5 T .

Therefore, the aim of this study was to measure and characterize the temperature dependence of T_1 and T_2 of adipose breast tissue samples, in order to investigate the feasibility of T_1 and T_2 based MR thermometry in breast adipose tissue. All data was acquired at 1.5 T,

which is the field strength currently used by our group for MR-guided high-intensity focused ultrasound (MR-HIFU) ablation of breast tumors, using a dedicated breast MR-HIFU system (22). The range in the inter-sample temperature dependence of the relaxation times was used to investigate the feasibility of relaxation-based relative and absolute thermometry.

5.2. Methods

In controlled heating and cooling experiments, relaxation times were measured at temperatures ranging from 25 to 65 °C. For each sample, the temperature dependence of the relaxation times was characterized by fitting a model to the measurements. The inter-sample variation in the temperature dependence was interpreted in terms of the expected temperature measurements errors that would occur when using an average calibration curve (as obtained by averaging the parameters of the model). Additionally, the heating-cooling reversibility of the relaxation time temperature dependence, and the comparison of the temperature dependence of the relaxation times for adipose tissue with those of only its fatty content was investigated to further determine the suitability of relaxation based MR thermometry for clinical applications in the breast.

5.2.1. Patient population and setup

Seven breast fat samples were obtained from seven women (age subject for sample nr. 1: 40, 2: 56, 3: 21, 4: 23, 5: 23, 6: 25, 7: 22 years) undergoing breast reduction surgery. Collection of these samples was approved by the Biobank review committee of the University Medical Center Utrecht. The samples were kept at room temperature and the MR experiments were performed on the day of surgery. Each sample was placed in a 50-mL Perspex cylindrical tube and heated in a temperature stabilized closed circuit water bath (Figure 1a). The water bath was placed at the iso-center of the bore of a 1.5-T MRI scanner (Achieva, Philips Healthcare, Best, The Netherlands) and two flexible receive coils (diameter = 20 cm) were used for signal detection. The actual temperature of the samples was monitored with a calibrated fiber optic probe (Luxtron, LumaSense, Santa Clara, California, USA), by placing the tip of the probe in the center of the sample. The MR scans were started when the probe temperature readings had been stable (within 0.2 °C) for at least 15 minutes.

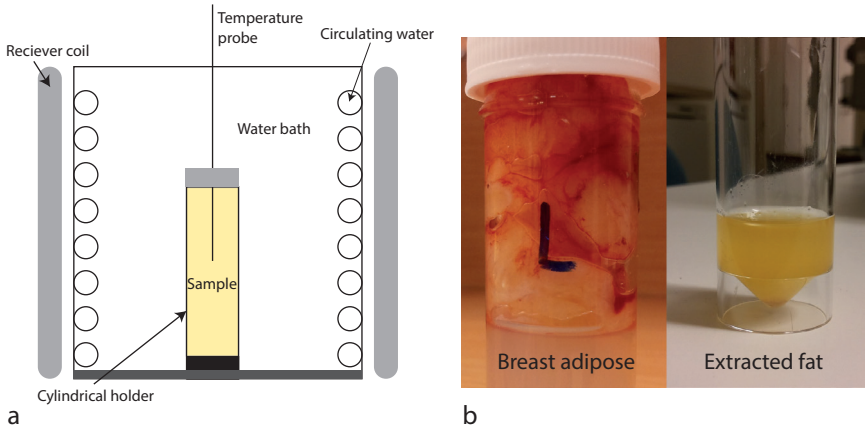

FIG. 1. (**a**) Schematic drawing of the water bath with the sample and (**b**) photos of fresh breast adipose tissue and the extracted fat.

5.2.2. MR protocol

The values of three relaxation times were measured: the longitudinal relaxation time (T_1), the transverse relaxation time (T_2), and the apparent transverse relaxation time obtained using a Turbo Spin Echo (TSE) sequence (T_{2TSE}). The most important parameter settings of the pulse sequences used are given below.

T_1: T_1 maps were calculated from a series of 2D inversion recovery TSE scans with inversion times = 150, 300, 800, and 3000 ms. The parameter settings were: field of view (FOV) = 160 × 160 mm^2, matrix = 80 × 80, slice thickness (ST) = 10 mm, repetition time (TR) = 4000 ms, number of signal averages (NSA) = 2, effective echo time = 20 ms, readout bandwidth = 0.5 Hz/pixel. TSE factor = 8, TSE echo spacing = 4.4 ms, total scan duration = 5 min 36 s. The scans were acquired with Spectral Inversion Water Suppression (SPIR-WS) because of the presence of a small amount of water in adipose tissue and possible presence of residual fibro-glandular tissue. Prior to the first inversion sequence, a full preparation scan was performed and it was checked whether the larmor frequency corresponded with the water peak.

T_2: T_2 mapping was performed with a multi spin echo sequence. The following parameters were used: 8 echo times = 25, 50, 75, 100, 125, 150, 175, and 200 ms, TR= 2500 ms, NSA =1, water-fat shift = 1 pixel, total scan duration = 1 min 30 s. The same FOV, matrix size, and slice thickness were used as for T_1 mapping. Similar to T_1 mapping, T_2 mapping was acquired with SPIR-WS.

T_{2TSE}: For faster temperature mapping in adipose tissue a dual echo TSE sequence was used, similar to the one previously used for T_2-based temperature mapping in abdominal fat for MR-HIFU near field monitoring (20). T_{2TSE} reflects mixed T_2 and T_1 relaxation effects due to the presence of stimulated and indirect echoes in a TSE echo train (23). The parameters were: FOV = 160 × 160 mm^2, acquired voxel size = 1.67 × 1.67 × 5 mm^3, effective echo times 40 and 180 ms. TR = 2000 ms, TSE factor = 38, refocusing pulse angle = 160°, echo spacing = 5.80 ms, NSA = 3, readout bandwidth = 429 Hz, total scan duration = 30 s, spectral water suppression (SPIR-WS). During the reconstruction, the in-plane pixel size was interpolated using zero padding to 1x1 mm^2.

5.2.3. Experiments

Temperature dependence of relaxation parameters

To compare the temperature dependence of the relaxation times, for all seven samples the temperature was increased stepwise from room temperature to 65 °C, and at five stable temperatures of 25, 35, 45, 55, and 65 °C, T_1, T_2, and T_{2TSE} maps were acquired.

Reversibility of temperature dependence

To investigate the reversibility of the temperature dependence of T_1, T_2, and T_{2TSE}, for two samples, T_1, T_2, and T_{2TSE} maps were acquired first during stepwise heating to 65 °C and then during stepwise cooling back down to 25 °C.

Adipose tissue compared with extracted fat

In one sample the T_1 and T_2 temperature dependence of adipose tissue was compared to the temperature dependence of the extracted fat component of the same tissue (Figure 1b). This was investigated because HIFU ablation of adipose tissue may result in changes in the water and fat spatial distribution (for example by merging of cell lipid droplets after membrane destruction). The lipid content was separated by compressing the tissue and mechanically extracting the fat.

Parameter calculation

For each voxel, T_1 was obtained by fitting simultaneously the real (S_r) and imaginary (S_i) transverse signal versus inversion time (TI) with the following equations (24):

$$S_r = S_{0r}\left(1-2\left(1+\varepsilon\right)e^{-\frac{TI}{T1}}\right), \qquad S_i = S_{0i}\left(1-2\left(1+\varepsilon\right)e^{-\frac{TI}{T1}}\right) \quad [1]$$

where $S_0 = S_{0r} + iS_{0i}$ is the signal from the thermal equilibrium magnetization and ε accounts for imperfect magnetization inversion by the 180° pulse. T_2 was calculated for each voxel by fitting the magnitude signal $|S|$ versus TE with:

$$|S| = |S_0|e^{-\frac{TE}{T2}} \quad [2]$$

For the fast T_2 mapping, T_{2TSE} was calculated for every voxel with:

$$T_{2TSE} = \frac{TE_2 - TE_1}{\ln\left(\frac{|S(TE_1)|}{|S(TE_2)|}\right)} \quad [3]$$

where $|S(TE_1)|$ and $|S(TE_2)|$ are the magnitude signals at the effective echo times of 40 and 180 ms respectively.

5.2.4. Models of relaxation temperature dependence

For all relaxation parameter maps, the mean and standard deviation of measured values within a region of interest (ROI) containing 30 voxels was calculated. The ROI was manually placed in a large adipose structure in the MR image. An exponential temperature dependence of T_1 with 1/T was used as a model for a free-state molecular system (25,26):

$$T_1 = A\,e^{-\frac{B}{T+273.15}} \quad [4]$$

where A (ms) and B (°C) are parameter constants and T is the tissue temperature (°C). For a smaller temperature range, the T_1 temperature dependence is commonly approximated by a linear function (17,19,25,27-30):

$$T_1 = C + DT \quad [5]$$

where C (ms) and D (ms/°C) are again parameter constants and D is the T_1 temperature dependence. Fewer studies have investigated the T_2 temperature dependence for tissues, but for adipose tissue a linear temperature dependence has been observed for a smaller temperature range (20,28). In the current study the choice of eq [4] or [5] was based on the best fit for the data (by comparing R^2 for the two fits). This resulted in using eq. [4] for T_1(T) and for T_{2TSE}(T), and using eq. [5] for T_2(T). The parameter constants were obtained for each of the 30 voxels by fitting the temperature-dependent models to the measurements obtained for the five temperatures (25 – 65 °C) during heating.

For the set of seven samples characterized by eq. [4], the range of absolute temperatures

(T) for the seven samples calculated using the fit function at a given relaxation time T_1 or T_{2TSE} was used to estimate the accuracy of absolute temperature measurements. Commonly, however, only changes in temperature are measured with MRI. To compare the temperature coefficients for the breast fat samples, parameter B (from eq [5]) was used for T_2(T). For T_1(T) and T_{2TSE}(T) the temperature coefficient depends on the initial temperature T_0. Given the parameters A and B from eq. [4], the T_1- and T_{2TSE}- temperature dependence at initial temperatures T_0 = 25, 35, 45, 55, and 65 °C was calculated using:

$$\left(\frac{dT_1}{dT} or \frac{dT_{2TSE}}{dT}\right)\Bigg|_{T=T_0} = A\frac{B}{T_0^2}e^{-\frac{B}{T_0}} \qquad [6]$$

The reversibility of the temperature dependence of T_1, T_2, and T_{2TSE} was also investigated by comparing the parameter temperature coefficients obtained during heating (25 to 65 °C) to those during cooling (65 to 25 °C). Additionally, the T_1 and T_2 temperature coefficients of adipose tissue were compared to those of its extracted fat component.

5.3. Results

5.3.1. Temperature dependence of relaxation parameters

T_1 and T_{2TSE} temperature dependence

Figure 2 shows the mean T_1 (Figure 2a) and T_{2TSE} (Figure 2b) measurements of the ROI plotted against the fiber optic probe temperature readings for the seven samples. The measurements were well fit with the exponential equation [4], having residuals less than 4%. Table 1 gives the mean and standard deviation of the found voxel parameters A and B (of eq. [4].) for the individual samples. The spread of temperature values for a given relaxation time measurement (red doubled-arrowed lines in Figure 2) indicates the expected accuracy of absolute temperature measurements for a sample based upon the data collected from the seven samples and was between 2.2 and 4.3 °C for T_1 and 0.7 and 2.2 °C for T_{2TSE}. The temperature coefficient at baseline temperatures 25, 35, 45, 55, and 65 °C are given in Table 2 for T_1 and Table 3 for T_{2TSE}. dT_1/dT increased from 5.35 ± 0.08 ms/°C at 25 °C to 9.50 ± 0.16 ms/°C at 65 °C. dT_{2TSE}/dT increased from 3.82 ± 0.06 ms/°C at 25 °C to 7.99 ± 0.38 ms/°C at 65 °C. The variation in inter-sample dT_1/dT and dT_{2TSE}/dT measurements (quantified with the standard deviation) was on the same order (or smaller than) the intra-sample variation.

T_1 and T_{2TSE} calibration lines:

Calibration lines were given as the average of the sample parameters A and B (Table 1), i.e. $T_1 = 2.57\times10^5\ e^{-2.08\times10^3/T}$ and $T_{2TSE} = 6.46\times10^5\ e^{-2.49\times10^3/T}$. Given these calibration lines, Figure 3 shows the maximum error in the measured temperature change from the set of seven samples, when assuming a baseline temperature before heating of 37 °C. The maximum error in the measured temperature change depends both on the initial sample temperature $T_{0\ sample}$ (which in practice may not have been 37 °C) and change in sample temperature .. from the initial temperature. For instance, if the initial sample temperature corresponds with the estimated initial temperature (37 °C, dashed vertical line in Figure 3), the maximum temperature change error was less than 1.0 °C for T_1 and less than 2.6 °C for T_{2TSE} for a temperature change up to 30 °C.

T_2 temperature dependence

In Figure 4 the T_2 measurements are plotted versus fiber optic temperature measurements, and the least squares fit ($R^2 > 0.97$) for eq. 6 is shown. Table 4 gives the average T_2-temperature dependence coefficients for the samples. The average value for all seven samples was 0.90 ± 0.03 ms/°C (range: 0.89 - 0.95 ms/°C). For all samples, the intra-sample $\Delta T_2 / \Delta T$ variation was larger than the inter-sample variation in $\Delta T_2 / \Delta T$.

5.3.2. Reversibility of temperature dependence

Figure 5 shows the T_1, T_2, and T_{2TSE} measurements during heating and cooling for two samples. Small differences were found between the temperature dependence of all relaxation times during the heating and cooling phase. The difference in the temperature dependence of T_1, T_2 and T_{2TSE} for the heating and cooling curves was less than 0.42 ms/°C (Table 2), 0.03 ms/°C (Table 3), and 0.16 ms/°C (Table 4) respectively.

5.3.3. Adipose tissue compared with extracted fat component

In Figure 6 the T_1 and T_2 temperature dependence of adipose tissue for one sample is compared with the temperature dependence of its extracted fat component. For T_1, the difference in temperature coefficients between adipose and the extracted fat was less than 0.3 ms/°C (Table 2). For T_2 the difference in temperature coefficients was 0.03 ms/°C (Table 4).

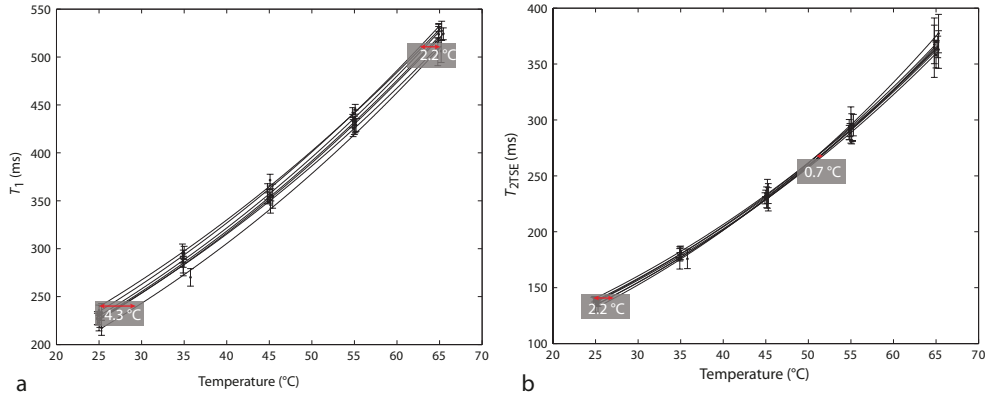

FIG. 2. Mean and standard deviation (error bars) of the (**a**) T_1 and (**b**) T_{2TSE} measurements versus temperature (N = 7 samples). The fit function is given by equation [4].

Table 1. The optimal values for parameters A and B of equation [4] for the T_1- and T_{2TSE} temperature dependence of the samples.

	T_1		T_{2TSE}	
Sample	**A $\times 10^5$ (ms)**	**B $\times 10^3$ (°C)**	**A $\times 10^5$ (ms)**	**B $\times 10^3$ (°C)**
1	2.00 ± 0.42	2.00 ± 0.07	4.51 ± 1.33	2.39 ± 0.09
2	2.56 ± 0.98	2.07 ± 0.13	4.96 ± 1.55	2.42 ± 0.09
3	3.25 ± 1.06	2.17 ± 0.10	9.75 ± 3.59	2.64 ± 0.12
4	2.58 ± 0.36	2.09 ± 0.05	5.86 ± 1.73	2.48 ± 0.09
5	2.32 ± 0.56	2.06 ± 0.08	7.62 ± 5.20	2.52 ± 0.18
6	2.67 ± 0.50	2.10 ± 0.06	5.04 ± 1.86	2.42 ± 0.12
7	2.62 ± 0.50	2.10 ± 0.07	7.46 ± 6.41	2.51 ± 0.18
Average:	**2.57 ± 0.38**	**2.08 ± 0.05**	**6.46 ± 1.90**	**2.49 ± 0.08**

Table 2. The T_1-temperature dependence (in ms/°C) at a given initial temperature T_0. For the individual samples ± denotes the standard deviation (N = 30) over the voxels of the ROI. For the average value, ± is the standard deviation over the mean of the seven samples.

Sample	**T_0 = 25 °C**	**T_0 = 35 °C**	**T_0 = 45 °C**	**T_0 = 55 °C**	**T_0 = 65 °C**
1 *heating*	5.39 ± 0.09	6.28 ± 0.14	7.23 ± 0.20	8.24 ± 0.27	9.30 ± 0.36
cooling	5.38 ±0.10	6.26 ±.0.13	7.20 ±0.16	8.20 ± 0.21	9.25 ± 0.27
extracted fat	5.48 ±0.12	6.41 ± 0.18	7.41 ±0.25	8.47 ± 0.33	9.60 ± 0.43
2 *heating*	5.45 ± 0.07	6.39 ± 0.14	7.41 ± 0.24	8.49 ± 0.36	9.64 ± 0.50
3 *heating*	5.25 ± 0.14	6.23 ± 0.22	7.29 ± 0.31	8.44 ± 0.43	9.67 ± 0.58
4 *heating*	5.40 ± 0.05	6.35 ± 0.12	7.38 ± 0.10	8.47 ± 0.15	9.63 ± 0.21
cooling	5.40 ± 0.09	6.27 ± 0.12	7.20 ± 0.17	8.18 ± 0.23	9.21 ± 0.31
5 *heating*	5.24 ± 0.15	6.14 ± 0.20	7.10 ± 0.27	8.13 ± 0.35	9.22 ± 0.45
6 *heating*	5.34 ± 0.06	6.28 ± 0.09	7.31 ± 0.13	8.40 ± 0.19	9.57 ± 0.27
7 *heating*	5.36 ± 0.09	6.30 ± 0.14	7.32 ± 0.21	8.41 ± 0.28	9.57 ± 0.37
Average (N=7): *(of heating)*	**5.35 ± 0.08**	**6.28 ± 0.08**	**7.29 ± 0.09**	**8.36 ± 0.12**	**9.50 ± 0.16**

Table 3. The T_{2TSE}-temperature dependence (in ms/°C) at a given initial temperature T_0. For the individual samples ± denotes the standard deviation (N = 30) over the voxels of the ROI. For the average value, ± is the standard deviation over the mean of the seven samples.

Sample	T_0 = 25 °C	T_0 = 35 °C	T_0 = 45 °C	T_0 = 55 °C	T_0 = 65 °C
1 *heating*	3.73 ± 0.09	4.51 ± 0.15	5.38 ± 0.23	6.34 ± 0.33	7.39 ± 0.44
cooling	3.74 ± 0.08	4.55 ± 0.12	5.45 ± 0.18	6.45 ± 0.25	7.55 ± 0.33
2 *heating*	3.74 ± 0.11	4.57 ± 0.17	5.49 ± 0.25	6.52 ± 0.36	7.64 ± 0.48
3 *heating*	3.90 ± 0.19	4.87 ± 0.25	5.98 ± 0.33	7.24 ± 0.45	8.65 ± 0.60
4 *heating*	3.86 ± 0.12	4.73 ± 0.18	5.73 ± 0.26	6.83 ± 0.35	8.05 ± 0.46
cooling	3.87 ± 0.13	4.75 ± 0.19	5.73 ± 0.27	6.84 ± 0.37	8.05 ± 0.49
5 *heating*	3.81 ± 0.25	4.70 ± 0.37	5.71 ± 0.54	6.85 ± 0.76	8.11 ± 1.02
6 *heating*	3.77 ± 0.16	4.60 ± 0.24	5.52 ± 0.36	6.55 ± 0.48	7.69 ± 0.64
7 *heating*	3.90 ± 0.16	4.79 ± 0.24	5.81 ± 0.36	6.95 ± 0.53	8.22 ± 0.75
Average (N=7): *(of heating)*	**3.82 ± 0.06**	**4.69 ± 0.11**	**5.67 ± 0.18**	**6.77 ± 0.27**	**7.99 ± 0.38**

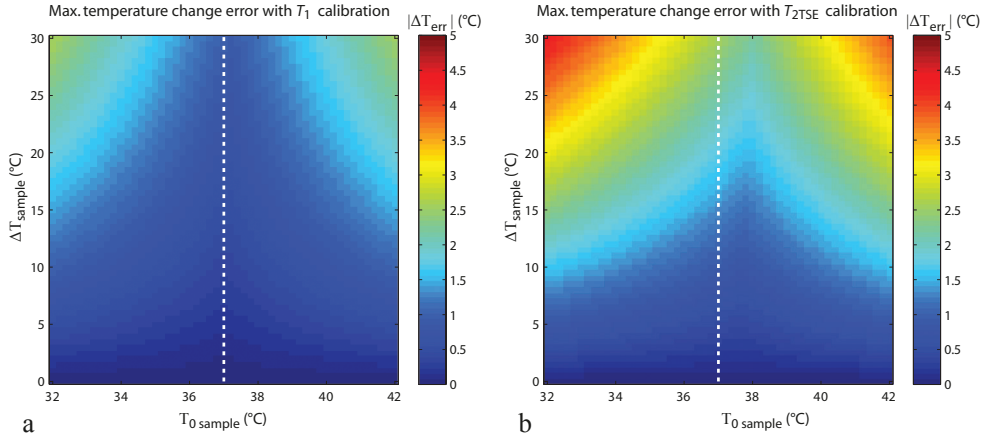

FIG. 3. The expected maximum absolute error in the measured temperature change from the set of seven samples when using the (**a**) T_1 and (**b**) T_{2TSE} average calibration line and assuming a baseline temperature of 37 °C.

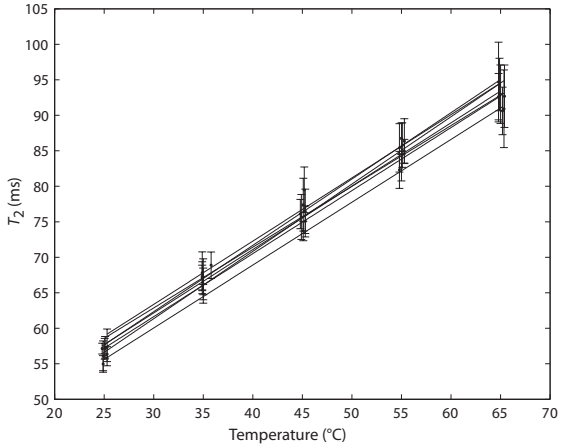

FIG. 4. Mean and standard deviation (error bars) of the T_2 measurements versus temperature (N = 7 samples). The fit is given by equation [6].

Table 4. The T_2-temperature dependence (in ms/°C). For the individual samples ± denotes the standard deviation (N = 30) over the voxels of the ROI. For the average value, ± is the standard deviation over the mean of the seven samples.

Sample	**$\Delta T_2/\Delta T$ (ms/°C)**
1 *heating*	0.89 ± 0.07
cooling	0.86 ± 0.08
extracted fat	0.92 ± 0.02
2 *heating*	0.89 ± 0.10
3 *heating*	0.89 ± 0.11
4 *heating*	0.89 ± 0.07
cooling	0.86 ± 0.07
5 *heating*	0.93 ± 0.15
6 *heating*	0.86 ± 0.12
7 *heating*	0.95 ± 0.10
Average (N=7): *(of heating)*	**0.90 ± 0.03**

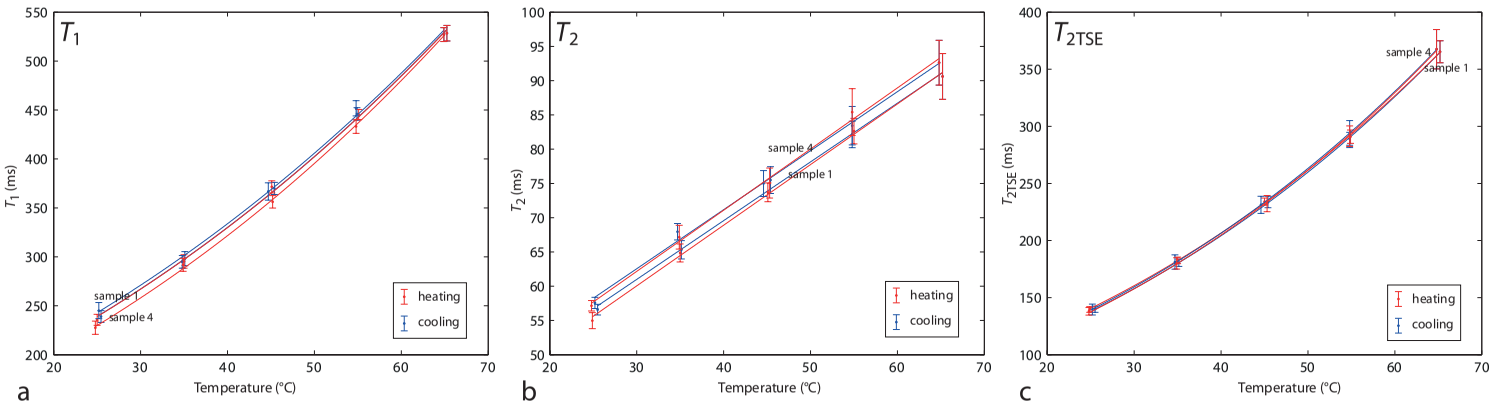

FIG. 5. The measured (**a**) T_1, (**b**) T_2, and (**c**) $T_{2\mathrm{TSE}}$ temperature dependence for two samples during heating (red line) and cooling (blue line).

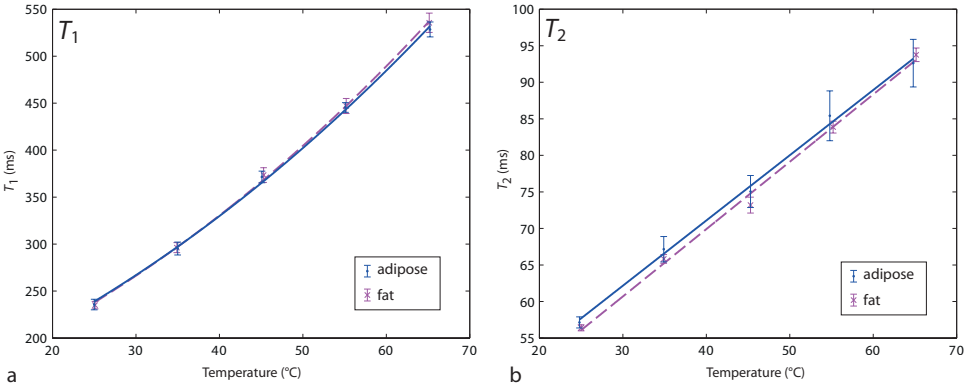

FIG. 6. The measured (**a**) T_1, and (**b**) T_2 temperature dependence for adipose tissue (solid blue line) and its extracted fat component (dashed magenta line).

5.4. Discussion

Small variations were found in the inter-sample temperature dependence of the three relaxation times T_1, T_2, and T_{2TSE} measured in this study (i.e. absolute differences less than 0.5 ms/°C for T_1 and 0.1 ms/°C for T_2 (Tables 2 and 4). Both T_1 and T_{2TSE} showed a non-linear temperature dependence (well modeled by the mono-exponential function in eq. [4].). The non-linearity demands a good baseline temperature estimate for reduced temperature measurement errors. For example: with an assumed baseline temperature of 37 °C, but an actual sample temperature between 34 and 40 °C and a sample temperature change of 30 °C, a maximum temperature change measurement error of 3 °C may be expected (Figure 3). The results (Figure 5) also suggest that T_1 and T_2 based thermometry is robust to heating of adipose tissue up to 65 °C (i.e. it is completely reversible) and not influenced by the cellular structures in which the fat resides (i.e. adipose tissue and fat showed a similar relaxation time temperature dependence). For measuring the absolute sample temperature, the best results were given by T_{2TSE} (Figure 2b), with a sample temperature accuracy of more than 2.2 °C.

The small inter-sample variation in the relaxation time-temperature dependence found in this study is consistent with the small variation in the apparent T_2-temperature dependence reported before for fresh adipose porcine samples (20). This small variation in coefficients would make relaxation-based MR thermometry also applicable to breast adipose tissue. In contrast, large inter-sample variations of the T_1 temperature dependence in breast fat samples have been reported by other studies (18), potentially resulting in temperature errors of up to 43%. The smaller variation found here may be due to the use of SPIR-water suppression in this study. Water suppression would reduce the influence of any residual water signal contributing to the measurement of the relaxation times. Additionally, the use of a temperature stabilized water bath, with the sample temperature kept constant during the MR acquisition may have resulted in more reproducible measurements. For all the relaxation parameters, the inter-sample temperature dependence was less or of the same order as the intra-sample variation (Tables 2-4). This may indicate that the current study was unable to probe very subtle differences in the sample temperature dependence for the relaxation times. However, the small variations found may also be due to differences in the fatty acid composition of the breast adipose samples (28). Whether variation in the temperature dependence of the relaxation times based on the whole fat signal could be linked to variation in fatty acid

composition would be interesting future work. One limitation to the current study was the relatively small sample size (N=7) and the homogeneity of some aspects of the patient group (i.e. all were undergoing a breast-reduction surgery operation.) However, there was a large variation in the age of the subjects (21 -56 years) included in this study.

To conclude, relaxation-based MR thermometry appears feasible for measuring temperature changes in adipose breast tissue during thermal therapy, for instance with MR-HIFU. The method will require adequate water suppression or reliable water-fat separation. In the future, relaxation based MR thermometry in adipose tissue (acquired for example with a turbo spin echo: i.e. T_{2TSE}) may be alternated with a PRFS acquisition in aqueous tissues for a complete temperature change map during thermal interventions in the breast.

5.5. Acknowledgements

This research was performed within the framework of CTMM, the Center for Translational Molecular Medicine, project VOLTA.

5.6. References

1. Ter haar G. Ultrasound Focal Beam Surgery. Ultrasound in Medicine and Biology 1995;21(9):1089-1100.
2. Jeffrey SS, Birdwell RL, Ikeda DM, Daniel BL, Nowels KW, Dirbas FM, Griffey SM. Radiofrequency ablation of breast cancer - First report of an emerging technology. Arch Surg-Chicago 1999;134(10):1064-1068.
3. Hallcraggs MA, Mumtaz H, Paley M, Wilkinson I, Chinn R, Bown SG. Laser Therapy for Treating Breast-Carcinoma - Mr-Histopathologic Correlation. Radiology 1995;197:136-136.
4. Gianfelice DC, Mallouche H, Lepanto L, Poisson R, Nassif E, Breton G. MR-guided focused ultrasound ablation of primary breast neoplasms: Works in progress. Radiology 1999;213P:106-107.
5. Raaphorst GP, Szekely JG. Thermal enhancement of cellular radiation damage: a review of complementary and synergistic effects. Scanning Microsc 1988;2(1):513-535.
6. Issels RD, Lindner LH, Verweij J, Wust P, Reichardt P, Schem BC, Abdel-Rahman S, Daugaard S, Salat C, Wendtner CM, Vujaskovic Z, Wessalowski R, Jauch KW, Durr HR, Ploner F, Baur-Melnyk A, Mansmann U, Hiddemann W, Blay JY, Hohenberger P. Neo-adjuvant chemotherapy alone or with regional hyperthermia for localised high-risk soft-tissue sarcoma: a randomised phase 3 multicentre study. Lancet Oncol 2010;11(6):561-570.
7. Grull H, Langereis S. Hyperthermia-triggered drug delivery from temperature-sensitive liposomes using MRI-guided high intensity focused ultrasound. Journal of Controlled Release 2012;161(2):317-327.
8. Taylor DG, Bore CF. A Review of the Magnetic-Resonance Response of Biological Tissue and Its Applicability to the Diagnosis of Cancer by NMR Radiology. Ct-J Comput Tomogr 1981;5(2):122-134.
9. Depoorter J. Noninvasive Mri Thermometry with the Proton-Resonance Frequency Method - Study of Susceptibility Effects. Magn Reson Med 1995;34(3):359-367.

10. Hindman JC. Proton Resonance Shift of Water in Gas and Liquid States. J Chem Phys 1966;44(12):4582.
11. Peters RD, Hinks RS, Henkelman RM. Ex vivo tissue-type independence in proton-resonance frequency shift MR thermometry. Magnet Reson Med 1998;40(3):454-459.
12. Schmitz AC, van den Bosch MAAJ, Loo CE, Mali WPTM, Bartelink H, Gertenbach M, Holland R, Peterse JL, Rutgers EJT, Gilhuijs KG. Precise correlation between MRI and histopathology - Exploring treatment margins for MRI-guided localized breast cancer therapy. Radiother Oncol 2010;97(2):225-232.
13. Henriques FC, Moritz AR. Studies of Thermal Injury .1. The Conduction of Heat to and through Skin and the Temperatures Attained Therein - a Theoretical and an Experimental Investigation. Am J Pathol 1947;23(4):531-&.
14. Cohen ML. Measurement of Thermal-Properties of Human-Skin - Review. J Invest Dermatol 1977;69(3):333-338.
15. Gandhi S, Daniel BL, Butts K. Temperature Dependence of Relaxation Times in Bovine Adipose Tissue. Proceedings 6th ISMRM; Sydney, Australia. 1998. p. 701.; 1998; Australia.
16. Peller M, Reinl HM, Weigel A, Meininger M, Issels RD, Reiser M. T1 relaxation time at 0.2 Tesla for monitoring regional hyperthermia: feasibility study in muscle and adipose tissue. Magn Reson Med 2002;47(6):1194-1201.
17. Hey S, de Smet M, Stehning C, Grull H, Keupp J, Moonen CT, Ries M. Simultaneous T1 measurements and proton resonance frequency shift based thermometry using variable flip angles. Magn Reson Med 2012;67(2):457-463.
18. Diakite M, Odeen H, Todd N, Payne A, Parker DL. Toward real-time temperature monitoring in fat and aqueous tissue during magnetic resonance-guided high-intensity focused ultrasound using a three-dimensional proton resonance frequency T1 method. Magn Reson Med 2014;72(1):178-187.
19. Todd N, Diakite M, Payne A, Parker DL. Hybrid proton resonance frequency/T1 technique for simultaneous temperature monitoring in adipose and aqueous tissues. Magn Reson Med 2013;69(1):62-70.
20. Baron P, Ries M, Deckers R, de Greef M, Tanttu J, Kohler M, Viergever MA, Moonen CT, Bartels LW. In vivo T2 -based MR thermometry in adipose tissue layers for high-intensity focused ultrasound near-field monitoring. Magn Reson Med 2014;72(4):1057-1064.
21. Hynynen K, McDannold N, Mulkern RV, Jolesz FA. Temperature monitoring in fat with MRI. Magnet Reson Med 2000;43(6):901-904.
22. Merckel LG, Bartels LW, Kohler MO, van den Bongard HJGD, Deckers R, Mali WPTM, Binkert CA, Moonen CT, Gilhuijs KGA, van den Bosch MAAJ. MR-Guided High-Intensity Focused Ultrasound Ablation of Breast Cancer with a Dedicated Breast Platform. Cardiovasc Inter Rad 2013;36(2):292-301.
23. Hennig J. Multiecho Imaging Sequences with Low Refocusing Flip Angles. J Magn Reson 1988;78(3):397-407.
24. Barral JK, Gudmundson E, Stikov N, Etezadi-Amoli M, Stoica P, Nishimura DG. A Robust Methodology for In Vivo T1 Mapping. Magn Reson Med 2010;64(4):1057-1067.
25. Parker DL, Smith V, Sheldon P, Crooks LE, Fussell L. Temperature distribution measurements in two-dimensional NMR imaging. Med Phys 1983;10(3):321-325.

26. Lewa J, Majewska Z. Temperature Relationships of Proton Spice-Lattice Relaxation Time T1 in Biological Tissues. Bulletin du Cancer 1980;67(5):525-530.
27. Nelson TR, Tung SM. Temperature-Dependence of Proton Relaxation-Times Invitro. Magn Reson Imaging 1987;5(3):189-199.
28. Kuroda K, Iwabuchi T, Obara M, Honda M, Saito K, Imai Y. Temperature Dependence of Relaxation Times in Proton Components of Fatty Acids. Magnetic Resonance in Medical Sciences 2011;10(3):177-183.
29. Cline HE, Hynynen K, Hardy CJ, Watkins RD, Schenck JF, Jolesz FA. Mr Temperature Mapping of Focused Ultrasound Surgery. Magn Reson Med 1994;31(6):628-636.
30. Bohris C, Schreiber WG, Jenne J, Simiantonakis I, Rastert R, Zabel HJ, Huber P, Bader R, Brix G. Quantitative MR temperature monitoring of high-intensity focused ultrasound therapy. Magn Reson Imaging 1999;17(4):603-610.

5

CHAPTER 6

General discussion

In this thesis, research with respect to several aspects of MR thermometry in tissues containing fat was presented and discussed. The research was carried out within the context of the VOLTA project funded by the Dutch Center for Translational Molecular Medicine (CTMM). The purpose of the VOLTA project was to develop an MR-HIFU technology platform for the ablation of breast and liver tumors.

Given the fact that breast tumors are often at least partially surrounded by fat tissue, the development and optimization of methods for MR thermometry in fatty tissues was indicated. Additionally a method to detect unwanted heating of subcutaneous adipose tissue during MR-HIFU ablation in the abdomen, e.g. of liver tumors, was proposed and investigated. Special attention was paid to the role of magnetic susceptibility in MR thermometry and the potential for relaxation based thermometry in adipose tissue.

6.1. Magnetic susceptibility of aqueous and fatty tissues

As mentioned in the introduction section of this thesis, the electron shielding constant of the water hydrogen proton has a low temperature sensitivity (0.01 ppm/°C), thereby making PRFS-based thermometry prone to errors caused by other sources of magnetic field changes that may easily overwhelm the effects of temperature on the observed proton resonance frequency. For example, a previous study showed that heat-induced magnetic susceptibility changes of fat give rise to magnetic field disturbances that may corrupt PRFS-thermometry in nearby aqueous tissues (1). This presented a challenge on how to separate (or account for the effects) of tissue magnetic susceptibility and electron shielding, which are both temperature dependent intrinsic tissue properties (chapter 2, equation 1). The magnetic susceptibility can be quantified using set-ups with special geometries (2) or making use of object rotations with respect to the direction of the main magnetic field (3), but this would be unpractical during HIFU ablations. Correction methods for magnetic field disturbances have generally fallen into two categories: the generic approach (eg. fat referencing (4)/referenceless MR thermometry (5)) or the direct approach (e.g. the multi-baseline correction algorithm (6)). In chapter 2 the direct approach was used to correct for heat-induced magnetic field disturbances. The change in heat-induced tissue magnetic susceptibility was estimated using a 3D thermal model with T_1 and/or PRFS temperature maps as input, and via a fast algorithm, the related magnetic field disturbance was calculated. The correction method was shown to be effective and has potential for real-time correction during HIFU.

For voxels containing both aqueous and fatty tissues, *internal referencing* has been proposed to compensate for general sources of magnetic field disturbances (7). The concept is to use fat, with a temperature independent electron screening constant as a probe for the magnetic field to correct for the field disturbance in the aqueous tissue in the same voxel. However, it was shown in chapter 3 that when heat-induced changes are the source of the field disturbance, using fat as an internal reference may work inadequately. This is because of the difference in temperature coefficient of magnetic susceptibility for aqueous and fatty tissues, resulting in intra-voxel spatial variations in the change of magnetic field. The choice of whether to use internal referencing may therefore depend on whether the heat-induced errors are expected to be higher or lower than other sources of magnetic field disturbances. However, given that the magnitude of these errors depends on the water/fat geometry, temperature change, and location and size of the voxel, this may have to be investigated for each application and situation.

Other than the heat-induced change in magnetic susceptibility, the inherent difference in magnetic susceptibility between aqueous and fatty tissues (of about 1 ppm) may also be an issue. If both aqueous and fatty tissues are present in a voxel, intra-voxel spatial magnetic field variations can be expected (chapter 3). Therefore, the measured intra-voxel difference in the water/fat resonance frequency is not only due to the difference in electron screening constants of water and fat, but also related to their spatial distribution. This complicates absolute thermometry techniques which are based on the difference in the resonance frequency between water and fat. Simulations and experiments confirmed that the spatial distribution of magnetic susceptibility was an important source of errors in the temperature measurement. With this knowledge, the large variations in absolute temperatures measured in the breast by McDannold et al. (2) may largely be explained by the spatial distribution of water and fat. Consequently, the spatial distribution of the magnetic susceptibility (as well as any other source of intra-voxel variation in magnetic field) should be considered when applying this technique. A more thorough investigation of this effect is warranted.

6.2. Relaxation based thermometry in adipose tissues

For thermal therapies in heterogeneous water/fat tissues, temperature information in both aqueous and fatty tissue compartments is desirable. For example, adipose tissue may accumulate heat during the thermal intervention and pose a risk to adjacent tissue structures, and tumor cells may be embedded in fat in the margins of a breast tumor. In chapters 4 and 5, MR thermometry based on the temperature dependence of relaxation times was investigated for adipose tissue. Very low inter-sample variations in the temperature coefficients for the relaxation times were found in breast and porcine adipose tissue. It was found to be important to apply water suppression, giving more reproducible temperature coefficients in adipose tissue (eg. chapter 4, Figure 4b). Additionally, for the temperature range measured (25 - 65 °C), and in both porcine and human breast adipose tissue, the relaxation times were completely reversible during cooling after the tissue had been heated. Both animal experiments in a pig model and calibration experiments in human breast adipose tissue samples suggest that relaxation-based MR thermometry is feasible in adipose tissue during MR-HIFU interventions.

6.3. Verification of MR thermometry

Commonly, calibrated temperature probes such as fiber-optic probes or thermocouples are used to verify MR temperature measurements, and are considered to provide the ground

truth. However, verifying the temperature information obtained from MR scans has proved to be difficult (8). In chapter 2 the use of ethylene glycol (EG) gel was introduced for this purpose. EG is an established solution used to calibrate temperatures of NMR spectrometers, by measuring the hydrogen proton resonance frequency difference between the -OH and -CH_2 chemical groups (9). In chapter 2, where a correction method was proposed, this property of EG was used to separate temperature changes from magnetic field changes. In chapter 4, which dealt with measuring the temperature change in subcutaneous adipose tissue, fiber optic probes were used to verify the temperature change in the pig's fat layer during a HIFU sonication. Although fiber optic probes provoke less susceptibility-related artefacts on the MR temperature maps, compared to metallic thermocouples, their use remains challenging. The ultrasound pressure waves may result in jumps in the temperature reading and finding the exact tip location on the MR image is challenging. Additionally, the influence of viscous heating of the probe itself can generally not be accounted for. In all chapters of this thesis, aspects regarding temperature verification have been addressed. In chapter 5, the temperature dependence of T_1 and T_2 in fat was investigated. Here a temperature-stabilized water bath was employed to make the temperature as spatially homogenous as possible to allow easier matching between the MR measurement and the temperature probe readings. In chapter 3, spherical tissue samples were maintained at room temperature for hours to ensure a temperature profile that is as homogenous as possible. Therefore, no field disturbing temperature probe was necessary, as the temperature was assumed to be spatially the same everywhere in the tissue.

6.4. Ongoing and future research

In this thesis, several issues were presented that may deserve further attention. The most important ones are described here. In chapter 2, a method to correct for PRFS thermometry errors due to heat-induced magnetic susceptibility changes was investigated. The correction method used prior knowledge of the temperature dependence of the magnetic susceptibility of tissues. Data on the temperature coefficient for the magnetic susceptibility were available for water, adipose tissue, and muscle, but not for tumor tissue. However, it would be good to have this data in order to estimate the effect of heat-induced magnetic susceptibility changes on PRFS-thermometry in tumors during HIFU interventions. For the same reason it would be interesting to investigate whether ex vivo and in vivo tissue have similar magnetic susceptibility properties. The correction method presented in this thesis assumed a small inter-sample variation in the temperature dependence of the tissue magnetic susceptibility. If this assumption is invalid, the proposed correction method may be ineffective. It is therefore desirable to investigate aspects that may influence these calibration measurements. For example, the temperature dependence of the susceptibility may be different for fast HIFU-heating (order of seconds) than for controlled heating experiments which may take hours. One study, for example, noted a dispersion of the lipid phase in experiments determining the temperature dependence of the magnetic susceptibility of breast adipose tissue (10). Additionally the preparation or origin of the tissue sample may influence the tissue magnetic susceptibility. Tissue refrigeration, centrifugation, and time between tissue extraction and calibration may all influence the magnetic susceptibility, and the temperature dependence hereof.

In chapter 3, the influence of water/fat heterogeneity on fat referenced thermometry was investigated. Fat referenced absolute thermometry was found to be challenging in more heterogeneous water/fat distributions like the breast. Further research is needed to investigate whether these effects may be corrected for, either directly by estimating the field

disturbance, or by analysis of the MR spectrum. Spectral characteristics have been used to characterize the geometry of simple magnetic field perturbers (11) but this concept may be much more difficult to apply to tissues with more complex geometries. Additionally, it would be interesting to investigate the influence of intra-voxel magnetic field variation on water/fat separation techniques. This is especially important because of the interest in techniques for simultaneous MR thermometry in water and fat. For example, by using a multi-flip angle, multi-echo gradient echo sequence, the water/fat signal may be separated with IDEAL (12), and the T_1 (13,14) and proton resonance frequency (shift) measured in water and fat. This would allow for T_1-based thermometry in fat and PRFS thermometry in water (15,16). However these water/fat separation algorithms commonly assume a fixed value for the water/fat resonance frequency separation, which was shown in chapter 3 not to be the case in the breast, even at a homogenous temperature. Being unable to sufficiently separate the water and fat signal may result in MR thermometry errors in both water and fat.

Regarding MR thermometry in adipose tissues, Kuroda et al. (17) measured the temperature dependence of T_1 and T_2 of adipose fatty acid components at 11 T. It is also important to measure the temperature dependence of relaxation times of fatty acid components at lower field strengths (1.5 T, 3 T) which are currently more clinically relevant for HIFU. This is necessary because of the possible influence of the variation of the fatty acid composition in adipose tissue on relaxation-based thermometry methods that don't separate these fatty acid components. In chapters 4 and 5 relaxation-based MR thermometry techniques were used that don't separate or account for the fatty acid composition. Despite this, small inter-sample variations in the temperature coefficients for the relaxation times were found suggesting that the influence of fatty acid compositions, at least in the population from which these samples were taken, is very small. However, due to the small sample size used in this thesis, this aspect should not be completely ignored. Therefore, to avoid unacceptable errors in relaxation-based thermometry, both investigating a larger number of samples is necessary, and the exact influence of the fatty acid composition on relaxation-based temperature measurements needs to be quantified. Another reason why measuring the temperature dependence of relaxation times of fatty acid components at lower field strengths is desirable, is to use this as prior knowledge for water/fat separation algorithms at different temperatures. Unfortunately, measuring the relaxation times of fatty acids in adipose tissue is challenging at lower field strengths because of the decreased spectral resolution. Also, the presence of J-coupling and the large number of fatty acid components present in adipose tissue complicate these measurements.

In chapter 3 it was shown that absolute thermometry based on the water/fat resonance frequency difference may not be straight-forward. As an alternative for adipose tissues, the absolute temperature may be derived from measurements of the relaxation times. Indeed, for the seven breast fat samples measured in chapter 5 (Figure 2b), a temperature error of less than 2.2 °C was found for the turbo spin echo based measurements. These findings should be confirmed in more breast samples. Furthermore, relaxation time measurement techniques would need to be developed that are sufficiently robust against B_1 and B_0 inhomogeneities, which may be quite large around the HIFU system.

In chapter 4, heat accumulation was measured in adipose tissue based on the change in the apparent T_2, i.e. the T_2 measured using a dual-echo turbo spin echo sequence. This sequence may be optimized, and the compromise between SNR, temperature sensitivity, scan time, and other imaging parameters investigated. This would allow for the implementation of this technique for different MR-HIFU platforms, and tissue regions, which may have considerably different SNR.

Lastly, the observed macroscopic tissue deformations during HIFU ablations observed in the breast in ex vivo studies (18) could seriously hamper MR-thermometry techniques used in this thesis (e.g. image subtraction methods), and the correction method presented in chapter 2. This observation needs to be confirmed with other MR imaging methods or imaging modalities and in the in vivo situation.

6.5. Conclusions

This work has contributed to the understanding, development, and application of MR thermometry methods in fat-containing tissues. The influence of magnetic susceptibility on chemical shift-based thermometry was shown with simulations and heating experiments. It was shown that relaxation based thermometry can sufficiently probe temperature changes in adipose tissue. MR thermometry is an active field of research, with new techniques being developed, evaluated, and applied, in order to improve patient care during thermal interventions.

6.6. References

1. Sprinkhuizen SM, Konings MK, van der Bom MJ, Viergever MA, Bakker CJ, Bartels LW. Temperature-induced tissue susceptibility changes lead to significant temperature errors in PRFS-based MR thermometry during thermal interventions. Magn Reson Med 2010;64(5):1360-1372.
2. Frei K, Bernstein HJ. Method for Determining Magnetic Susceptibilities by NMR. J Chem Phys 1962;37(8):1891-&.
3. De Poorter J. Noninvasive MRI thermometry with the proton resonance frequency method: study of susceptibility effects. Magn Reson Med 1995;34(3):359-367.
4. Kuroda K, Oshio K, Chung AH, Hynynen K, Jolesz FA. Temperature mapping using the water proton chemical shift: A chemical shift selective phase mapping method. Magn Reson Med 1997;38(5):845-851.
5. Rieke V, Vigen KK, Sommer G, Daniel BL, Pauly JM, Butts K. Referenceless PRF shift thermometry. Magn Reson Med 2004;51(6):1223-1231.
6. Vigen KK, Daniel BL, Pauly JM, Butts K. Triggered, navigated, multi-baseline method for proton resonance frequency temperature mapping with respiratory motion. Magn Reson Med 2003;50(5):1003-1010.
7. Kuroda K, Mulkern RV, Oshio K, Panych LP, Nakai T, Moriya T, Okuda S, Hynynen K, Jolesz FA. Temperature mapping using the water proton chemical shift: self-referenced method with echo-planar spectroscopic imaging. Magn Reson Med 2000;44(1):167.
8. Baron P, Deckers R, de Greef M, Merckel LG, Bakker CJG, Bouwman JG, Bleys RLAW, van den Bosch MAAJ, Bartels LW. Correction of Proton Resonance Frequency Shift MR-Thermometry Errors Caused by Heat-Induced Magnetic Susceptibility Changes during High Intensity Focused Ultrasound Ablations in Tissues Containing Fat. Magn Reson Med 2014;72(6):1580-1589.
9. Ammann C, Meier P, Merbach AE. A Simple Multi-Nuclear NMR Thermometer. J Magn Reson 1982;46(2):319-321.
10. Sprinkhuizen SM, Bakker CJG, Ippel JH, Boelens R, Viergever MA, Bartels LW. Temperature dependence of the magnetic volume susceptibility of human breast fat tissue: an NMR study. Magn Reson Mater Phy 2012;25(1):33-39.

11. Seppenwoolde JH, van Zijtveld M, Bakker CJ. Spectral characterization of local magnetic field inhomogeneities. Phys Med Biol 2005;50(2):361-372.
12. Reeder SB, Wen ZF, Yu HZ, Pineda AR, Gold GE, Markl M, Pelc NJ. Multicoil Dixon chemical species separation with an iterative least-squares estimation method. Magn Reson Med 2004;51(1):35-45.
13. Kuroda K, Iwabuchi T, Lam MK, Obara M, Honda M, Saito K, Cauteren MV, Imai Y. Fat Temperature Imaging with T1 of Fatty Acid Species using Multiple Flip Angle Multipoint Dixon Acquistions. In Proceedings of the 18th Annual Meeting of the ISMRM, Stockholm, Sweden, 2010. p. 1818.
14. Deoni SC, Rutt BK, Peters TM. Rapid combined T1 and T2 mapping using gradient recalled acquisition in the steady state. Magn Reson Med 2003;49(3):515-526.
15. Diakite M, Odeen H, Todd N, Payne A, Parker DL. Toward real-time temperature monitoring in fat and aqueous tissue during magnetic resonance-guided high-intensity focused ultrasound using a three-dimensional proton resonance frequency T1 method. Magn Reson Med 2014;72(1):178-187.
16. Soher BJ, Wyatt C, Reeder SB, MacFall JR. Noninvasive temperature mapping with MRI using chemical shift water-fat separation. Magn Reson Med 2010;63(5):1238-1246.
17. Kuroda K, Iwabuchi T, Obara M, Honda M, Saito K, Imai Y. Temperature Dependence of Relaxation Times in Proton Components of Fatty Acids. Magn Reson Med Sci 2011;10(3):177-183.
18. Merckel LG, Deckers R, Baron P, Bleys RLAW, van Diest PJ, Moonen CTW, Mali WPTM, van den Bosch MAAJ, Bartels LW. The effects of magnetic resonance imaging-guided high-intensity focused ultrasound ablation on human cadaver breast tissue. Eur J Pharmacol 2013;717(1-3):21-30.

6

CHAPTER 7

Summary

The aim of the research described in this thesis was to improve and apply MR thermometry techniques in fat containing tissues. These thermometry methods were researched with the aim of applying them for MR-guided HIFU treatment of tumors in the female breast and in the liver.

In **chapter 2** the sensitivity of proton resonance frequency shift (PRFS)-based thermometry to heat-induced magnetic susceptibility changes was demonstrated and a model-based correction procedure was presented and evaluated. To demonstrate the theoretically expected temperature-induced effect on the magnetic field, field disturbances during high intensity focused ultrasound sonications were monitored in breast fat samples with a three-dimensional (3D) gradient echo sequence. To evaluate the correction procedure, phantom experiments were performed in which an interface of tissue mimicking ethylene glycol gel and fat was sonicated. During sonication, the temperature was monitored with a 2D dual flip angle multi-echo gradient echo sequence, allowing for PRFS based relative and referenced temperature measurements in the gel and T_1-based temperature measurements in fat. The PRFS-based measurement in the gel was corrected by minimizing the discrepancy between the observed 2D temperature profile and the profile predicted by a 3D thermal model. The HIFU sonications of breast fat resulted in a magnetic field disturbance which completely disappeared after cooling. For the correction method, the 5th to 95th percentile interval of the PRFS-thermometry error in the gel decreased from 3.8 °C before correction to 2.0 – 2.3 °C after correction. This study showed the effects of magnetic susceptibility changes induced by heating of breast fatty tissue samples. The resultant errors could be reduced by the use of a model-based correction procedure.

In **chapter 3** the effect of the aqueous and fatty tissue magnetic susceptibility distribution on absolute and relative temperature measurements as obtained directly from the water/fat frequency difference was investigated. Absolute thermometry was investigated using spherical phantoms filled with (macroscopically heterogeneous) pork and (more homogeneous) margarine, which were scanned in three orthogonal orientations. To evaluate relative fat referencing, multi-gradient echo scans were acquired before and after heating pork tissue by high intensity focused ultrasound (HIFU). Simulations were performed to estimate the errors that can be expected in human breast tissue. The sphere experiment showed susceptibility-related errors of 8.4 °C and 0.2 °C for pork and margarine, respectively. For relative fat referencing measurements, fat showed pronounced phase changes of opposite polarity to aqueous tissue. The apparent mean temperature for a numerical breast model (assumed to be at 37 °C) was 47.2 ± 21.6 °C. Simulations of relative fat referencing for a HIFU sonication

($\Delta T = 29.7$ °C) gave a maximum temperature error of 6.6 °C compared to 2.5 °C without fat referencing. Variations in the observed frequency difference between water and fat are largely due to variations in the water/fat spatial distribution. This effect may lead to considerable errors in absolute MR thermometry. Additionally, fat referencing may exacerbate rather than correct for PRFS-temperature measurement errors.

During MR-guided high-intensity focused ultrasound (HIFU) therapy, ultrasound absorption in the near field represents a safety risk and limits efficient energy deposition at the target. In **chapter 4** the feasibility of using T_2 mapping to monitor the temperature change in subcutaneous adipose tissue layers was investigated. The T_2 temperature dependence and reversibility was determined for fresh adipose porcine samples. The accuracy was evaluated by comparing T_2-based temperature measurements with probe readings in an ex vivo HIFU experiment. The in vivo feasibility of T_2-based thermometry was studied during HIFU ablations in the liver in pigs and of uterine fibroids in human patients. T_2 changed linearly and reversibly with temperature with an average coefficient of 5.2 ± 0.1 ms/°C. For the ex vivo HIFU experiment, the difference between the T_2-based temperature change and the probe temperature was < 0.9 °C. All in vivo experiments showed temperature-related T_2 changes in the near field directly after sonications. As expected, considerable inter-subject variations in the cooling times were measured in the in vivo porcine experiments. The reversibility and linearity of the T_2-temperature dependence of adipose tissue allows for the monitoring of the temperature in the subcutaneous adipose tissue layers.

In **chapter 5** the T_1 and T_2 temperature dependence of female human breast adipose tissue at 1.5T was investigated in order to evaluate the applicability of relaxation-based MR thermometry for temperature monitoring in fat during thermal therapy in the breast. Relaxation times T_1, T_2, and T_{2TSE} (apparent T_2 measured using a turbo spin echo readout sequence) were measured in seven fresh adipose breast samples for temperatures from 25 to 65 °C. Spectral water suppression was used to reduce the influence of residual water signal. The temperature dependence of the relaxation times was characterized. The expected maximum temperature measurement errors based on average calibration lines were calculated. Additionally, the heating-cooling reversibility was investigated for two samples. The T_1 and T_{2TSE} temperature (T) dependence could be well fit with an exponential function of 1/T. A linear relationship between T_2 and temperature was found. The temperature coefficients (mean ± inter-sample standard deviation) of T_1 and T_{2TSE} increased from 25 °C (T_1 = 5.35 ± 0.08 ms/°C, T_{2TSE} = 3.82 ± 0.06 ms/°C) to 65 °C (T_1 = 9.50 ± 0.16 ms/°C, T_{2TSE} = 7.99 ± 0.38 ms/°C). The temperature coefficient of T_2 was 0.90±0.03 ms/°C. The temperature-induced changes in the relaxation times were found to be reversible after heating to 65 °C. Given the small inter-sample variation of the temperature coefficients, relaxation-based MR thermometry appears feasible in breast adipose tissue.

7

CHAPTER 8

Nederlandse Samenvatting

Het doel van het onderzoek beschreven in dit proefschrift was om MR thermometrie in vethoudende weefsels toe te passen en te verbeteren. Deze thermometrie methoden zijn onderzocht met het doel in gedachten om deze te gebruiken in MR-geleide HIFU behandelingen van tumoren in de borst en lever.

In **hoofdstuk 2** wordt de gevoeligheid van proton resonance frequency shift (PRFS) thermometrie voor susceptibiliteitsveranderingen veroorzaakt door verhitting gedemonstreerd en een modelgebaseerde correctie procedure gepresenteerd en geëvalueerd. Om de theoretisch verwachte temperatuur-geïnduceerde effecten te laten zien, werd de magnetisch veldverstoringen tijdens HIFU sonicaties van borstvetmonsters met een driedimensionale (3D) gradiënt echo sequentie gemeten. Om de correctieprocedure te evalueren, werden fantoom experimenten uitgevoerd waarbij een raakvlak van ethyleenglycol gel en vet werd gesoniceerd. Tijdens de sonicatie werd een 2D dubbele-fliphoek multi-echo gradiënt echo pulssequentie toegepast, waardoor op de PRFS gebaseerde relatieve en referentietemperatuurmetingen in de gel en op T_1 gebaseerde temperatuurmetingen in vet kon werden gedaan. De op PRFS gebaseerde metingen in de gel werd gecorrigeerd door het verschil tussen het waargenomen 2D temperatuurprofiel en het profiel voorspeld door een 3D thermisch model te minimaliseren. De HIFU sonicaties in borstvet resulteerde in een verstoring van het magnetisch veld die verdween na afkoeling. De breedte van het interval van 5e tot de 95e percentiel van de verdeling van PRFS-thermometriefouten in de gel daalde van 3.8 °C voor de correctie naar 2.0 - 2.3 °C na correctie. Deze studie toonde de effecten aan van magnetische susceptibiliteitveranderingen bij het verwarmen van borstvetweefsel met HIFU. De resulterende fouten kunnen worden verminderd door het gebruik van een modelgebaseerde correctieprocedure.

In **hoofdstuk 3** werd het effect van de distributie van de magnetische susceptibiliteit van waterhoudend weefsel en vetweefsel op absolute en relatieve temperatuurmetingen, rechtstreeks verkregen uit het water/vet frequentieverschil, onderzocht. Absolute thermometrie werd onderzocht met behulp van bolfantomen gevuld met (macroscopisch heterogeen) varkensvlees en (homogenere) margarine, die in drie orthogonale richtingen werden gescand. Om relatieve thermometrie met vet als referentie te evalueren, werden multi-gradiënt echo scans geacquireerd voor en na het verwarmen van varkensvlees met HIFU. Simulaties werden uitgevoerd om de verwachte fouten in menselijk borstweefsel af te schatten. Het bolexperiment toonde susceptibiliteits-gerelateerde fouten van respectievelijk 8.4 °C en 0.2 °C voor varkensvlees en margarine. De relatieve temperatuurmetingen toonde duidelijke faseveranderingen van tegengestelde polariteit in vet en in waterig weefsel. De

schijnbare gemiddelde temperatuur van een numeriek borstmodel (met een veronderstelde temperatuur van 37 °C) was 47.2 ± 21.6 °C. Simulaties van relatieve temperatuurmetingen voor een HIFU sonicatie (ΔT = 29.7 °C) gaf een maximale temperatuurfout van 6.6 °C in vergelijking met 2.5 °C zonder gebruik te maken van vet als referentie. Variaties in het waargenomen frequentieverschil tussen water en vet zijn grotendeels te wijten aan variaties in de ruimtelijke verdeling van water en vet. Dit effect kan leiden tot aanzienlijke fouten in absolute MR thermometrie. Daarnaast kan het gebruik van vet als referentie meetfouten in PRFS-thermometrie gerelateerd aan susceptibiliteit groter maken.

Tijdens MR-geleide HIFU therapie, vormt ultrageluidabsorptie in het nabije veld een veiligheidsrisico dat efficiënte energie-depositie in het doelgebied beperkt. In **hoofdstuk 4** wordt de haalbaarheid van het gebruik van metingen van de transversale relaxatietijd T_2 om de temperatuursverandering in onderhuids vetweefsel te monitoren onderzocht. De temperatuursafhankelijkheid van T_2 en de omkeerbaarheid daarvan werd bepaald voor monsters van vers varkensvet. De precisie werd geëvalueerd door temperaturen bepaald op basis van T_2 te vergelijken met metingen uitgevoerd met een gekalibreerde thermometer in een ex vivo HIFU experiment. De haalbaarheid in vivo van thermometrie op basis van T2 werd bestudeerd tijdens HIFU ablaties in de lever tijdens dierexperimenten in een varkensmodel en van uterine myomen in patiënten. T_2 veranderde lineair en reversibel met temperatuur met een gemiddelde coëfficiënt van 5.2 ± 0.1 ms/°C. In het ex vivo HIFU experiment werd een verschil kleiner dan 0.9 °C tussen de T_2-gebaseerde temperatuurveranderingen en de probe metingen gevonden. Bij alle in vivo experimenten werden direct na sonicaties temperatuurgerelateerde T_2 veranderingen in het nabije veld gezien. Zoals werd verwacht, werden er een aanzienlijke inter-individuele variatie in de karakteristieke afkoeltijd gemeten in de in vivo varkensexperimenten. De reversibiliteit en lineariteit van de temperatuursafhankelijkheid van T_2 van vetweefsel maakt het meten van de temperatuur in onderhuids vetweefsel mogelijk.

In **hoofdstuk 5** werd de temperatuursafhankelijkheid van de longitudinale relaxatietijd T_1 en van de transversale relaxatietijd T_2 van humaan vetweefsel uit de borst bij 1.5 T onderzocht om te bepalen of deze parameters te gebruiken zijn voor temperatuursmetingen tijdens thermische behandeling in de borst. De relaxatietijden T_1, T_2 en T_{2TSE} (dat is de schijnbare T_2, gemeten met een turbo spin-echo sequentie) werden gemeten in zeven verse humane borstvet monsters in het temperatuurbereik van 25 - 65 °C. Spectrale wateronderdrukking werd gebruikt om de invloed van het signaal afkomstig van water te verminderen. De temperatuursafhankelijkheid van de relaxatietijden werden gemodelleerd en de verwachte maximale meetfouten in de temperatuur gebaseerd op gemiddelde kalibratielijnen werd berekend. Daarnaast werd de verwarming-koeling reversibiliteit onderzocht in twee monsters. De relaties tussen zowel T_1 als T_{2TSE} en de temperatuur (T) werden goed gefit met een exponentiële functie van 1/T. Een lineair verband tussen T_2 en de temperatuur werd gevonden. De temperatuurscoëfficiënten (gemiddelde ± inter-sample standaarddeviatie) van T_1 en T_{2TSE} nam toe in het temperatuursbereik van 25 ° C (T_1 = 5.35 ± 0.08 ms/°C, T_{2TSE} = 3.82 ± 0.06 ms/°C) tot 65 °C (T_1 = 9.50 ± 0.16 ms/°C, T_{2TSE} = 7.99 ± 0.38 ms/°C). De temperatuurcoëfficiënt van T_2 was 0.90 ± 0.03 ms/°C. De door temperatuurveranderingen veroorzaakte veranderingen in de relaxatietijden bleken reversibel te zijn na verwarmen tot 65 °C. Gezien de kleine variatie tussen de monsters van de temperatuurcoëfficiënten, lijkt op relaxatie gebaseerde MR thermometrie haalbaar te zijn in borstvet weefsel.

List of abbreviations

CTMM	Center for Translational Molecular Medicine
EG	Ethylene glycol
FOV	Field of view
HIFU	High Intensity Focused Ultrasound
mac	Macroscopic
meas/cor	Measured/corrected
MRI	Magnetic Resonance Imaging
NSA	Number of signal averages
nuc	Nuclear
obj	Object
ppm	parts per million
PRESS	Point resolved spectroscopy
PRFS	Proton resonance frequency shift
ref	Reference
RF	Radio frequency
ROI	Region of interest
SD	Standard deviation
SNR	Signal to noise ratio
SPGR	Spoiled gradient echo
SPIR(-WS)	Spectral presaturation with inversion recovery (-Water suppression)
ST	Slice thickness
suc	Susceptibility
TE	Echo time
TR	Repetition time
TSE	Turbo spin echo
US	Ultrasound
VOLTA	Volumetric thermal ablation project
w/f	Water/fat

Acknowledgments

I want to thank colleagues, family and friends for supporting me during my PhD program. It was a privilege to be part of the VOLTA project, which involved an exciting combination of MRI and ultrasound. I have learned so much, both work related and through personal development.

This thesis would not be possible without the dedicated support from my daily supervisor and co-promotor Dr. ir. Wilbert Bartels. Wilbert, thank you for your supervision during my PhD research. You have helped me through our discussions on MRI and HIFU, read and reviewed countless of my manuscript drafts, and have encouraged me to give presentations. Thanks!

Prof. dr. ir. Max Viergever, thank you for giving me the opportunity to work at the Image Science Institute. Thank you for supporting me in achieving my research goals.

Prof. dr. Chrit Moonen, I was happy to see your group come to Utrecht. This gave a great impulse to the MR-HIFU research in Utrecht. Thank you for supporting my PhD project.

Roel, you have extensive MR-HIFU knowledge and have helped me throughout my PhD with experiments, writing manuscripts, and discussions. Thank you for all your extensive support and being part of my daily supervision. Chris, I have always admired your patience in trying to understand my MR problems. You have helped me to develop my own research skills. You have an amazing enthusiasm to discover more and more. Job, I have gone to you countless number of times with questions and problems, both work related and personal. You have always been there to help me. Thank you for all your help and it has been nice working with you.

I want to thank the examining committee: Prof. dr. P.J. van Diest, Prof. dr. ir. J.J.W. Lagendijk, Prof. dr. M.A.A.J. van den Bosch, Prof. dr. B.W. Raaymakers, Prof. dr. D.L. Parker, Prof. dr. K. Butts Pauly and Dr. Edwin Heijman for taking the time to evaluate my thesis.

Mario, thank you for supervising me with the liver near-field project. You have a great drive to get things done. Martijn, thank you for your help with simulations and explaining ultrasound physics to me. Gerald, thank you for all your help with the animal experiments. Thank you Laura, Floor, Joost, Marlijne, and Merel, for working with me on the HIFU projects, supplying tissue samples for my experiments, and supporting me during my first international oral presentation in Washington! Also, thanks to our colleagues from Philips Healthcare for their support. Thank you Jukka for working on T_2 thermometry in fat with me. Thank you Max K. for supporting the MR-HIFU group in Utrecht.

Thank you Kagayaki for working with me on MR thermometry in adipose tissue. Yolanda, thank you for the breast segmentation. Jaco, thanks for the Pulse Programming Environment support. Peter S. and Sjoerd van G., thanks for our MR physics discussions. Gerard, thanks for making my computer virus-free. Cyril, I will never again bet on beer with you! Thank you for our MR relaxometry discussions. Yinghe, you are a nice colleague. It really is time you

learned some more Dutch so you can pick up on the latest gossip during lunch. Hendrik, you were a colleague during the first part of my PhD and I was sad to see you leave. You always showed interest in my work and have a lot of MR knowledge- thank you for this. Sara, thank you for introducing me to MR Thermometry and passing the subject on to me. Hugo and Marijn, thanks for your help with MevisLab. Thank you Frank S. and Nico for the helpful MR thermometry discussions. Thank you Rennert and Chris O. for your help with experiments and letting me use the lab at the Nuclear Medicine department. Thessa, thank you for helping me with InDesign and the layout of my thesis. Special thanks to all my fellow PhD students and colleagues (including some names not yet mentioned: Bruno, Chantal, Lisette, Marc, Szabolcs, Sjoerd V., Floor, Pim, Jurica, Mike, Hui Shan, Fenghua, Bas, Bob, Jelmer, Frank Z., Yulia, Sandra, Miekee, Clemens, Kenneth, Hans, Ivana, Alexander, Rick, Dennis, Josien, Koen, Paul S., Erwin, Vincent, Baudouin, Anneriet, Adrienee, Jeroen S., Jeroen de B., Pieter, Christian, Noburu, Bart, Baudouin, Angelique, Pascal, Irene, Cornel, Manon, Luc, Greet, Niels, Gerrit, Ronald, Jaap, Ewoud, Maartje, Maaike, Judith, Renee, Marjan, and Jacqueline) for helping to create a ‘gezellig’ working atmosphere.

Floris, you have been a great office roommate. You have a wide range of knowledge and have contributed so much to my research. It was enjoyable having you as a colleague. We have explored the hidden passage ways of the hospital together, and you have introduced me to Pacha! Nynke, thank you for all your healthy food choice advice (although the occasional consumption of a greasy hamburger does still occur). Floris and Nynke – thank you for hanging around with me, and eating the delicious food at the Brink restaurant with me. Mitko- cool relaxed guy, thank you for all your advice on all types of issues, and for inviting me to hang around with you. Daniel, thanks for all the fun times going out in the city and enjoying different restaurants. Robin, thanks for introducing me to the Wombats music and for your funny Facebook comments! Thank you Hristina, Henriette, Irene, Mattheijs and Nelleke for being my friends and giving some relief during some stressful PhD moments. Thanks to my parents Wietze and Dorothy, and brother and sister Wiebe and Ruth for supporting me. Thank you Junier for your help with the thesis layout and nephew and niece Joshua and Noemi for letting me be part of your life.

List of publications

Baron P, Deckers R, Bouwman JG, Bakker CJG, de Greef M, Viergever MA, Moonen CTW, Bartels LW. On the influence of water and fat heterogeneity on fat referenced MR thermometry. Magn Reson Med. (Submitted)

Baron P, Ries M, Deckers R, Greef M, Tanttu J, Kohler M, Viergever MA, Moonen CTW, Bartels LW. In Vivo T2-Based MR Thermometry in Adipose Tissue Layers for High-Intensity Focused Ultrasound Near-Field Monitoring. Magn Reson Med 2014;72(4):1057-1064.

Baron P, Deckers R, de Greef M, Merckel LG, Bakker CJG, Bouwman JG, Bleys RLAW, van den Bosch MAAJ, Bartels LW. Correction of Proton Resonance Frequency Shift MR-Thermometry Errors Caused by Heat-Induced Magnetic Susceptibility Changes during High Intensity Focused Ultrasound Ablations in Tissues Containing Fat. Magn Reson Med 2014;72(6):1580-1589.

Merckel LG, Deckers R, **Baron P**, Bleys RLAW, van Diest PJ, Moonen CTW, Mali WPTM, van den Bosch MAAJ, Bartels LW. The effects of magnetic resonance imaging-guided high-intensity focused ultrasound ablation on human cadaver breast tissue. Eur J Pharmacol 2013;717(1-3):21-30.

Dijkstra H, **Baron P**, Kappert P, Oudkerk M, Sijens PE. Effects of microperfusion in hepatic diffusion weighted imaging. Eur Radiol 2012;22(4):891-899.

Baron P, Dorrius MD, Kappert P, Oudkerk M, Sijens PE. Diffusion-weighted imaging of normal fibroglandular breast tissue: influence of microperfusion and fat suppression technique on the apparent diffusion coefficient. NMR Biomed 2010;23(4):399-405.

Sijens PE, Dorrius MD, Kappert P, **Baron P**, Pijnappel RM, Oudkerk M. Quantitative multivoxel proton chemical shift imaging of the breast. Magn Reson Imaging 2010;28(3):314-319.

van der Houwen EB, **Baron P**, Veldhuizen AG, Burgerhof JGM, van Ooijen PMA, Verkerke GJ. Geometry of the Intervertebral Volume and Vertebral Endplates of the Human Spine. Ann Biomed Eng 2010;38(1):33-40.

Biography

Paul Baron was born in Papua New Guinea and lived there for about 11 years. After living a few years in Scotland his family moved to The Netherlands. He followed his secondary education at the Maartenscollege - an international school in Groningen. In Groningen he also completed his masters study Applied Physics with specialization Biomedical Technology. From 2006 to 2008 he worked at the Department of Radiology at the University Medical Center in Groningen on diffusion weighted imaging of breast tissue. In 2009 Paul started his PhD project at the Image Science Institute at the University Medical Center in Utrecht. He researched MR thermometry techniques in fat-containing tissues for MR-guided High Intensity Focused Ultrasound (MR-HIFU) therapy. His PhD program was part of a larger project (CTMM-VOLTA) concerned with the development of MR-HIFU technologies for the ablation of breast and liver tumors.